POLITECNICO DI MILANO

Dipartimento di Energia

Doctoral program in Energy - XXIV Cycle

Solar Cooling Systems Utilizing Concentrating Solar Collectors; Design, Experimental Evaluation & Optimization

Doctoral dissertation of:

Ing. Osama Ayadi

Supervisor

Prof. Mario Motta

Tutor

Prof. Livio Mazzarella

Coordinator of the PhD course

Prof. Carlo Bottani

2011- XXIV Cycle

Abstract

This thesis reports on the design, experimental evaluation and optimization of a novel solar cooling concept that allows a high temperature lift. Through applying this concept, very low temperatures (about –10 °C) on the cold side can be achieved in hot climates while employing a dry air heat rejection system that does not need water.

Under these operating conditions, thermodynamic analysis revealed that high efficient solar collector system is needed, and thus the system configuration consists of an air-cooled single-effect water ammonia absorption chiller that is driven by a medium temperature heat source (e.g. parabolic trough and Linear Fresnel reflector collectors).

Throughout the present work, two pilot plants based on this concept were designed and installed for a Tunisian beverage factory and a Moroccan dairy factory. The development of the system concept, the detailed design and the components sizing have been implemented through simulations of the system behavior using the TRNSYS's simulation platform. For this purpose mathematical models of the concentrating collector and the absorption chiller were implemented.

A monitoring system, based on the unified monitoring procedure developed within the experts group of Task 38 SHCP-IEA, was designed and all monitoring sensors have been calibrated and a data acquisition system was programmed using the software LabVIEW. The results of the extensive experimental work on the pilot plants have been used to assess the performance of the systems as well as to calibrate and validate the TRNSYS models.

The validated models were used for further simulation campaigns aiming at defining the optimum operating points of the whole system and tracing a path towards the plant performance improvement. Several parameters of the control strategy have been studied through the coupling of TRNSYS simulation software with GenOpt optimization software. The results highlighted the higher impact of some optimization options. Monitoring results showed that 44% improvement of the primary energy savings of the system has been achieved by applying the optimization procedure. Further optimization options investigating components design showed that 45% improvement of the primary energy savings of the system could be achieved.

Abstract

In questa tesi di dottorato si affronta la progettazione, l'analisi sperimentale e l'ottimizzazione di un innovativo concetto di solar cooling ad elevato salto di temperatura. La peculiarità del sistema in esame consiste nell'elevata differenza che esiste tra la bassa temperatura del refrigerante nell'evaporatore (circa -10°C) e l'alto livello di temperatura ambiente (superiore anche a 40°C) al quale il sistema di smaltimento del calore può lavorare.

L'analisi termodinamica ci ha consentito di determinare le principali caratteristiche di configurazione del sistema a queste condizioni operative, che consistono in un chiller ad assorbimento acqua/ammoniaca a singolo effetto raffreddato ad aria alimentato da una sorgente di calore a media temperatura (ad esempio un collettore parabolico o di tipo lineare Fresnel)

Durante lo sviluppo del presente lavoro, due impianti pilota, basati su questo concetto, sono stati progettati e installati a servizio di una cantina tunisina e di un caseificio marocchino.

Lo sviluppo del sistema, la progettazione di dettaglio e il dimensionamento delle varie componenti sono stati realizzati mediante l'uso della piattaforma di simulazione TRNSYS. A questo scopo sono stati implementati i modelli matematici del collettore a concentrazione e del chiller ad assorbimento.

Un sistema di monitoraggio è stato progettato sulla base della procedura unificata di monitoraggio adottata all'interno del gruppo di esperti del TASK 38 SHCP-IEA e tutti i sensori sono stati calibrati. Il sistema di acquisizione dati è stato programmato utilizzando il software LabVIEW.

I risultati delle attività di monitoraggio effettuati sugli impianti sperimentali sono stati utilizzati per valutare le prestazioni del sistema, nonché per calibrare e validare i modelli realizzati in TRNSYS.

I modelli validati sono stati poi usati per ulteriori campagne di simulazione con l'intento di definire i punti di funzionamento ottimale dell'intero sistema e delle singole componenti ed individuare le strategie per ottimizzare le performance dell'impianto. Sono state quindi studiate differenti opzioni di controllo mediante l'uso congiunto del software di simulazione TRNSYS con quello di ottimizzazione GenOpt. I risultati hanno sottolineano l'impatto più elevato di alcune scelte rispetto ad altre. I risultati di monitoraggio hanno dimostrato che la procedura di ottimizzazione ha comportato un miglioramento del 44% in termini di risparmio di energia primaria del sistema. Ulteriori opzioni di ottimizzazione hanno evidenziato che Il risparmio di energia primaria del sistema potrebbe essere migliorato ancora del 45%.

Acknowledgments

Nomenclature

ABS	Absorption Chiller
CPC	Compound Parabolic Concentrator
CSP	Concentrating Solar Power Plant
DHW	Domestic Hot Water
FPC	Flat-Plate Collector
G	Total Solar Radiation
Gb	Beam Solar Radiation
G_{bn}	Direct Normal Solar Radiation
Gd	Diffused Radiation
GHP	Gross Heat Production
IAM	Incident Angle Modifier
IPRT	Platinum Resistance Thermometers
LFC	Linear Fresnel Collector
PCM	Phase Change Material
PTC	Parabolic Trough Collector
RTD	Resistance Temperature Detectors
SC	Solar Cooling
SCR	Solar Cooling Ratio
SF	Solar Fraction
SH	Space Heating

Greek letters

γ	Surface Azimuth Angle
γ_s	Solar Azimuth Angle
δ	Declination Angle
θ	Angle Of Incidence
$\theta_{\|\|}$	Longitudinal Angle
θi	Incidence Angle
θz	Zenith Angle
ω	Hour Angle
ϕ	Latitude
η_{total}	Total Efficiency

Contents

Introduction

The utilization of cooling technologies for refrigeration and air conditioning continues to grow worldwide and is directly influenced by the increased living standards, consumption habits, comfort demands as well as building architectural characteristics and trends.

Refrigeration technologies play a vital role in many industrial applications. Notably in the food field where reduction of post-harvest losses, improved food safety and hygiene, promotion of international trade and improved food supply to the cities are considered as top-priority objectives. (Billard and Dupont 2002) The food industry relies heavily on the vapor compression refrigeration cycle for food preservation and processing. (Tassou et al. 2010) Unfortunately, in developing countries, hot weather often causes large post-harvest production losses due to the scarcity of electricity sources that run conventional cooling equipments.

Air-conditioning is the dominant energy consuming service in buildings in many countries. (IEA Solar Heating and Cooling 2002) In Europe, a strong cooling market expansion has taken place during the last decade and that the cooling market will show a fourfold increase between 2000 and 2018. (Pär Dalin, Nilsson, and Rubenhag 2006) In the United States, space cooling and refrigeration shared 25.8% of the total electrical consumption in the residential sector in 2009. (The U.S. Energy Information Administration (EIA) 2011)

Conventional cooling technologies used for refrigeration and air-conditioning cause high electricity peak loads because of their concurrent operation during periods of high ambient temperature. Not only that but also the refrigerants generally used in conventional cooling systems are adding significantly to climatic change and ozone depletion.(The U.S. Energy Information Administration (EIA) 2011)(Earthcare Products Limited 2008)

As such, the process of cooling creates a double threat to the global environment. It is no wonder, therefore, that in recent years, more and more attention has been paid to the application potential of solar cooling to meet this increasing demand in an environmentally sound way.

Several obstacles still need to be overcome in order to facilitate larger market penetration of solar cooling systems; beside the high first cost, are the lack of practical experience and acquaintance among architects, builders and planners with the design, control and operation of these systems. As consequence substantial R&D efforts are required before the solar cooling systems could reach the early market stage.(Henning 2007)(Langniß et al. 2007)

Research goals

This research aims to develop, test and optimize solar thermally driven cooling concepts for the food and agro industry in the Mediterranean region. The objective is to asses which systems could better suit the actual and future demand of the food and conservation industry sectors in the south edge of the basin of the Mediterranean and estimate in technical and economical terms the most appropriate approach for the application of solar thermally driven systems.

The majority of activities carried out through this PhD project perform part of the EC co-funded project MEDISCO "MEDiterranean food and agro Industry applications of Solar Cooling technologies".

Methodology

In order to accomplish the aforementioned goals, several research activities were carried out as shown in the flow diagram (Figure 0-1)

1. Two system concepts have been developed for two end-users selected among the agro-food industries in Tunisia and Morocco.
2. The detailed designs have been made with the assistance of system simulations to size main system components.
3. Monitoring systems have been designed, installed and calibrated to evaluate the system performance in accordance with the unified monitoring procedure.
4. System simulation models have been validated using the performance data in order to be used for optimization and future simulations.
5. The first system installed has been optimized using system simulation.
6. Solar cooling application potential has been identified by simulating developed system configurations working in different climates.
7. The experience gained through the project duration is summarized as guidelines for future designs and installations.

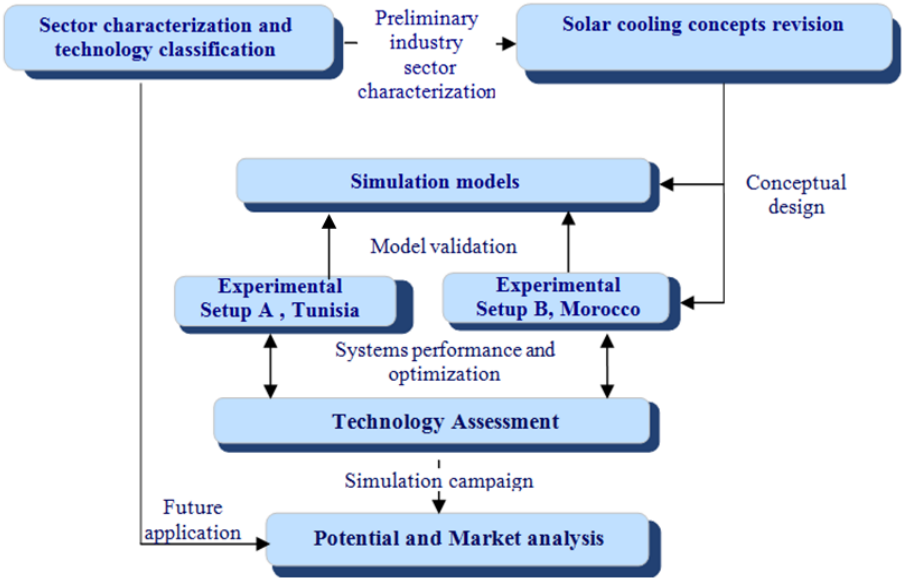

Figure 0-1: Flow diagram of the research project activities.

Thesis plan (Chapters overview)

In the first chapter, a general review of solar cooling systems is presented explaining the drivers behind the usage/implementation of solar cooling systems, market status, growth barriers and the measures for alleviation of these barriers. This general review is followed by a more dedicated review of the solar cooling system technology adopted in this project *i.e.* solar cooling systems utilizing concentrating solar collectors.

The concept development of the two experimental setups is described in the second chapter. The thermodynamic analysis behind the selected system configuration is explained and cooling load profiles of the selected end users obtained from site visits and energy audit are presented with their implications on the solar cooling system design and components selection.

The third chapter presents the detailed designs of the two experimental setups and the main features of the systems components.

The Fourth chapter describes the performance figures used to assess the system's behavior as well as the monitoring system designed to measure system parameters that are required for the performance figures evaluation.

The Fifth chapter describes the results of the experimental activities that established the basis for the performance assessment of the systems and for validation of the simulation models.

The results included the typical daily performance of the system, performance of the main system components and the system electrical consumption. The energetic analysis and the performance figures developed in the previous chapter are used to analyze the system performance data.

The sixth chapter is focused on modeling and simulation activities carried throughout the project, experimental validation of simulation models, and system simulation during design phase.

In the seventh chapter, the validated simulation models were used for further simulation campaign aiming at defining the optimum operating points of the entire system and trace a path towards plant performance improvement.

Conclusions and open issues are presented in chapter eight.

References

Billard, F., and J. Dupont. 2002. “Industry as a partner for sustainable development - Refrigeration” by International Institute of Refrigeration (IIR), Final Report prepared for UNEP - United Nations Environment Programme. Environment. Paris, France. http://www.sustainablecropnutrition.info/ifacontent/download/5895/93832/version/1/file/NOUVEAU+Fertiliser+Report.pdf.

Earthcare Products Limited. 2008. The Use of Natural Refrigerants in Supermarket Systems. In *International Technical Meeting on HCFC phase-out*. Montreal, Canada. http://ec.europa.eu/clima/events/0007/earthcare_natural_refrigerants_supermarkets.pdf.

Hartmann, N., C. Glueck, and F.P. Schmidt. 2010. “Solar cooling for small office buildings: Comparison of solar thermal and photovoltaic options for two different European climates.” *Renewable Energy* (December). doi:10.1016/j.renene.2010.11.006. http://linkinghub.elsevier.com/retrieve/pii/S0960148110005082.

Henning, Hans-Martin. 2007. “Solar assisted air conditioning of buildings - an overview.” *Applied Thermal Engineering* 27 (10) (July): 1734-1749. http://www.sciencedirect.com/science/article/pii/S1359431106002547.

IEA Solar Heating and Cooling. 2002. *Ongoing research relevant for solar assisted air conditioning systems*. http://www.iea-shc.org/task25/publications/Task25-Subtask_C-2-final_report.pdf.

Langniß, Ole, Kristin Seyboth, Luuk Beurskens, André Wakker, Ralph Sims, Frieder Frasch, and Lex Bosselaar. 2007. *Renewables for Heating and Cooling*. http://www.iea.org/textbase/nppdf/free/2007/Renewable_Heating_Cooling_Final_WEB.pdf.

Pär Dalin, Joakim Nilsson, and Anders Rubenhag. 2006. *ECOHEATCOOL Project*. *Final Report*. http://www.pdfdownload.org/pdf2html/view_online.php?url=http://www.euroheat.org/files/filer/ecoheatcool/documents/Ecoheatcool_WP2_Web.pdf.

Tassou, S A, J S Lewis, Y T Ge, A Hadawey, and I Chaer. 2010. “A review of emerging technologies for food refrigeration applications.” *Applied Thermal Engineering* 30 (4) (March): 263-276. http://www.sciencedirect.com/science/article/pii/S1359431109002737.

The U.S. Energy Information Administration (EIA). 2011. How is electricity used in U.S. homes? http://www.eia.gov/tools/faqs/faq.cfm?id=96&t=3.

1. Chapter one: Review of Solar Cooling Systems

Although the absorption refrigeration cycle has an earlier origin (Carre´, 1857) than the vapour compression cycle (Linde, 1875), the refrigeration market has been since its origins dominated by the vapor compression cycles, and especially since 1930 with the introduction of halogenated hydrocarbons as working fluids from the refrigeration machines (Garcia Casals 2006)

The first demonstration of solar-assisted absorption cooling machine was made during the Paris World Exhibition in 1878 by Augustin Mouchot, based on a technique developed by Edmond Carré. This system has consisted of an ammonia/water absorption chiller and a parabolic reflector to produce ice. (Mouchot & Weber 1987). (See Figure 1-1)

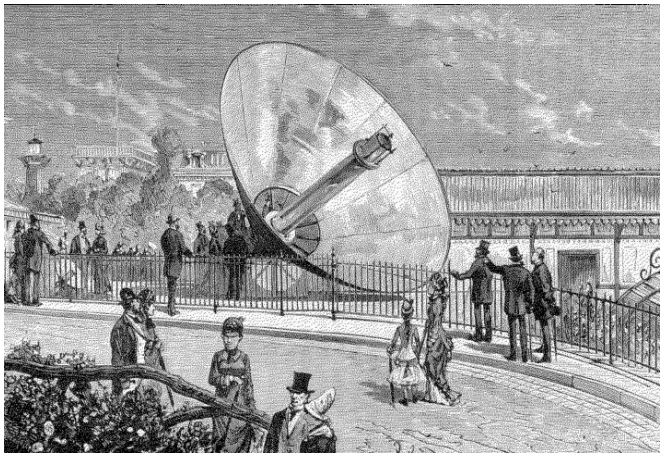

Figure 1-1 World exhibition 1878, Paris: Augustin Mouchot produced the first ice block through solar energy (Mouchot & Weber 1987)

The first commercial solar cooling systems for air-conditioning were developed in Europe and the USA one hundred years later, e.g. by the companies Dornier-Prinz Solartechnik, Germany (Schubert & Dreyer 1977) and Arkla Industries, USA (part of which today is Robur, Italy) (Grossman 2002). These systems have been realized in several demonstration projects.

Following intensive research and development activities in this field in the United States and Japan mainly during the 1980s, there was a slow-down during the 1990s. (Sayigh & McVeigh 1992) However, recently solar cooling has attracted new interest in many countries. And the reasons for this new renaissance are manifold.

1.1.Solar cooling motivations

1. There is an increased consciousness of the environmental problems which are created by the use of fossil fuels for generating electricity consumed by conventional cooling systems.
2. The use of common working fluids (refrigerants), with their ozone-depleting and/or global warming potential, has become a serious environmental problem.
3. The impact of air-conditioning in increasing the peak power demand and contributing to shortages in the electricity supply have caused serious problems in several countries. A growing number of countries experience a switch of peak electricity from winter to summer. This underlines the need to implement advanced, new concepts in building air-conditioning.
4. Solar energy is available almost at the same time when cooling is needed.
5. Comparatively low noise and vibration-free operation of thermally driven chillers.

1.2. Solar cooling systems market status

In 2007, about 70 solar air-conditioning systems driven by the solar energy were reported in operation in Europe, mainly in Germany and Spain. About 59% of systems use absorption chillers. In about 11% of the installations adsorption chiller is installed and in about 23% of the installations a desiccant cooling system using a sorption wheel. Only about 6% of all installation use liquid desiccant technology. (Henning 2007)

A total of only 300 – 400 operating systems worldwide were reported in the "State of the Art on Existing Solar Heating and Cooling Systems" technical report prepared within the International energy agency Task 38- Solar Heating and Cooling programme in 2009; the vast majority of which are in Europe, where the market has increased in the last five years by 50%–100% annually.(Sparber et al. 2009). During the fourth 4th international conference solar air-conditioning Otti, held during October 2011, (Henning 2011b) estimated the number of installed solar cooling system in the world to be about 1000 systems.

It has to be mentioned that the previous three studies as well as most of the review articles ((Lamp & Ziegler 1998), (Li & Sumathy 2000), (Grossman 2002) and (Henning 2007)) are limited to the solar thermal, especially sorption cooling technologies. Even though there are different technologies that are available to deliver refrigeration from solar energy including solar electric, thermo-mechanical, sorption and also some newly emerging technologies. (Kim & Infante Ferreira 2008).

An important aspect that can be concluded from the previous studies is that even though the solar cooling market is small (about 1000 systems), the growth rates are high, and in spite of the effort spent in collecting information about realized systems, no information about many installed systems can be found in the literature. The latter since they are considered as commercial systems and not as a research projects, or prototypes, those need to be documented. This is especially true for the small

installations which usually are for private residential applications. And thus it is believed that the number of installed systems is higher than reported in the previous studies.

1.3. Barriers against solar cooling growth

In spite of the tremendous research effort made in theoretical analysis and experimental projects since the 70s, and the enormous interest related to solar air-conditioning and refrigeration systems, their commercial implementation is still at a very early stage, several are the barriers to its growth and can be summarized as follows:

1. Costs: The main barrier of the market deployment of this technology is the high cost-gap relative to conventional technologies as can be seen in Figure 1-2)
   1.1. Higher initial investment costs compared with conventional cooling systems
   1.2. To date, not cost efficient from a business point of view.
   1.3. Often forgotten in today's financial incentive schemes for solar thermal.

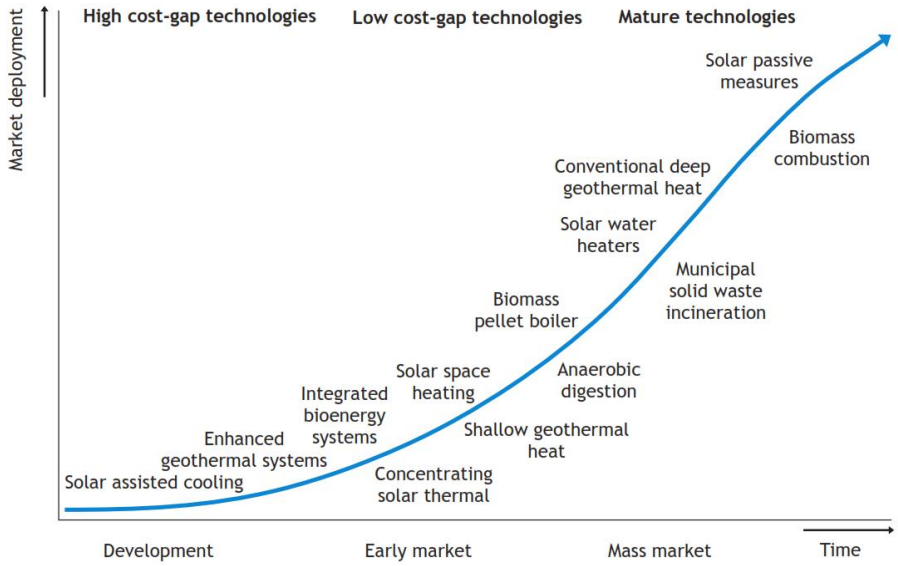

Figure 1-2 Indication of the current state of deployment of Renewable heating and cooling technologies from development to application in the mass market. (Langniß et al. 2007)

2. Technical barriers
   2.1. Hardware
      2.1.1. Lack of units with small capacities
      2.1.2. Lack of package-solutions for residential and small commercial applications
      2.1.3. Only few available medium temperature collectors
      2.1.4. Low thermal efficiency (COP)
      2.1.5. Often: Need for wet cooling tower
   2.2. Software (e.g. planning guidelines, training)
      2.2.1. No skills today among professionals.
      2.2.2. Lack of standardized hydraulic schemes, planning guidelines and simple design tools.

3. Lack of awareness: Lack of awareness of solar cooling will become a key barrier to growth in the near future. (European Thermal Solar Industry Federation 2006), (Henning 2011b) (Langniß et al. 2007)

1.4. Measures and recommendations against growth barriers

In the last few years, substantial R&D efforts were done aiming at pushing the solar cooling to reach the early market stage, both in terms of technical and economical terms.

As a part of the R&D during the last few years, especially in Europe, various new sorption chillers with small- and medium-scale cooling capacity have been developed (up to approximately 35 kWcold). Many of these absorption and adsorption chillers have now passed from prototype and pre-commercial installations into small serial production and consequently a rising number of products are expected to enter the market in the coming years and correspondingly significant reductions in cost can be expected here. (Appleyard 2010) (Henning 2011b).

Moreover, it has to be mentioned that the market of solar medium temperature collectors, required for double and triple effect chillers, is on the move. In just two years, not only the number of the commercial suppliers of tracked process heat collectors increased about five-fold, bur compared to a previous market overview done by (Sun & wind energy magazine in 2009) a remarkable variety of products has developed as well. (Mohart 2011).

While most of the previous solar cooling research was focused on the detailed thermal chiller models, which are mainly used for chiller optimization and design and not for yearly system simulation, several recent studies focused on system level simulation, and coupled models of chillers, solar thermal systems and cooling loads. (Ursula Eicker & Pietruschka 2009).

A recent trend is the development of (solar) cooling kits, that is pre-engineered package solutions that consist of all-important components of a system and where the components are well adjusted to each other. These kits are mainly developed for small capacities up to about 35 kW cooling capacity. Prices excluding installation cost and distribution system to the building for the package solutions dropped from about 6000€ per kW in 2007 to about 4500 € per kW in 2009 and are expected to reduce further to about 3000€ per kW in 2012. (Jakob & Kohlenbach 2010) (Henning 2011a)

Recently, a number of countries are considering special stimulation programs for a larger market deployment of Solar Air-Conditioning and Refrigeration (SAC) technologies. One of the most encouraging programmes has been implemented in France; SAC installations here will be supported by substantial investment funds in order to overcome the existing cost barriers if they prove high quality performance and a high level of reliability. However, in most countries incentive programs provide support schemes for solar thermal systems in general and do not put a particular focus on SAC. (Henning 2011a)

1.5. General solar cooling technology overview

The solar cooling system is generally comprised of three sub-systems: the solar energy conversion system, refrigeration system, and the cooling load. The appropriate cycle in each application depends on cooling demand, power, and the temperature levels of the refrigerated object, as well as the environment. A number of possible "paths" from solar energy to "cooling services" are shown in Figure 1-3. (Henning 2007) (Pridasawas 2006)

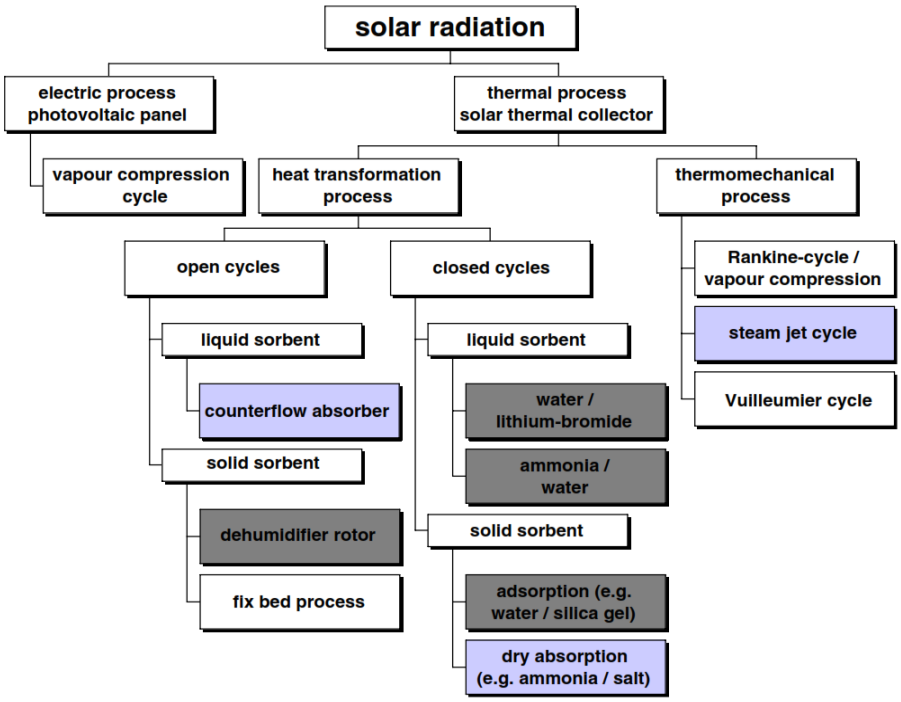

Figure 1-3 Overview on physical ways to convert solar radiation into cooling or air-conditioning. Processes marked in dark grey: market available technologies which are used for solar assisted air-conditioning. Processes marked in light grey: technologies in status of pilot projects or system testing. (Henning 2007)

Solar energy can be converted into cooling using two main principles:

1. Electricity generated with photovoltaic modules can be converted into cooling using well-known refrigeration technologies that are mainly based on vapor compression cycles.

2. Heat generated with solar thermal collectors can be converted into cooling using thermally driven refrigeration or air-conditioning technologies. Most of these systems employ the physical phenomena of sorption in either an open or closed thermodynamic cycle. Other technologies, such as steam jet cycles or other cycles using a conversion of heat to mechanical energy and of mechanical energy to cooling are less significant.

Today, the first principle – solar electricity driven cooling – is mainly used for solar driven refrigerators for cooling medicine in remote, sunny regions, while the second principle – solar thermally driven

cooling – is mainly applied for comfort cooling and air-conditioning in buildings and first pilot installations have been realized for large capacity refrigeration applications. The first principle installed in buildings is normally not considered a “solar cooling system” today since most photovoltaic plants are connected to the electric grid and are operated completely independent from the HVAC installations used in buildings or the refrigeration machines used in industrial applications.

Nevertheless, this research project aimed at developing a solar thermal cooling system, and thus the focus of this review is on the dominating technology using the second principle – heat driven air-conditioning and refrigeration systems using solar thermal energy as the main driving energy.

For solar thermal collectors, different collector types produce heat at different temperature levels. This indicates that the temperature level can be matched to various cycle demands. For example, the Rankine cycle requires a rather high driving temperature whereas the desiccant cycle manages at a lower temperature level of heat supply.

The same type of temperature matching is important for the cold side of the solar cooling path, i.e in the cold object. Since several cycles typically operates with water as a working fluid, it is impossible to achieve temperatures below 0°C for some cycles. The solar thermal-driven air conditioning cycles can be based on absorption cycles, adsorption cycles, duplex Rankine, desiccant cooling cycles, or ejector refrigeration cycles.

Regarding the main component of the solar cooling system, the thermally driven chillers, Table **1-1** classifies the market available thermally driven sorption systems based on several aspects; the system cools water in a closed thermodynamic cycle (absorption and adsorption) or directly treats the air in an open thermodynamic cycle (desiccant system), the physical phase of the sorption material, the absorbent and the refrigerant materials and the type of the cycle.

An absorbent and a refrigerant in an absorption cycle form a working pair. The most common working pairs in absorption refrigeration are lithium bromide-water and water-ammonia. The lithium bromide-water pair is widely used for air cooling applications, with evaporation temperatures about 5-10 ^{o}C; while the water-ammonia pair is mostly used when evaporation temperatures are below 0^{o}C for some small size air conditioning and large industrial applications.

1.6. Review of solar cooling technology suitable for the requirements of this project

Under operating conditions of the solar cooling plants planned in this project i.e. (high ambient temperature in which wet cooling tower cannot be employed and low temperatures required on the cold side below zero degree), It can be seen in Table 1-1 that the single effect ammonia/water absorption chiller driven by temperatures of (120 -180^{o} C) provided by concentrating temperature

collectors is the only market available thermally driven cooling system. It uses Ammonia as a refrigerant, and thus can produce temperatures below 0°C for refrigeration purpose. The thermodynamic reasoning behind this will be described in details in the concept development chapter.

Further investigations of ammonia/water single effect chillers is carried out here both for the market available products and prototypes which is under development.

A review of medium temperature concentrating collectors was done based on technical and economical terms in the concept development chapter. And a review of the solar cooling systems utilizing concentrating collectors is presented in this chapter with respect to the reasons behind their utilization and the applications at which they are used and the prospective.

Table 1-1 Overview on market available thermally driven cooling systems based on sorption technology. (Henning 2011b)

Type of system	**Water chillers (closed thermodynamic cycles)**						**Direct air treatment (open thermodynamic cycles**	
Physical phase of sorption material	Liquid			Solid			Liquid	Solid
Sorption material	Water	Lithium-bromide		Zeolite	Silica gel	Lithium-chloride	Lithium-chloride	Silica gel (or zeolite), cellulose matrix with lithium-chloride
Refrigerant	Ammonia	Water		Water	Water	Water	Water	Water
Type of cycle[1]	1-effect	1-effect	2-effect	1-effect	1-effect	1-effect	Cooled sorption process	Desiccant rotor
$EER_{thermal}$ range	0.5-0.75	0.65-0.8	1.1-1.4	0.5-0.75	0.5-0.75	0.5-0.75	0.7-1.1	0.6-0.8
Driving temperature range, °C	70 … 100 120 …180[2]	70 … 100	140 … 180	65 … 90	65 … 90	65 … 90	60 … 85	60 … 80
Solar collector technology[3]	FPC, ETC SAT[2]	FPC, ETC	SAT	FPC, ETC	FPC, ETC	FPC, ETC	FPC, ETC, SAHC	FPC, ETC, SAHC

Comments:

1 1-effect: single-effect thermodynamic cycle (no internal heat cascade); 2-effect: double-effect thermodynamic cycle (with internal heat cascade)
2 Valid for production of cold at temperatures significantly below the freezing point of water, i.e. < 0°C
3 Abbreviations for solar thermal collector types: FPC = flat plate collector; ETC = evacuated tube collector; SAT = single-axis tracking solar collector (e.g. parabolic trough collectors or Fresnel type collectors); SAHC = solar air heating collector

1.6.1. Review of single effect ammonia/water absorption chillers

1.6.1.1. Market available products

A 12 kW ammonia/water (NH3/H2O) absorption chiller has been available since the end of the year 2006. The chiller uses a newly developed membrane pump and is a product of the Austrian company Pink, distributed by SolarNext from Germany. The driving temperatures are in the range of 65 to 95°C. The COPs range between 0.6 and 0.65 depending on the design and heat rejection conditions. Other ammonia/water chillers have been available since 2008 from the German company AGO, with 50 to 500 kW capacities and from Solarice, Germany, with 25 and 40 kW capacities. (Jakob & Kohlenbach 2010).

1.6.1.2. Prototype developments

A directly air-cooled ammonia/water absorption chiller manufactured by the Italian company Robur has a 17 kW cooling capacity. This machine can be indirectly fired (prototype) and this version is a modified version of Robur's standard gas-fired product. This chiller requires heat at 180 to 200°C. (Henning et al. 2006)

The National Institute of Engineering, Technology and Innovation (INETI) of the University of Lisbon has developed together with the Portuguese company AoSol an air-cooled ammonia/water chiller prototype with a 6 kW cooling capacity for the Southern European market.(Jakob & Kohlenbach 2010)

The Graz University of Technology, Austria, has developed a prototype of an ammonia/water absorption heat pump/chiller with a 5 kW cooling capacity for the Austrian company Heliotherm/Helioplus.(Moser & Rieberer 2007)

At the ITW Stuttgart in Germany, another ammonia/water absorption chiller prototype with a 10 kW cooling capacity is being developed (Zetzsche et al. 2009). The pressure lift of the solution to the required high pressure level is achieved by a membrane pump. At driving temperatures of 100°C and heat rejection temperatures of 27 to 32°C, cold water temperatures of 14°C can be achieved with a cooling capacity of 10 kW and a COP of 0.72.

The German company Makatec has developed a 6 kW NH3/H2O absorption chiller using a membrane absorber.

Different diffusion absorption chiller prototypes with the working pair ammonia/water and helium as auxiliary gas are being developed at the zafh.net of the Stuttgart University of Applied Sciences, Germany.(Jakob U et al. 2008) The chiller has no mechanical solution pump, but does have an indirectly driven bubble pump. The latest cooling capacity reached with the third prototype is 3 kW.

1.6.2. Review of solar cooling systems utilizing concentrating collectors

The main reasons for employing concentrating collectors in solar cooling systems:

a) Increasing the primary energy savings is crucial for the justification of a solar thermal cooling concept. However, the primary energy savings that could be achieved with single stage absorption chillers (generally having a COP_{th} value around 0.6) is quite small. Thus, double and triple effect absorption chillers with higher COP_{th} (1-1.4-2) are required for higher primary energy savings. However, double and triple effect chillers require high driving temperatures, which can be achieved by concentrating collectors working at these temperatures with reasonable efficiency.

b) High potential for refrigeration at temperatures below 0°C exist specially for industrial applications. However this requires Ammonia/ Water absorption chillers which require high temperature input for the generator in the range of (120-180°C) which can only be satisfied by concentrating solar collectors.

c) Several industrial applications require both cooling and steam for processes, and concentrating solar collectors can be very advantageous in the sense it maximize the use of solar thermal collectors.

d) In many cases, available area for the collector's installation makes the utilization of single effect chillers with large flat plate or evacuated tube collectors not feasible. And this can be solved using double or triple effect absorption chiller with a concentrating collector.

Air-conditioning and refrigeration facilities driven by concentrating solar collectors are still infrequent. However, several test facilities using this technology have appeared in the literature during the last 50 years. The configurations of the reviewed installed solar cooling systems utilizing concentrating solar collectors fall into one of the categories shown in Figure 1-4.

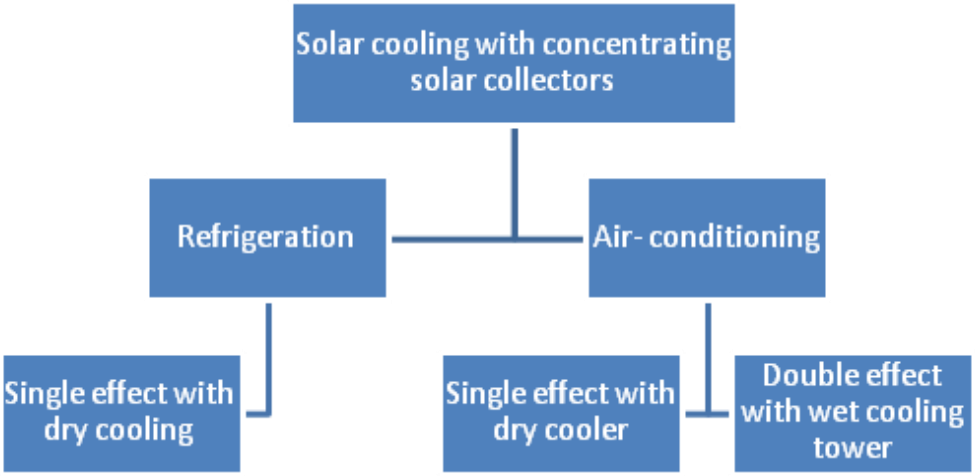

Figure 1-4 Categories of high temperature solar cooling systems utilizing concentrating solar collectors.

In 1956, two small solar cooling systems with concentrating collectors were reported in Montlouis in France and in Flordia in US consisting of parabolic trough collectors coupled to prototype single stage water-ammonia absorption chillers (Trombe & Foex 1957) (Farber et al. 1966). A similar system configuration was reported few years later in Bangladesh in 1964 by the East Pakistan University of Engineering (DESA 1964).

In 1979 a solar heating and cooling plant was reported in U.S. Army Yuma Proving Ground with a 1191 m^2 powered by parabolic trough collector (PTC) from solar kinetics company. (Fernández-García et al. 2010)

A solar cooling and heating system was installed in Sulaibiya in Kuwait in 1984 utilizing a prototoype PTC collectors and the single effect H_2O/LiBr absorption chiller Arkla Solaire 501. (Osman 1985)

The Indian Institute of technology tested a small 0.25 k W chiller from Himalux, coupled to a 1.5 m^2 prototype PTC collector in 1989. (Raheman & Gupta 1989)

The University of Jordan tested a prototype absorption chiller for air-conditioning by coupling the chiller to a prototype flat plate collector with a PTC collector in 1991.And later (Hammad & Audi 1992) in 2000 tested a prototype PTC with an absorption chiller for refrigeration purpose in the desert areas. (Hammad & Habali 2000)

Another study in 2000 was done by the Polytechnic University of Madrid on a prototype PTC collector using thermal oil as a heat transfer fluid coupled to a single effect ammonia/water absorption chiller. (De Francisco et al. 2002)

(Gee 2004) reported the first system of double effect absorption chiller coupled with PTC from Power Roof™ for air-conditioning application in North Carolina in USA in 2002.

A solar cooling and heating system was installed in San Antonio (Texas) in USA in 2003 using 420 m^2 of PTC collectors (The National Renewable Energy Laboratory. DOE/GO-102004-1914 2004).

From the year 2004 onward, a high growth rate was noticed, several concentrating collectors start to be commercially available, and most of the reported solar cooling systems after this date utilized one of the commercialized collectors rather than developing a prototype one.

The main concentrating collectors coupled to solar cooling systems were produced by: SOLITEM GmbH based in Aachen, Germany with branches in Turkey, (PSE/Mirroxx/Industrial Solar GmbH based in Freiburg, Germay), NEP SOLAR Pty Ltd based in Australia and (Industrial Solar Technology Corporation/Abengoa Solar S.A. based in Spain).

A review list for systems installed after 2004 are presented in Table 1-2. Information about these systems was obtained from scientific papers, specialized publications, the web and direct contact with manufacturers.

The outcomes of this review clearly present the small, but steadily growing market of solar cooling systems coupled with concentrating collectors (see Figure 1-5).

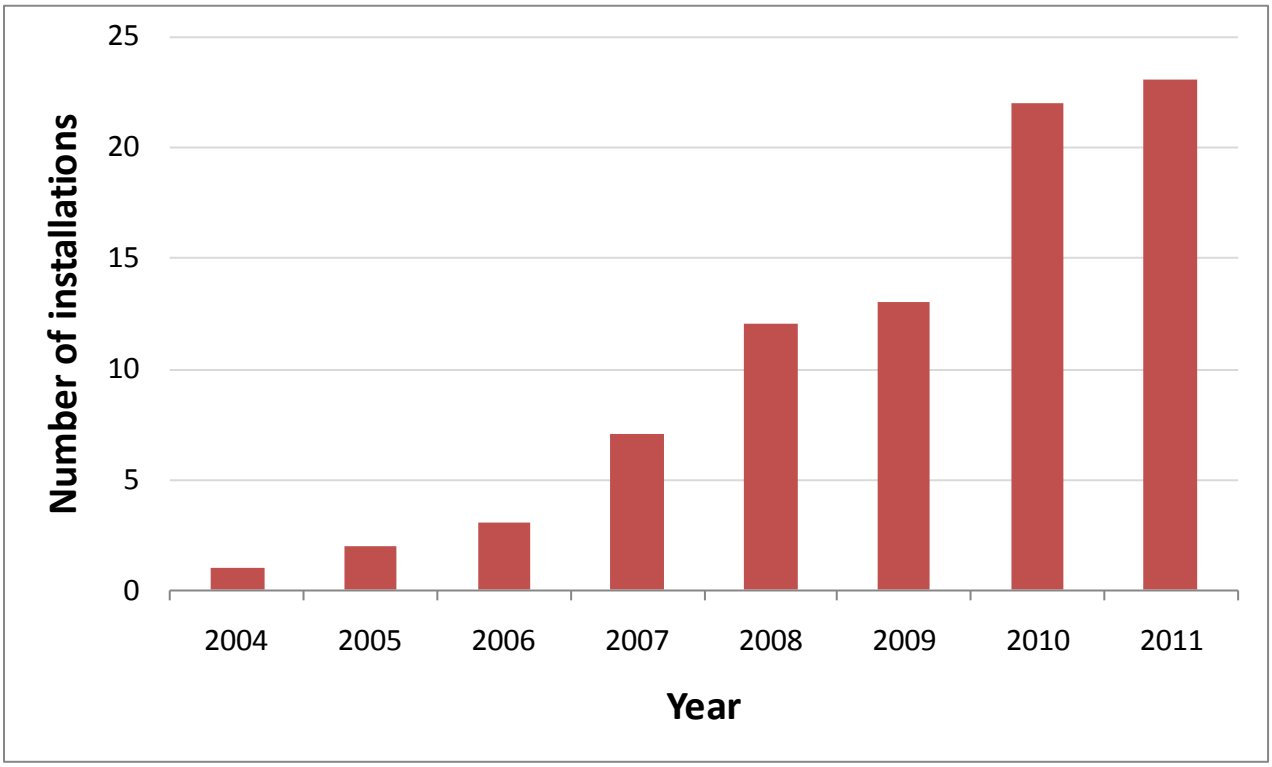

Figure 1-5 The number of installed solar cooling systems utilizing concentrating collectors.

Table 1-2 Review of solar cooling systems utilizing concentrating collector (2004-present).

Collector producer	*Location*	*Company or institution/ Application*	*year*	*Application*	*Aperture Area*	*Fluid*	*Chillertype/model/ fluid pairs/power (kW)*
Solitem							
1	Turkey / Dalman	Iberotel Sarigerme Park	2004	SC, Steam	360	pressur. water	DE/Broad/LiBr-H2O/140
2	Turkey / Alanya	Grand Kaptan	2005	SC	360	pressur. water	DE/Broad/LiBr-H2O/150
3	Turkey / Gebz	Gebz High technology Institute	2008	SC, DHW	324	pressur. water	DE/Broad/LiBr-H2O/a
4	Turkey / Antalya	Metro	2008	SHC	432	pressur. water	DE/Broad/LiBr-H2O/300
5	Jordan/ Dead sea	Dead Sea hotel	2010	SC	126	pressur. water	SE/Robur/NH3-H2O/13
6	Turkey / Tarsus	FritolayPepsico	2008	SC, steam	1440	pressur. water	a/a/a/420
7	Morocco / Casablanca	Moulay Youssef Hospital	2010	SHC	108	Thermal oil	SE/Robur/NH3-H2O/13
9	Firenze / Italy	Misericordia	2010	SHC	108	Saturated steam	SE/Robur/NH3-H2O/17
10	North republic of Cyprus	METU campus	2010	SHCP	756	pressur. water	SE/Thermax/LiBr-H2O/130
PSE							
11	Bergamo /Italy	Robur	2006	SC	132	pressur. water	SE/Robur/NH3-H2O/2*13
12	Seville /Spain	Seville University	2007	SHC	354	pressur. water	DE/Broad/LiBr-H2O/175
13	Grombalia/Tunisia	Politecnico di Milano	2008	SC	88	pressur. water	SE/Robur/NH3-H2O/13
14	Abu Dhabi/UAE	Masdar	2010	SC	132 +334 PTC	pressur. water	DE/Broad/LiBr-H2O/ 175

15	Qatar/ Doha	Showcase football stadium	2010	SC	1408	pressur. water	DE/Thermax/LiBr-H2O/750
16	Freiburg/ Germany	PSE/ Fraunhofer ISE	2011	SC	132	pressur. Water or steam	SE/Robur/NH3-H2O/2*13
NEP							
17	Brisbane, QLD/Australia	Ipswich Hospital	2007	SC	570	pressur. water	DE/Broad/LiBr-H2O/ 290
18	Padstow, NSW/ Australia,	SERDF Demo. Project	2008	SC	165	pressur. water	DE/Broad/LiBr-H2O/ 175
19	Newcastle/ Australia	Cinema Complex	2010	SC	354	pressur. water	DE/a/LiBr-H2O/230
21	Araluen, NT/ Australia	Art gallery	2010	SC	450	n/a	n/a /n/a /n/a /230
20	Newcastle/ Australia	(CSIRO)	2007	SC	50	pressur. water	SE/ chillii®/LiBr-H2O/18
IST/ Abengoa Solar							
22	Long Island/NY/USA	Piano factory	2009	SC	533	pressur. water	DE/Broad/LiBr-H2O/315
23	Marrakech/ Morocco	Politecnico di Milano	2010	SC	78	Thermal oil	SE/Robur/NH3-H2O/13
Broad							
24	Pittsburgh/ USA	Carnegie Mellon University	2007	SHC	52	pressur. water	DE/Broad/LiBr-H2O/16

Application		**Chiller**	
SHC	solar heating and cooling	SE	single effect
DHW	domestic hot water	DE	double effect
SC	solar cooling		
n/a	Not available information		

1.7. References

Appleyard, D., 2010. Chilling Out in the Sun: Solar Cooling. Available at: http://www.renewableenergyworld.com/rea/news/article/2010/06/chilling-out-in-the-sun-solar-cooling [Accessed July 2, 2011].

DESA, V., 1964. Experiments with solar-energy utilization at Dacca. *Solar Energy*, 8(3), pp.83-90. Available at: http://dx.doi.org/10.1016/0038-092X(64)90082-9 [Accessed May 2, 2011].

Eicker, Ursula & Pietruschka, D., 2009. Design and performance of solar powered absorption cooling systems in office buildings. *Energy Build*, 41, pp.81-91.

European Thermal Solar Industry Federation, 2006. *Solar Assisted Cooling – State of the Art –*, Available at: http://www.estif.org/fileadmin/estif/content/policies/downloads/D23-solar-assisted-cooling.pdf.

Farber, E. et al., 1966. Operation and performance of the University of Florida solar air-conditioning system☆. *Solar Energy*, 10(2), pp.91-95. Available at: http://dx.doi.org/10.1016/0038-092X(66)90043-0 [Accessed April 28, 2011].

Fernández-García, A. et al., 2010. Parabolic-trough solar collectors and their applications. *Renewable and Sustainable Energy Reviews*, 14(7), pp.1695-1721. Available at: http://dx.doi.org/10.1016/j.rser.2010.03.012 [Accessed September 5, 2010].

De Francisco, A. et al., 2002. Development and testing of a prototype of low-power water–ammonia absorption equipment for solar energy applications. *Renewable Energy*, 25(4), pp.537-544. Available at: http://dx.doi.org/10.1016/S0960-1481(01)00093-3 [Accessed May 2, 2011].

Garcia Casals, X., 2006. Solar absorption cooling in Spain: Perspectives and outcomes from the simulation of recent installations. *Renewable Energy*, 31(9), pp.1371-1389. Available at: http://www.sciencedirect.com/science/article/pii/S0960148105001783.

Gee, R.C., 2004. *Solar powering of high efficiency absorption chiller*, Available at: http://www.osti.gov/bridge/product.biblio.jsp?query_id=0&page=0&osti_id=840264&Row=0 [Accessed May 2, 2011].

Grossman, G., 2002. Solar-powered systems for cooling, dehumidification and air-conditioning. *Solar Energy*, 72(1), pp.53-62. Available at: http://www.sciencedirect.com/science/article/pii/S0038092X01000901.

Hammad, M. & Audi, M., 1992. Performance of a solar LiBr-water absorption refrigeration system. *Renewable Energy*, 2(3), pp.275-282. Available at: http://dx.doi.org/10.1016/0960-1481(92)90039-6 [Accessed April 28, 2011].

Hammad, M. & Habali, S., 2000. Design and performance study of a solar energy powered vaccine cabinet. *Applied Thermal Engineering*, 20(18), pp.1785-1798. Available at: http://dx.doi.org/10.1016/S1359-4311(99)00099-X [Accessed April 28, 2011].

Henning, H.-M., 2011a. *Solar Air -Conditioning and Refr iger ation Solar Cooling Position Paper*,

Henning, H.-M., 2007. Solar assisted air conditioning of buildings - an overview. *Applied Thermal Engineering*, 27(10), pp.1734-1749. Available at: http://www.sciencedirect.com/science/article/pii/S1359431106002547.

Henning, H.-M., 2011b. Status and Perspectives of Solar Air-Conditioning and Refrigeration. In *4th INTERNATIONAL CONFERENCE SOLAR AIR-CONDITIONING 2011*. Larnaca, Cyprus, pp. 18-33.

Henning, H.-M. et al., 2006. Solar Cooling and Refrigeration with High Temperature Lifts - Thermodynamic Background and Technical Solution. In *National Congess of the Italian Thermotechnical Association (ATI) of Solar Heating and Cooling*. Perugia, pp. 105-110.

Jakob U et al., 2008. Simulation and experimental investigation diffusion absorption cooling machines for air-conditioning applications. *Applied Thermal Engineering*, 28(10), pp.1138-1150.

Jakob, U. & Kohlenbach, P., 2010. Recent Developments of Sorption Chillers in Europe. In *9th IIR-Gustav Lorentzen Conference on Natural Refrigerants*. Sydney, Australia.

Kim, D.S. & Infante Ferreira, C.A., 2008. Solar refrigeration options – a state-of-the-art review. *International Journal of Refrigeration*, 31(1), pp.3-15. Available at: http://linkinghub.elsevier.com/retrieve/pii/S0140700707001478 [Accessed April 3, 2011].

Lamp, P. & Ziegler, F., 1998. European research on solar-assisted air conditioning. *International Journal of Refrigeration*, 21(2), pp.89-99. Available at: http://www.sciencedirect.com/science/article/pii/S0140700798000085.

Langniß, O. et al., 2007. *Renewables for Heating and Cooling*, Available at: http://www.iea.org/textbase/nppdf/free/2007/Renewable_Heating_Cooling_Final_WEB.pdf [Accessed June 7, 2011].

Li, Z.F. & Sumathy, K., 2000. Technology development in the solar absorption air-conditioning systems. *Renewable and Sustainable Energy Reviews*, 4(3), pp.267-293. Available at: http://www.sciencedirect.com/science/article/pii/S1364032199000167.

Mohart, A., 2011. Solar process heat is becoming sexy. *Sund & wind energy*, pp.70-77.

Moser, H. & Rieberer, R., 2007. SMALL-CAPACITY AMMONIA / WATER ABSORPTION HEAT PUMP FOR HEATING AND COOLING - USED FOR SOLAR COOLING APPLICATIONS. In *2nd International Conference Solar Air-Conditioning*. Tarragona, Spain.

Mouchot, A.; & Weber, R., 1987. *Die Sonnenwaŕme und ihre industriellen Anwendungen*, Oberbözberg, Schweiz : Olynthus,.

Osman, M., 1985. Performance analysis and loadmatching for tracking cylindrical parabolic collectors for solar cooling in arid zones. *Energy Conversion and Management*, 25(3), pp.295-302. Available at: http://dx.doi.org/10.1016/0196-8904(85)90046-9 [Accessed April 28, 2011].

Pridasawas, W., 2006. *Solar-driven refrigeration systems with focus on the ejector cycle*. Royal Institute of Technology, KTH. Available at: http://www.dissertations.se/dissertation/529c43abcd/ [Accessed July 9, 2011].

Raheman, H. & Gupta, C.R., 1989. Development of a Solar-Energy-Operated Vapour-Absorption-Type Refrigerator. *Applied Energy*, 34, pp.89-98.

Sayigh, A.A.M. & McVeigh, J.C., 1992. *Solar Air Conditioning and Refrigeration*, Pergamon Press, Oxford/UK.

Schubert, K.. & Dreyer, J., 1977. Cooling with solar energy. *Dornier-Post*, 1, pp.9-11.

Sparber, W. et al., 2009. *State of the art on existing solar heating and cooling systems*, Available at: http://www.iea-shc.org/publications/downloads/Report_B1_final.pdf [Accessed June 7, 2011].

The National Renewable Energy Laboratory. DOE/GO-102004-1914, 2004. *Heating Water with Solar Energy Costs Less at the Phoenix Federal Correctional Institution*,

Trombe, F. & Foex, M., 1957. The production of cold by means of solar radiation. *Solar Energy*, 1(1), pp.51-52. Available at: http://dx.doi.org/10.1016/0038-092X(57)90055-5 [Accessed April 28, 2011].

Zetzsche, M. et al., 2009. SOLAR COOLING WITH AN ICE-STORAGE BACK-UP SYSTEM. In *3rd International Conference Solar Air-Conditioning*. Palermo, Italy.

2. Chapter Two: Concept Development

The aim of this research project is to develop an innovative solar thermally driven cooling concept, to be used for refrigeration in the agro-food industry in the south Mediterranean countries.

The peculiarity of the system is the high temperature difference between the chilled refrigerant temperature, about –5°C and the condenser temperature (ambient temperature, which could exceed 40°C) in which hardly a wet cooling tower can be employed, due to high wet bulb temperatures or no availability of water.

The thermodynamic analysis behind the definition of the system configuration is presented in the first section of this chapter.

The main components of the solar cooling system are explained (the solar collectors, the absorption chiller and the cold and hot storages). A main attention is paid at the procedure of selection of a specific technological solution among several options; this is especially true for the selection of the solar collectors and the cold and hot storages.

During the project in order to implement the developed concept, two agro-food industrial sites have been selected; the first is a beverage factory in Tunisia, and the second is a Dairy factory in Morocco.

Within the selected industrial sites, several production processes required cooling. In order to select the most suitable cooling process to be supplied by the solar cooling systems, selection criteria have been defined. And the hourly cooling load profiles have been analyzed in order to develop the solar cooling system design that can best fit this cooling load profile.

2.1.Thermodynamic analysis

The general solar cooling system scheme is presented in Figure 2-1, the heat supplied by the solar collectors Q_{Heat} at temperature T_H drives the generator of the sorption chiller, which absorbs the heat from the cooling load Q_{Cold} at a temperature of T_C and rejects that heat Q_M to the ambient at temperature T_M.

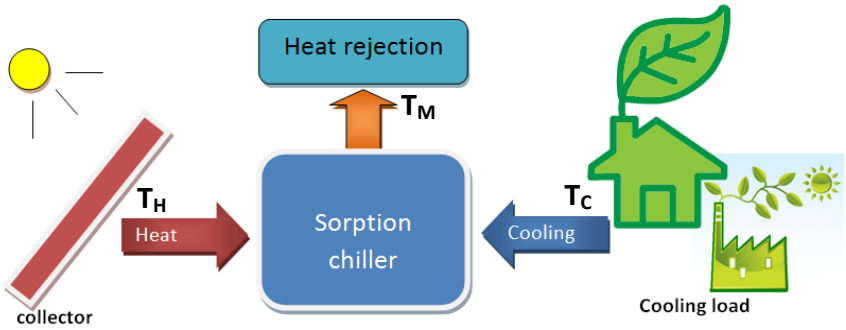

Figure 2-1 General scheme of solar cooling system.

A basic figure to describe the quality of the conversion of heat into cold is the thermal Coefficient of Performance, COP, defined as the useful cold, Q_{cold}, per unit of invested driving heat, Q_{heat}:

$$COP = \frac{Q_{cold}}{Q_{heat}} \qquad \text{Equation 1}$$

A detailed thermodynamic analysis for closed cycle's solar cooling systems was done by (Henning et al. 2006) .

The first and second law of thermodynamics applied to the basic process of a thermally driven chiller according to a scheme shown in Figure 1, lead to an expression for the maximum possible Coefficient of Performance, COP_{ideal}, in which the COP is only dependent of the three temperature levels:

$$COP_{ideal} = \frac{T_C}{T_H} \cdot \frac{T_H - T_M}{T_M - T_C} \qquad \text{Equation 2}$$

The COP calculated according to equation (2) gives the upper thermodynamic limit which can never be achieved in practice. The fraction between real COP and maximum, ideal COP at the same conditions is called Carnot Efficiency Factor:

$$\xi_{Carnot} = \frac{COP_{real}}{COP_{ideal}} \qquad \text{Equation 3}$$

This factor lies in the range of 0.3 to 0.4 for common market available systems. The ξ_{Carnot} can be increased by any measure which reduces the impact o thermodynamic irreversibility, such as improved heat recovery in the internal cycle, optimized heat exchanger etc..

The difference between the heat rejection temperature T_M and the temperature of the low temperature heat source, T_C is called the required temperature lift ΔT:

$$\Delta T = T_M - T_C \qquad \text{Equation 4}$$

In Figure 2-2 the required temperature of the heat source – the solar collector in case of solar cooling – is plotted as function of the required temperature lift; the curves are based on the COP of an ideal thermally driven chiller according to equation (2), multiplied with the Carnot Efficiency Factor ξ_{Carnot}.

Although this characteristic of an ideal cycle is not completely identical to that of real systems it can be well used to demonstrate the influence of the temperature lift on the required driving temperature and thus with the selection of the appropriate solar collector technology at different load conditions. Four different lines are shown which refer to different COP-values, namely 0.7 and 1.1, and different Carnot Efficiency Factors, namely 0.3 and 0.4. Typical operation temperature ranges of different solar collector technologies are marked by colored areas. The ellipses indicate different system designs.

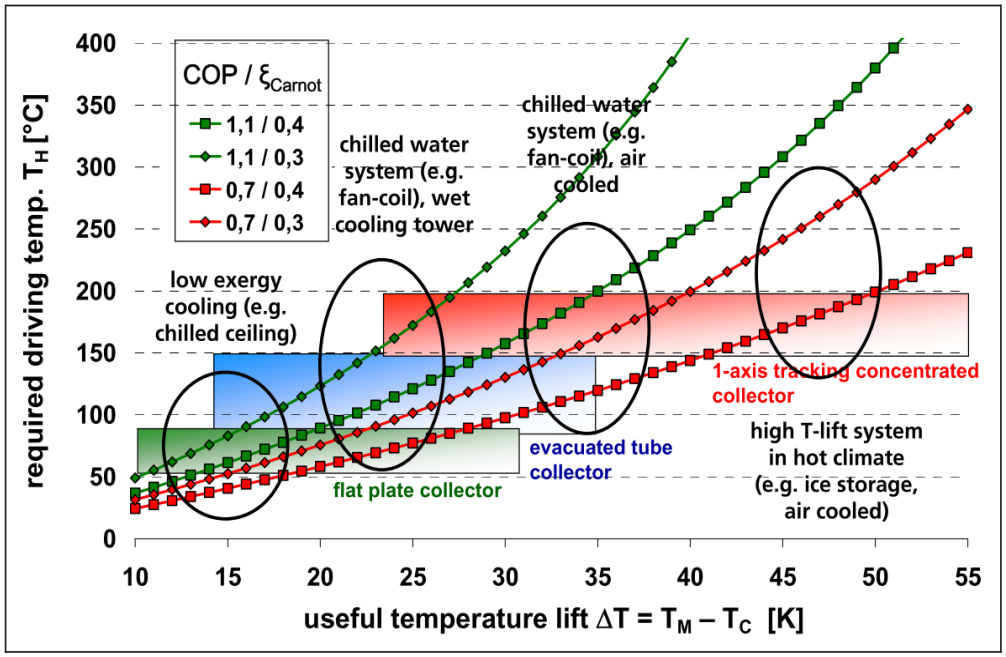

Figure 2-2 Required heat source temperature TH as function of the required temperature lift ΔT between required temperature of cold production (low temperature heat source) and temperature for heat rejection. Curves refer to different COP/ξCarnot combinations. Typical operation temperature ranges of different solar collector technologies are marked by colored areas. The ellipses indicate different system designs.

A first important step in the design process of solar cooling systems is to define the required temperature lift. Different systems and applications can be compared and some important examples are described below:

In case of a low exergy cooling system, i.e., a system which can be operated with a low temperature difference between room temperature and temperature of the cold water such as a chilled ceiling, a low temperature lift in the range of 15 K will be sufficient, at least in moderate climates. Such system can be operated using flat plate collectors.

A common fan-coil system, in which dehumidification is realized by cooling the air below the dew point needs chiller water in the range of 6-8 K. With a temperature for heat rejection in the range of 35 ^{o}C a temperature lift of about 25 -30 K is necessary. For this example a medium temperature lift system very high efficient flat plate collectors or evacuated tube collectors are necessary in case of single effect chillers.

For double effect chillers, possibly high efficiency evacuated tube collectors can be employed, but in most cases collector systems with optical concentration which are tracking the sun will be necessary.

Under conditions of high ambient temperature (e.g. Higher than 35 ^{o}C) in which cooling tower cannot be employed (e.g. due to high wet bulb temperature or scarcity of water) a high temperature lift will be necessary, This is even more valid if a low temperature on the cold side is needed, e.g. in case of ice production or using and ice storage to overcome mismatches between cooling load and solar gain. Under those conditions only a single-effect chiller can be used if driving temperatures up to approximately 200 ^{o}C are available. A collector system with an optical concentration will be necessary in such case. These conditions correspond very much to the needs in hot, arid regions in which fresh water is costly or a scarce commodity.

2.2.System concept development

Based on the aforementioned thermodynamic analysis the system concept consists of an air cooled single-effect ammonia-water absorption chiller driven by heat produced by a medium temperature concentrating collector that could be a Linear Fresnel Reflector (LFR) collector or a Parabolic Trough Collector (PTC) as presented in Figure 2-3.

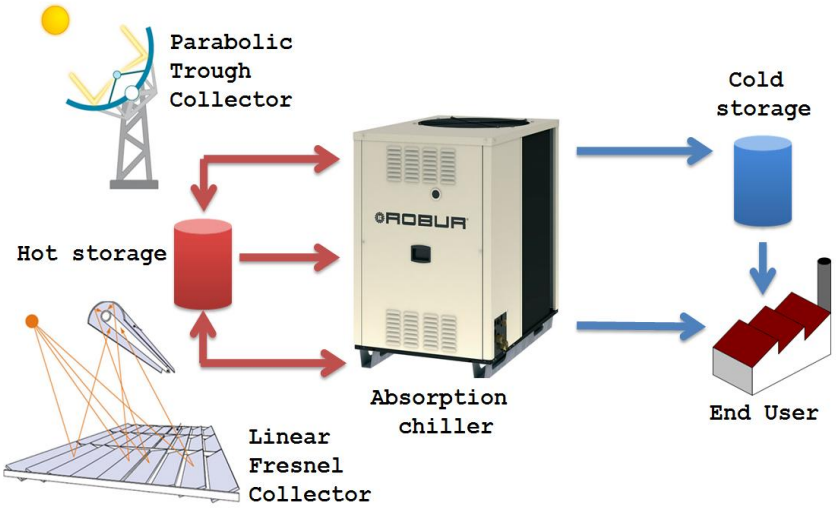

Figure 2-3 General scheme of a solar cooling system.

In addition to the main system components i.e. the collector and the chiller, a hot and/or cold storage might be required to match the cooling production in the chiller during the sunny hours of the day with the cooling required by the end user. The general scheme of a solar cooling system presented the LFR and the PTC collectors as the different approaches to integrate a hot and cold storages to the system is presented in Figure 2-3.

In the next paragraphs, the main components used in the system are presented. Further, the system configuration is discussed based on its ability to match the end user's cooling load demand.

2.3.System components

2.3.1. Absorption Chiller used in the project:

Based on the review of the market ready and prototypes under development, the only tested available air-cooled ammonia/water single effect chiller that can produce refrigeration effect while working at higher than 40 ^{o}C ambient temperatures with a cooling potential above 10 kW is the chiller developed by the Italian company Robur. (Aprile and Motta 2007)

The absorption chiller is a derivation of Robur model ACF RTCF-LB, which is a single stage - gas fired - air cooled – ammonia/water absorption chiller for low temperature brine generation. The chiller was adapted to cope with solar heat by replacing the gas burner placed at the bottom side of the generator with a heat exchanger. The gas fired version of this chiller was experimentally tested by Horuz and Callander (Horuz and Callander 2004). And later, it was analyzed using Aspen Plus flowsheet simulator in the study of Darwish et al.(Darwish, Al-Hashimi, and Al-Mansoori 2008).

2.3.2. Chiller working principle

The solar operated absorption chiller schematic shown in Figure 2-4 presents the operation of the chiller with the main components numbered from 1 to 9;

The ammonia-water mixture in the pool type generator (1) is heated by the solar energy delivered from the solar loop heat transfer fluid (pressurized water, thermal oil or steam) to the jacket type heat exchanger (9) surrounding the generator. The vapor of refrigerant (ammonia) evolves from the generator, since absorbent (water) is volatile, a rectifier (2) is needed in order to condensate the water vapor in excess and transfer it back to the generator by gravity.

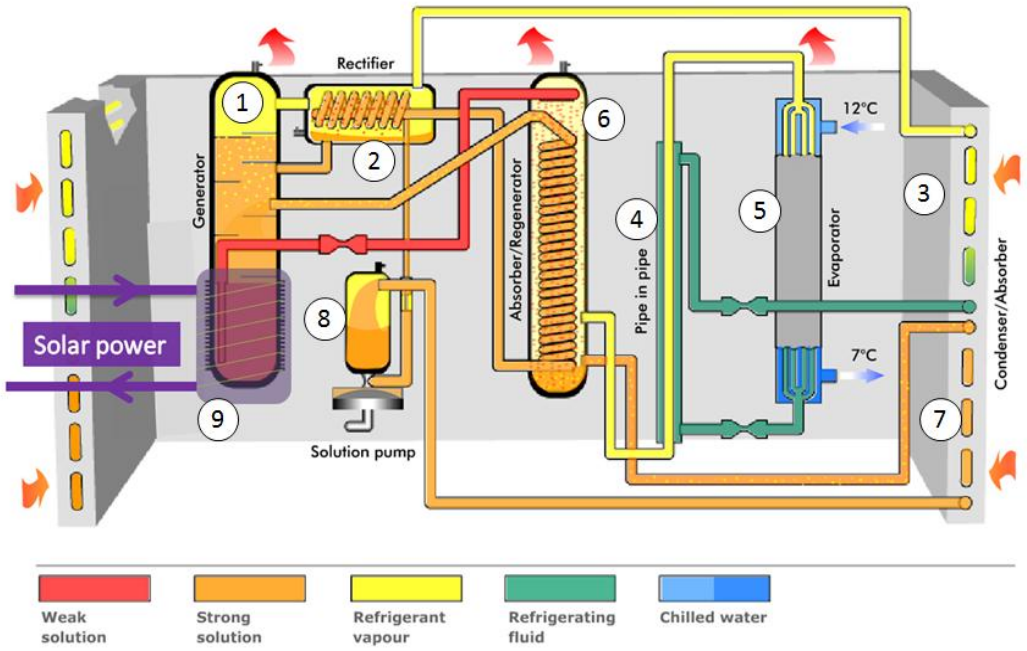

Figure 2-4 Solar operated absorption chiller schematic.

Water vapor condensation is made possible by the medium temperature strong1 solution flowing in a serpentine inside the rectifier. The almost pure refrigerant vapor proceeds to the condenser (3), cooled by air (the cooling coils all around the machine). At the exit of the condenser, an expansion valve adiabatically lowers pressure. The pipe in pipe arrangement (4) with the cold vapor leaving the evaporator (5) provides additional cold for the complete condensation of the low pressure refrigerant before entering the evaporator. In the evaporator, the low pressure liquid refrigerant evaporates, thus subtracting heat from the low temperature brine circulating in the evaporator. Low pressure vapor enters the recuperator / absorber (6), where it gets mixed with the weak solution coming from the generator. The serpentine in the recuperator / absorber subtracts heat from the absorption reaction between weak solution and refrigerant, thus pre-heating the strong solution that enters the generator. At the exit of the recuperator / absorber, the mixture of weak solution and refrigerant is cooled by the fan coil absorber (7), in order to subtract the heat generated by the absorption reaction, thus completing the formation of the strong solution. The volumetric pump (8) pressurizes the strong solution that, after passing through the above mentioned recuperators, enters the generator.

2.3.3. Chiller technical data

The main technical specifications and operating parameters for the operation of the chiller are reported in Table 2-1.

[1] Strong solution is the solution of absorbent (water) and refrigerant (ammonia) that is rich in refrigerant. On the contrary, weak solution is the solution of absorbent and refrigerant that is poor in refrigerant.

Table 2-1 Robur ACF RTCF-LB technical specifications.

Chiller's operational characteristics			
Cooling power at the follow Conditions:		kW	12.8
T inlet , driving heat source		°C	240
T amb, ambient temperature		°C	35
T inlet chiller water		°C	0
T outlet chilled water		°C	-5
Chilled water flowrate	Nominal	l/h	2600
	Max		2900
	Min		2300
Hot fluid flow rate	Nominal	l/h	3500
Operating temperature (T_{Air})	Min	°C	-12
	Max	°C	45
Chilled water inlet temperature	Min	°C	-10
	Max	°C	45
Initial charge of H_2O		kg	11.5
Initial charge of NH_3		kg	8

2.3.4. Solar collectors

The solar thermal collector is the device in charge of transforming the incident solar radiation energy into thermal energy by means of heat exchange through a thermal fluid that circulates within. This is the most important element in a solar facility. The thermal fluid can be water, air, oil, water-antifreeze mixture, etc. There are different types of solar thermal collectors and its selection depends on the necessities of the user.

Flat-Plate Collector (FPC) can be designed for applications requiring energy delivery at moderate temperatures, up to perhaps 100°C above ambient temperature. The major applications of these units are in solar water heating, building heating, air-conditioning and industrial process heat. (Duffie and Beckman 2006)

Evacuated tube collectors (ETC) have lower heat losses than FPC due to the vacuum surrounding the absorber plates, and thus are capable of working at higher temperatures than FPC.

An improvement that can be done to ETC is to integrate them with compound parabolic concentrators (CPC) which are non-imaging concentrators, having the capability of reflecting to the absorber all of the total (direct and diffuse) incident radiation within wide limits. Using this device it is possible to achieve higher temperatures, than with a simple ETC, moreover, this kind of collector doesn't need a tracking system.

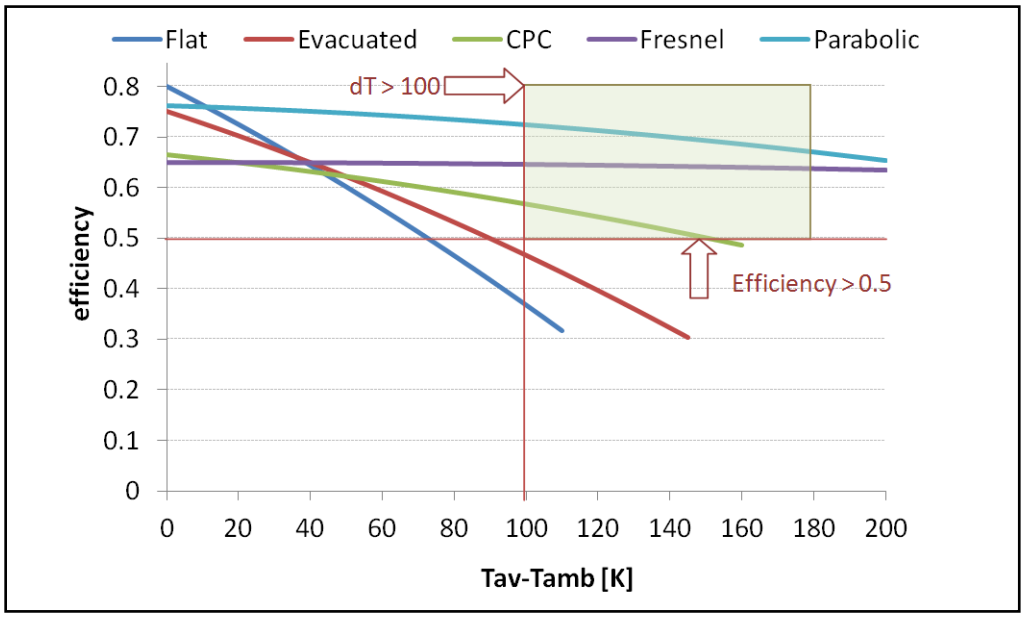

Figure 2-5 Typical efficiency curves for different types of solar collectors.

Based on the operating temperature and heat transfer medium required by the absorption chiller, that is 120 °C - 180 °C, a pre-selection of typologies of collectors has been done. The typologies of collectors that work with a reasonable efficiency (η>50%) at such temperatures (120 °C - 180 °C) are highlighted in the efficiency curves in Figure 2-5.

2.3.2.1. Solar collectors typologies investigated:

According to the efficiency curve, three types of solar collectors have been investigated:

1. Parabolic trough collectors (PTC)
2. Linear Fresnel Reflector collectors (LFR)
3. Evacuated tube collectors with compound parabolic concentrator (ETC with CPC)

Hereafter a brief overview on physical principles and technical characteristics of solar collectors mentioned above is presented.

2.3.2.1.1. Parabolic trough collectors

Parabolic Trough Collectors (PTC) are made by bending sheets of reflective material into a parabolic shape. A high absorbing black metal tube, covered with a glass tube to reduce heat losses, is placed along the focal line of the mirror (see Figure 2-6). When the parabola is pointed towards the sun, parallel rays incident are reflected onto the receiver tube. Such a collector is able to concentrate only the beam radiation. The main advantages of the parabolic trough collector are:

- No use of secondary reflector, thus high optical efficiency;
- Ability to capture sunlight in the early morning and late evening hours.

Because of the apparent movement of the sun across the sky, conventional concentrating collectors must follow the sun's daily motion so that a tracking system is required. Temperatures up to 400 °C can be reached.

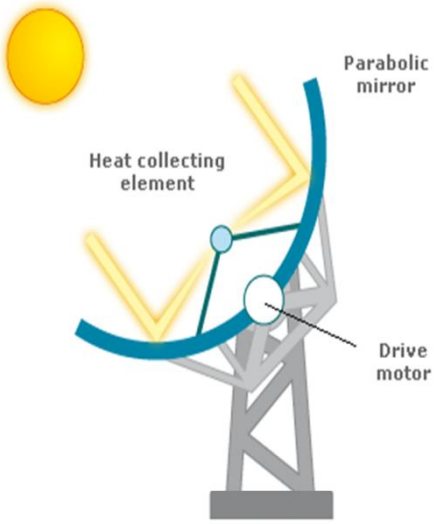

Figure 2-6 Linear parabolic trough concentrating collector.

2.3.2.1.2. Linear Fresnel type collectors

Linear Fresnel reflector (LFR) technology relies on an array of linear mirror strips which concentrate light on to a fixed receiver mounted on the array. The Fresnel collector is made of a primary planar Fresnel reflector, a secondary compound parabolic reflector and an absorber tube. The primary reflector is composed of several reflecting stripes, which concentrate direct beam radiation on the secondary reflector Figure 2-7. Mirror strips orientation can be varied according to radiation incident angle by means of a tracking system in order to maintain a fixed focus line.
The main advantages of the Fresnel collector, compared to trough collectors, are:

- Planar mirrors are easier to manufacture, consequently the collector is less expensive;
- The tracking system is simpler and more reliable;
- The absorber tube doesn't need flexible high pressure joints;
- The planar reflector offers less resistance to the wind, consequently the risk of breakages due to storming is reduced and larger mirrors can be used;
- Overheating protection can be easily made by setting part of the mirrors out of focus.

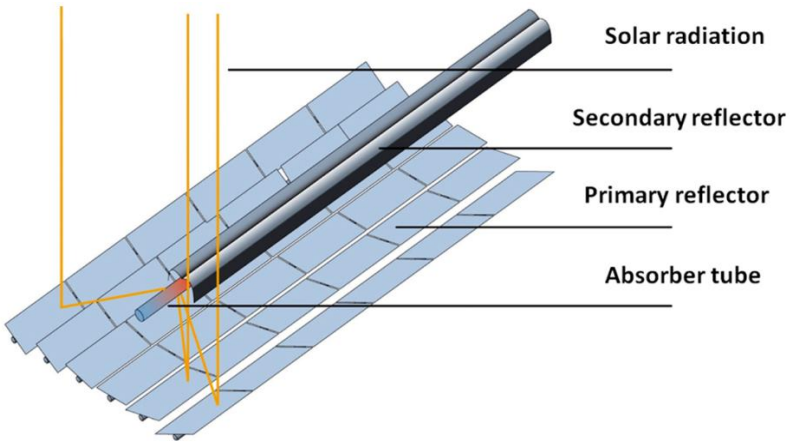

Figure 2-7 Linear Fresnel collector.

2.3.2.1.3. Evacuate tube collectors with compound parabolic concentrator.

In order to increase the efficiency of a collector, beyond selective surfaces, it's possible to create a vacuum envelope between the absorber and the glass cover. In this way it's possible to reduce convection and conduction losses, so the collectors can operate at higher temperatures than flat plate collectors (FPC). This is very difficult to be accomplished in FPC due to both the mechanical resistance of the glass as well as problems related to a state of vacuum. It's easier instead to create vacuum in a tubular structure; an evacuated tube collector (ETC) is made of a certain number of glass tubes, in which there is an absorbing plate sealed to a tube. Typical operational range of ETC is 80 – 110 °C.

There are two kinds of ETC classified based on how the heat is transferred from the tubes is done:

- Direct connections "flow through"
  Direct means that the fluid of the solar circuit is directly going through the collector,

- Dry connection "heat pipe"
  In the heat pipe systems the working fluid is not in contact with the inner tube, that instead contains a small amount of fluid (e.g. methanol),that undergoing an evaporating-condensing cycle, transfers heat to working fluid at high efficiency level.

Compound parabolic concentrators (CPC) are non-imaging concentrators, having the capability of reflecting to the absorber all of the total (direct and diffuse) incident radiation within wide limits **Error! Reference source not found.**. Using this device it is possible to achieve higher temperatures, han with a simple ETC, in the range of (80 °C – 135 °C). This kind of collector does not need a tracking system. (See Figure 2-8)

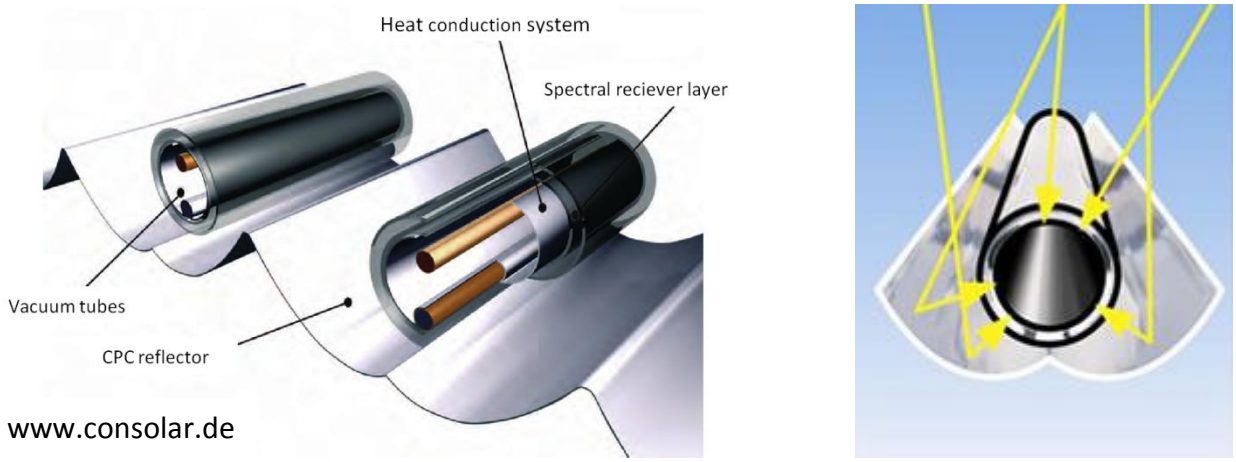

Figure 2-8 Schematic structure of a direct connection CPC collector.

2.3.2.2. Selection methodology

The selection process described here was done in 2008 and 2009. And the aim was to find a suitable collector for the two solar cooling systems described earlier. The attention has not paid only to commercially available collectors but also to prototypes.

It has to be mentioned that the solar medium temperature heating market is on the move, in just two years, not only the number of the commercial suppliers of tracked process heat collectors increased about five-fold. Compared to a previous market overview done by (Sun & wind energy magazine in 2009) a remarkable variety of products has developed as well. (Mohart 2011)

As a first step, research was carried out in order to collect information on companies and research institutes selling or developing medium temperature solar collectors. During this phase the research was carried out using various sources – scientific articles, specialized publications, and the Web to name a few – after which a database of contacts was created. In particular the documents issued by the IEA Task 33 working group were very useful (Weiss and Romme 2008) . Once the database was created it was necessary to choose the parameters to be used for the evaluation of the offers considering both technical and economic aspects. These parameters include: Optical and thermal performance; Availability; Cost and delivery time.

Over the course of this work, twenty contacts were individualized between companies and research institutes. To facilitate the collection of data a questionnaire was developed and sent to the individual contacts.

2.3.2.3. Solar collectors survey outcomes:

2.3.2.3.1. Evacuated tube collectors with CPC

Apart from the efficiency curve of CPC collectors which shows an efficiency higher than 50% at temperatures above 150°C, practically, only one prototype utilizing thin gases and optimized geometry showed an experimental results for operation at 150°C of the. (Buttinger et al. 2010)

The majority of other CPC collectors are experimentally tested at working temperatures below 135°C which do not present an optimal value for the operation of the chiller. And thus, CPC collectors were excluded from the selection procedure.

2.3.2.3.2. Parabolic trough collectors

Several producers have been contacted, but only the collectors from the American company IST was ready to be provided within the available budget and time limits of the project. IST's PT-1 collector presents very good thermal performance and technical characteristics. Another important aspect is that it is a commercial product that has proven to be a very successful in several systems, some of which have been operating continuously for more than fifteen years "reliability aspects".

2.3.2.3.3. Linear Fresnel Reflector Collector

Two LFR collectors have been found suitable for the application, but only the German company PSE was able to supply a prototype suitable for a pilot plant. The thermal performance, the technical characteristics and the price of such a collector make it suitable for the solar cooling concept.
Moreover, regarding the fact that two plants are planned within the project, it would be preferred to test both typologies of concentrating collector i.e. the PTC and the LFR in order to test and compare their performance.

2.3.5. Cold and hot storage

In cooling systems using chilled water as the cooling medium, a cold storage component can be integrated. This allows the chiller to be operated at times other than when cooling in the rooms is needed. In conventional cooling systems, storage has become one of the primary solutions to overcome the electric power imbalance between daytime demand and nocturnal abundance. The storage unit uses off-peak power to provide cooling capacity by extracting heat from a storage medium. Typically, a storage system uses refrigeration equipment at night to operate more efficiently than during the day, reducing the power consumption, and to create a reservoir of cold material. During the day, the reservoir is tapped to provide cooling power.

In a solar-assisted air-conditioning system, the reason to install a storage unit is somewhat different. The main purpose is to increase the use of solar energy in order to overcome periods of low radiation,

in which the solar heat is not sufficient to cover the cooling load. This is achieved by generating more cooling power than needed during periods of high solar gains. Different time scales are of importance:

- Shortages of the solar radiation on time scales of seconds to minutes are due to clouds; if heat cannot be stored, the cooling process has to follow the available solar heat and in phases when the load exceeds the generated cooling power, a reservoir to allow further cooling is needed. In such cases, the cold reservoir has to be designed to cover the load only for a short time.
- Mismatches between solar gains and loads on a diurnal level can occur due to typical load patterns with a peak of the required cooling in the afternoon or evening, whereas the solar gains have their peak at noon. In such cases, the storage system has to be designed to cover the load on the order of hours.

The advantages of storing cold in comparison to the storage of heat in a solar-assisted air-conditioning system are:

- The amount of energy to be stored to cover a certain load is lower for a cold medium than for heat if the COP is less than 1.0 as it is the case for most thermally driven chillers. This fact is also demonstrated in Figure 2-9 .
- The temperature of chilled water is generally closer to the temperature of the air surrounding the storage unit. This causes lower heat losses for the same standard of insulation.

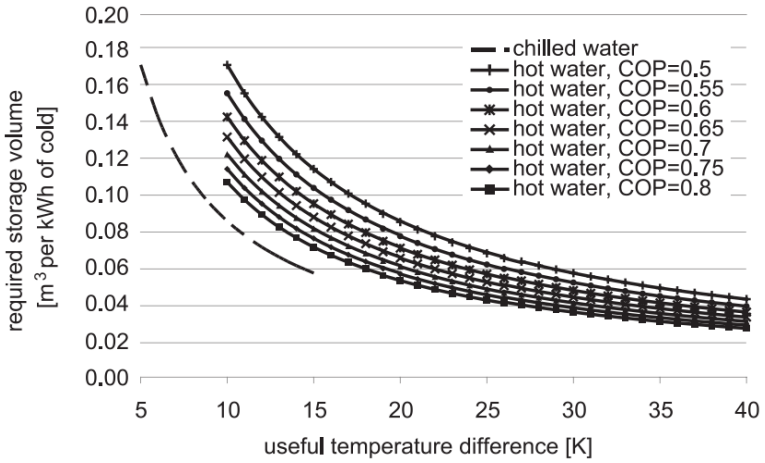

Figure 2-9 Required storage volume for chiller water storage and hot water storage for different values of the COP of thermally driven chillers as a function of the useful temperature difference. The required storage volume is given in m^3 required to provide 1 kWh of cold.

A major disadvantage is that the storage density is lower because of the lower useful temperature difference. Chilled water storages require much larger storage tanks than the other storage media. Also the insulation quality has to be higher in comparison to hot water storage since condensation on the tank walls and particularly on the pipe connections has to be prevented.

On the other hand, to store 1 kWh of cold produced with a chiller which has 0.7 of thermal COP, means that on the hot side we would have needed to store about 1,43 kWh of "hot" thermal energy.

2.4. Cooling process selection criteria

The criteria to select the two end users among the agro-food industry where solar cooling plants to be installed as well as to select the specific industrial cooling process which will be cooled by the solar cooling system are presented in the check list in Table 2-2. It can be seen that in addition to the energy and technical aspects considered, the practical and logistic aspects are also highly important for the success of the pilot plants.

Table 2-2 Criteria to end user and industrial cooling process selection.

Criteria	Yes	No
Cooling loads and solar radiation availability have to be in phase as much as possible. It is preferable to have high cooling loads in summer (peak)		
Replication potential of the pilot plants in other agro-food industrial processes.		
Suitability of the location with respect to solar energy (solar radiation level, land availability and exposition to solar radiation).		
Production process requirements (refrigeration load at temperature around 0°C, distributed along the year and peaking during summer).		
Availability of space where to install the solar collector field (Minimum 300 m2)		
Low probability of sandstorms and dust.		
Availability of structure where to install the collectors: if flat roof is available (check possible load on the structure) it is better than building a steel structure on purpose.		
The distance from solar collectors field installation site and actual technical room is less than 100 m		
Availability in the technical room of about 30-50m^2		

Level of interest and commitment of the end-user in sustainable and innovative production processes.		
Preferable if the end-user has previous experience with customs (import-export activities)		
The selected process has to be in the same order of magnitude as the solar cooling plant in terms of capacity (power): no peak load higher than 60 kW		
It is preferable if there is a need for heat (particularly when there is no cold demand)		

Based on the aforementioned criteria two factories where the solar cooling systems to be installed have been selected; the first is a Tunisian beverage factory and the second is a Moroccan dairy.

Having identified the two end-users, the first step was to evaluate their energy needs in order to derive a typical hourly load profile (i.e. the refrigeration power needs sampled at hourly intervals) to be used in the next project phase of sizing and performance prediction of the solar refrigeration plant.

2.5. End user requirement

The objective of this work is to describe the end-users requirements in terms of:

- Cool energy load pattern;
- Cool peak power;
- Control and operating parameters;
- Requirements for integration of the solar refrigeration plant with the existing (conventional) one.

The energy analysis was carried out by both collecting actual energy consumption data and simulating the production process energy load. By reconciling the actual and the simulated data, it has been possible to derive an hourly load profile for the refrigeration load.

Since hourly load profiles for a whole year are typically not available, a “bottom-up” approach has been used in order to reconstruct a typical hourly load profile. According to this approach, the facility electricity needs, including chiller electricity consumption, refrigerant circulation and production machineries electricity consumption, have been simulated by assessing the technical features (e.g. nominal power, efficiency) of all electrical appliances and estimating their operating time. The simulated data was finally reconciled with the monthly electricity bill in order to validate the model.

The study has gone through the following methodological steps:

- Inspection of the production facility (location of machines, nominal power of coolers, pumps and any electrical appliance)
- Interviews (technicians, manager) in order to collect information on the production process and its energy needs (batch volumes, duration and frequency, transformation sequence)
- Energy bill collection (monthly electricity consumption, kWh/month)
- Production process modelling (batch volumes and frequency, transformations)
- Physics of the climatic data impact (effect of radiation, temperature and air humidity on the production process in terms of refrigeration energy needs)
- Simulation of cool energy requirement (hourly load profile process and climate)
- Data reconciliation (energy bill as compared to simulation output data)

2.5.1. Tunisia Plant

The selected agro-food industrial plant in Tunisia is a beverage factory. Fermentation which is an exothermic reaction is a vital process in the production of the beverage, in order to guarantee the quality of the beverages during the fermentation process the temperature needs to be stable, and thus cooling is required. Fermentation is done in twenty three fermenting tanks which are cooled by chilled water flowing in jacket type heat exchangers (see Figure 2-10 and Figure 2-11).

Figure 2-10 Fermenting tanks with chilled water circuit and jacket heat exchangers before insulation.

Figure 2-11 Fermenting tanks after insulation.

The existing conventional refrigerator plant is composed of the following machineries: Refrigerator, Cooling tower, Cold water storage tank. Hydraulic circuit (pumps, valves and pipes).

Further, the plant hydraulic scheme is presented and the control mechanism briefly described (see Figure 2-12 and Figure 2-13):

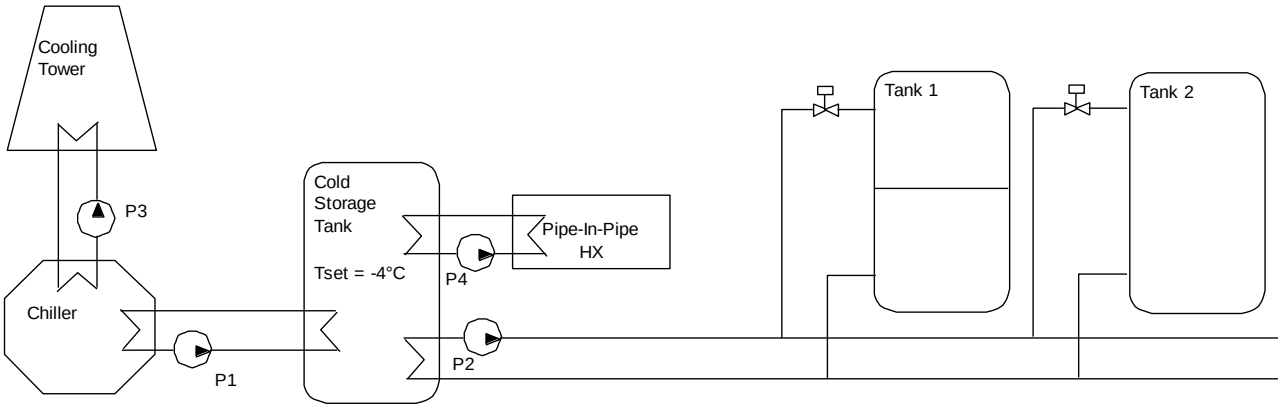

Figure 2-12 Existing Refrigeration plant hydraulic scheme (only 2 out of the 23 fermenting tanks are represented)

The pumps P1 and P3 is set always on, in order to keep the cold water storage always fully mixed and guarantee continuous water circulation in the wet cooling tower. The chiller turns on when the temperature in the cold storage tank raises above -2 °C and turns off when the same temperature falls below -6 °C.

The pump P2 turns on when at least one of the fermenting tank valves is open. The valves open according to the set-point temperature of each tank, which is set according to the on-going production phase.

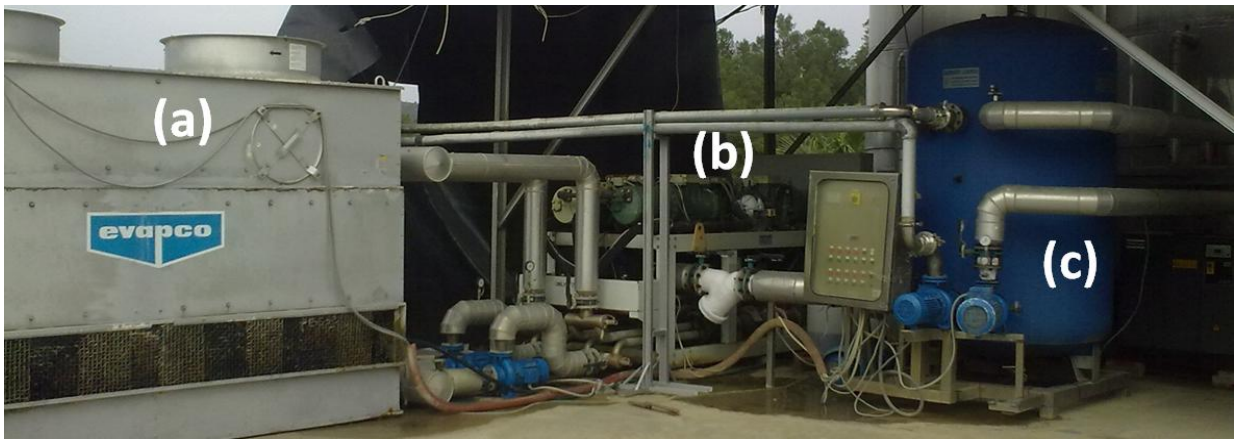

Figure 2-13 The existing conventional cooling plant; Evaporative cooling tower (a), the compression unit (b) and cold storage (c).

Based on the work done by (Aprile and Aronne 2008), a representative yearly load profile for the refrigeration system can be derived from the analysis. In particular, the following three data profiles have been reconstructed: Daily average refrigeration power (see Figure 2-14), daily peak refrigeration power (see Figure 2-15), and typical hourly refrigeration profile for the typical day in each month of the year (see Figure 2-16).

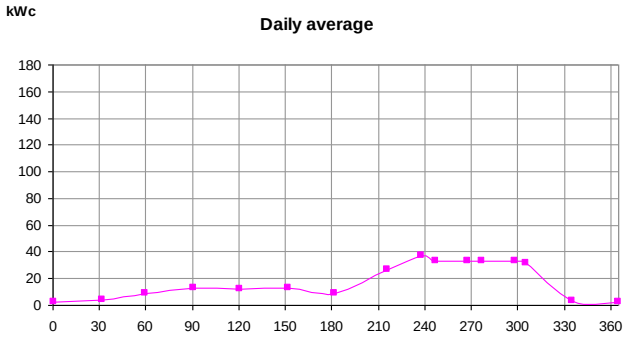

Figure 2-14 Daily average refrigeration power at -4 °C, year 2006, day 1 (January 1st) till day 365 (December 31st)

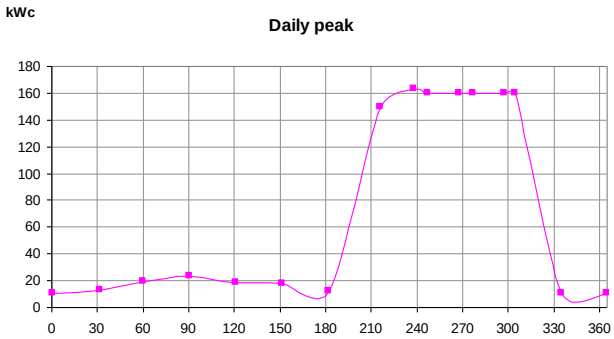

Figure 2-15 Daily peak refrigeration power at -4 °C, day 1 (January 1st) till day 365 (December 31st)

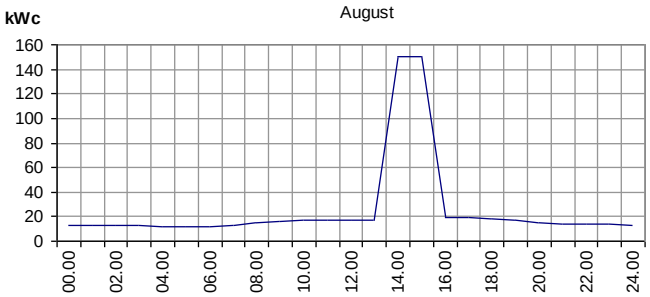

Figure 2-16 Hourly refrigeration power profile at -4 °C, year 2006, typical day in each month

According to the simulation results, the most relevant share of the yearly electricity consumption is due to hydraulic (44.7 %), followed by refrigeration (20.8 %), air conditioning & lighting (14.7 %) and mechanical (13.0 %), while heating is negligible (only 0.2 %). The hydraulic load seems quite high and it could be possible to reduce it by optimising the control procedure of the different pumps.

For what concerns the monthly profile, the electricity consumption peaks in summer due to refrigeration of the beverage production area and conditioning of the office building. In particular, a peak in the refrigeration load during August and September is the consequence of the pre-cooling operation.

The daily average refrigeration load at -4 °C it is only a few kW up to June, and suddenly raises to some 40 kW during summer to nearly vanish in December. Similarly, the daily peak refrigeration is only 10-20 kW up to June and raises up to 160-170 kW during summer. On this regard, it can be argued that the installed refrigeration power of some 800 kW seems too large when compared to peak load, even considering the decrease in chiller capacity due to the low value of chilled water temperature (-4 °C).

The hourly load profile reveals that a certain refrigeration power of some 10 kW is required during night time. However, the refrigeration load peaks during day time in every day of the year, and especially during spring time, when it doubles, and summer, when it concentrates in the mid of day due to the pre-cooling operation. All this makes the beverage refrigeration load particularly suitable to solar cooling applications.

2.5.2. Moroccan Plant

The second agro-food industrial plant selected is a diary factory which is located in the city of Marrakech in Morocco. This factory is considered to be the second largest dairy factory in Morocco which receives milk from a vast number of dairy farms and processes it to milk products.

After studying the plant operation lines and processing schemes, site visits have been done in order to investigate the existing cooling plant, cooling process and the optimal integration of the solar cooling system with the existing plant.

Several other processes found to be suitable to be coupled with the solar cooling system, for example the pasteurization process which includes the simultaneous heating and cooling. However, due to the high cooling power demand compared with the limits of the cooling potential of the absorption chiller used in this pilot plant the focused was kept on the first investigated process of cooling the raw milk, which has a high replication potential in dairy farms and factories.

Cows are milked early in the morning in small dairy farms in villages around Marrakech, and then milk is collected in several collecting centres and transported by road milk tankers to the diary factory in the city. Generally milk tankers arrive to the factory by midday and the milk temperature ranges between (9-28 °C) depending on the availability of refrigeration systems at the collecting centre and the ambient temperature. According to the process engineers, the milk has to be cooled after the first milking to 7.3°C or less within 4 hours of the start of the first milking.

The received milk is discharged into holding tanks, and then it is pumped to a clarifier which removes debris, some bacteria, and any sediment that may be present in the raw milk. Afterward the clarified raw milk is cooled via two plate heat exchangers, supplied on their cold side with chilled water at about 2°C. Afterward, the cooled milk is stored in storage tanks to be ready for processing in the various factory production lines. (See Figure 2-17)

In order to ensure the quality of the milk, the quality control lab of the factory was taking a sample from each milk tanker to test it; this was useful because this allowed having data about the temperatures and the amount of received milk for about two years. This information allowed evaluating the hourly and the annual cooling load profiles of the process of cooling of raw milk.

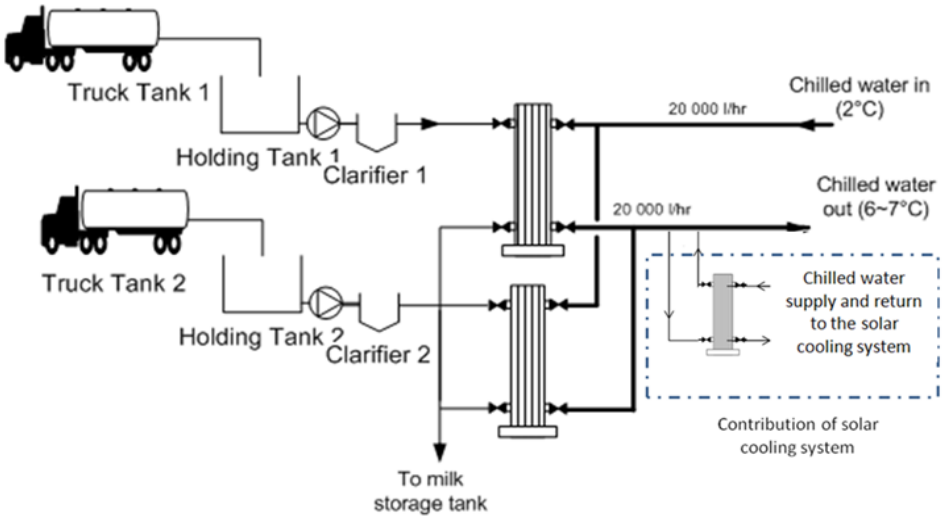

Figure 2-17 Fresh milk cooling system and the integration of the solar cooling system.

Figure 2-18 presents the amount of fresh milk received by the factory per month; it can be seen that the amount of milk received during spring and summer months are higher than the amounts received during autumn and winter months. This is due to the fact that cows and sheep produce more milk in the sunny seasons due to the longer days and higher availability of grass and nutrition elements.

Moreover, the ambient temperatures in the sunny months are higher, and this temperature has a direct impact on the temperature of the received milk by the factory, and this explains the higher cooling loads during spring and summer months compared to the other period of the year.

This annual cooling load profile for cooling the fresh milk highly matches the solar radiation availability during the year, which confirms the high potential of applying solar cooling system for this type of applications.

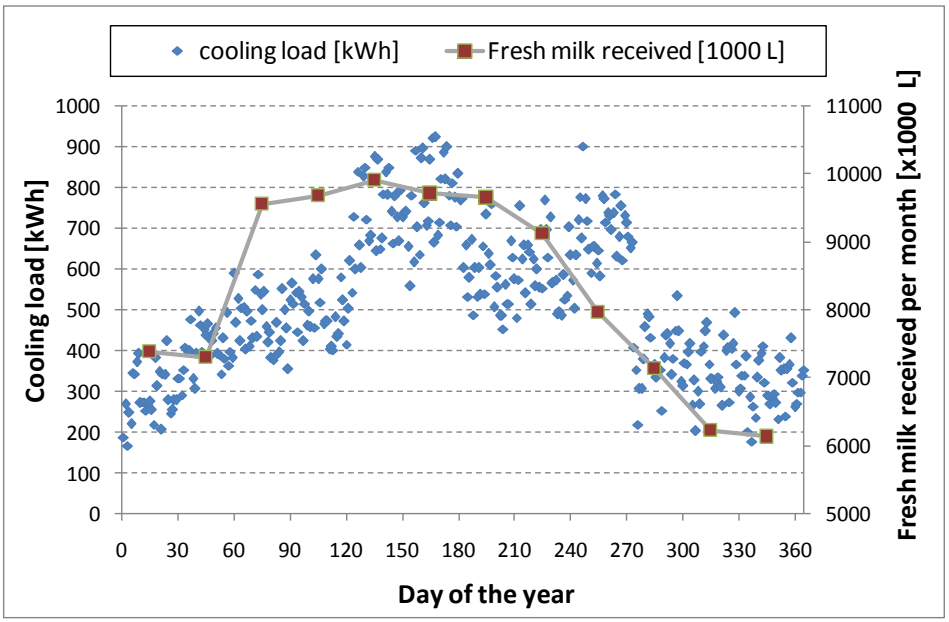

Figure 2-18 The daily cooling load in [kWh] and the monthly amount of fresh milk received in [1000 L].

In order to investigate the opportunities of utilizing the solar cooling system in the fresh milk cooling process, both, the cooling load profile and the solar radiation for one typical summer day were studied; it was concluded that due to the mismatch between the two profiles an inertial component was needed. A cold storage has been selected to store cold energy in the phases when the availability of solar radiation allows cold production, without having concurrent cooling demand. Also, due to the existing system configuration- where there are two heat exchangers to cool milk, and they are used alternatively- it was decided to connect the solar cooled heat exchanger to play a role on cooling the return chilled water to the existing chiller as this is common between the two existing milk heat exchangers. The load profiles worked out - an example of a daily profile is presented in Figure 2-19- highlighted, on a daily basis, that four operation phases take place as further described.

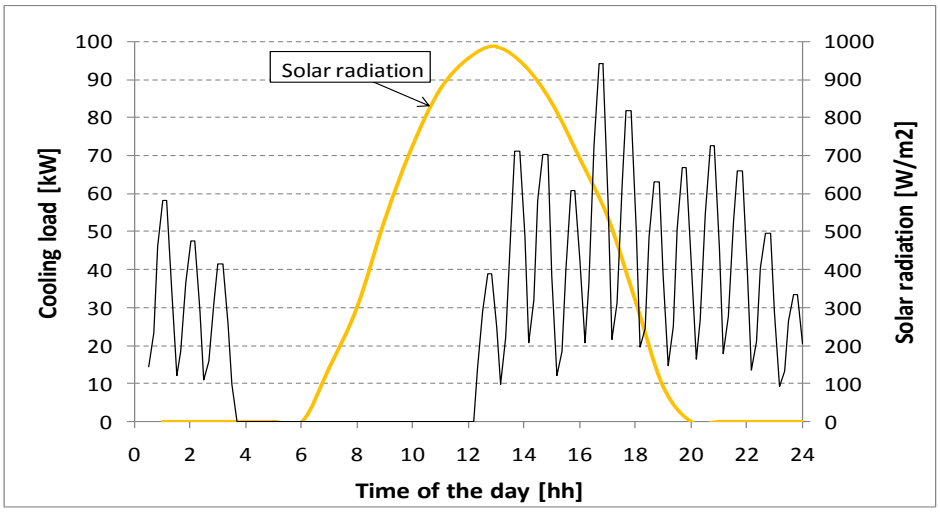

Figure 2-19 The hourly cooling power [kW] and the solar radiation [W/m2].

Operation phase:

- Direct cooling: This is the default mode of operation of the system when there are simultaneous solar energy and cooling load.
- Charging the cold storage: This basically happens early in the day when there is enough solar radiation to run the chiller but there is no cooling load as the milk didn't arrived yet to the factory.
- Discharging the cold storage: As soon as the supply energy by the solar radiation is not sufficient to run the chiller, the system turns to discharge mode, where cold energy started to be discharge to the load.
- System Off: Obviously, when there is no load and there is no solar radiation the system goes off, this mainly happens in the very late hours of the night and before sunrise.

Moreover, It can be seen that cooling load power is much higher that the nominal cooling potential of the absorption chiller (12.8 kW) and as the system design need to be done in a way to increase replication potential; it has been decided to work on a portion of the industrial process (i.e., a portion of the milk volume flow) which allows to speculate on the possible behavior of the a solar refrigeration system correctly sized for the application (i.e., about seven times in capacity). A scheme of the process is given in Figure 2-17.

2.6.References

Aprile, Marcello, and Marco Aronne. 2008. *Medisco Project Deliverable 2.1: Detailed report of the end-user requirements, including load patterns and operating parameters for the Tunisian plant*.

Aprile, Marcello, and Mario Motta. 2007. SIMULATIONS OF A NOVEL SOLAR ABSORPTION COOLING CONCEPT: A COMPARISON OF STATIC AND DYNAMIC SYSTEM MODELS. In *2nd International Conference Solar Air-Conditioning*. Tarragona, Spain.

Buttinger, Frank, Thomas Beikircher, Markus Pröll, and Wolfgang Schölkopf. 2010. "Development of a new flat stationary evacuated CPC-collector for process heat applications." *Solar Energy* 84 (7) (July): 1166-1174. http://www.sciencedirect.com/science/article/pii/S0038092X10001386.

Darwish, N A, S H Al-Hashimi, and A S Al-Mansoori. 2008. "Performance analysis and evaluation of a commercial absorption-refrigeration water-ammonia (ARWA) system." *International Journal of Refrigeration* 31 (7) (November): 1214-1223. http://www.sciencedirect.com/science/article/pii/S0140700708000364.

Duffie, John A., and William A. Beckman. 2006. *Solar Engineering of Thermal Processes*. Wiley. http://www.amazon.com/Solar-Engineering-Thermal-Processes-Duffie/dp/0471698679.

Henning, Hans-Martin, Andreas Häberle, Marco Guerra, and Mario Motta. 2006. Solar Cooling and Refrigeration with High Temperature Lifts - Thermodynamic Background and Technical Solution. In *National Congess of the Italian Thermotechnical Association (ATI) of Solar Heating and Cooling*, 105-110. Perugia.

Horuz, I, and T M S Callander. 2004. "Experimental investigation of a vapor absorption refrigeration system." *International Journal of Refrigeration* 27 (1) (January): 10-16. http://www.sciencedirect.com/science/article/pii/S0140700703001191.

Mohart, Alexandar. 2011. "Solar process heat is becoming sexy." *Sund & wind energy*.

Weiss, Werner, and Matthias Romme. 2008. *Process Heat Collectors*.

3. Chapter Three: Experimental Setups

3.1.The first experimental setup in Tunisia

The plant serves as industrial refrigerator for a beverage factory in Grombalia, Tunisia (Figure 3-1, Figure 3-2). One of the main energy consuming processes in the factory is the cooling of the twenty fermenting tanks in order to avoid the excess heat resulted from the exothermic fermentation process. The solar cooling plant is connected to three of these fermenters in parallel with the existing cooling system which serves as a cooling backup for them. The solar cooling system is requested to supply low temperature down to -8°C to the fermenting tanks' jacket heat exchangers.

Figure 3-1 Fresnel solar thermal collector in the solar cooling system in Tunisia

Figure 3-2 Fermenting tanks behind the installed solar thermal collector

The system (Figure 3-3) consists of a concentrating linear Fresnel collector. Heat absorbed by the collector is supplied to the generator of a single-effect water-ammonia absorption chiller which cools a water-glycol cold storage. Water-ammonia chiller was selected to supply cold water at temperature below zero degrees. The water-glycol cold storage is connected with the cooling load represented by the three 300 hl fermenting tanks.

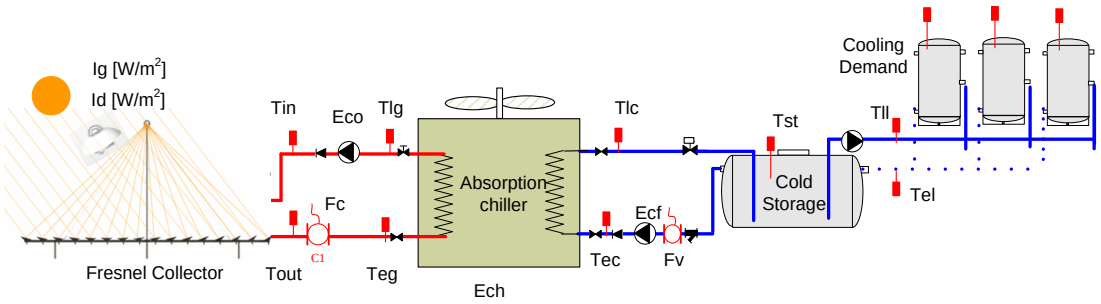

Figure 3-3 General scheme of the first experimental setup in Tunisia.

The technical data of the main system components are presented in Table 3-1. These components are; the solar collector, the absorption chiller and the cold storage. In the following sections, a detailed description of the LFR collector and the cold storage is presented.

Table 3-1 Technical data of the first experimental setup in Tunisia.

Thermally driven cooling systems	Technology	Ammonia-water Absorption chiller
	Nominal capacity	12.8 kW_{cold}
	Heat rejection system	Integrated Air Cooled Condenser
Solar thermal collectors fields	Technology	Concentrating Linear Fresnel Collector
	Gross area	120 m² gross area/ 88 m² aperture area
	Tilt angle, orientation	Single axis tracking, North-South
	Typical operation temperature	110 - 180°C
Storage system	Cold storage	3 m³ water-glycol
	Heat storage	none

3.1.1. Linear Fresnel reflector solar collector (LFR)

The Fresnel solar collector used in our project was manufactured and installed on the ground of the Tunisian factory by the company PSE AG, which has recently transferred all activities concerning concentrating solar collectors to its newly founded subsidiary Industrial Solar GmbH. It consists on a solar field with a total surface area of a 120 m^2 made up of eleven rows of 4 modules (16 m long) that concentrate the sunlight on a tubular vacuum receiver SCHOTT PTR©70 with secondary aluminum compound parabolic concentrator (CPC) 4m above the mirror field, see Figure 3-4. The thermal-fluid is pressurized water, which is heated up to a maximum operating temperature of 180 °C (12 bars). The main parts of the collector (see Figure 3-4) are described in the following sections:

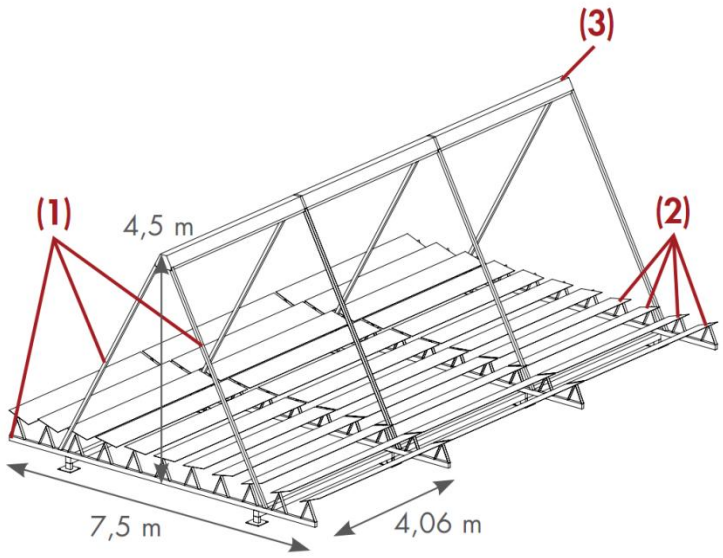

Figure 3-4 Schematic diagram of the Linear Fresnel reflector, 1 is the steel structure. 2 is the primary reflector mirrors, and 3 is the receiver.

3.1.1.1. Steel Structure

The steel structure supports reflective mirrors, theirs bearings and drive actuators, absorption pipe and secondary reflector. (See Figure 3-5) This structure defines the boundary of the reflective mirrors area. Because of its structural constitution, the structure has been painted with a solar reflective varnish. This particular varnish is oil-based and designed with glass micro-balls specifically treated to increase the reflectivity. A special treatment like this has been made to limit the reduction of mirrors reflective area caused by the reflection of the steel structure on them. Unfortunately, mirrors area reduction due to pipe's reflection and shadows cannot be avoided, because the pipe cannot be painted with the varnish, in order to not affect pipe's thermal properties.

Figure 3-5 The civil foundations and the steel structure of collector during installation.

3.1.1.2. Primary reflector, Reflective Mirrors

Reflective mirrors are made of security glass, slightly curved with a radius of curvature of 9.6 meters. Being the radius of curvature so large, construction costs are reduced and at first sight mirrors seem to be flat. The solar glass that constitutes reflective mirrors is made of a glass substrate and a reflective layer. The reflective layer is designed to reflect the maximum amount of solar energy incident upon it and it comprises a highly reflective layer of thin silver plating. Each mirror is attached to the load-bearing structure by ten steel supports and it is moved by a drive actuator that allows for solar-tracking. The reflective mirrors on solar-tracking mode are presented in (Figure 3-6).

Figure 3-6 Mirrors in tracking mode.

3.1.1.3. Receiver

The receiver consists of a secondary reflector and vacuum absorber tubes. The secondary reflector (see Figure 3-7) is formed by an aluminum thin envelop covered with a reflective mirror (with nominal reflectivity of 0.77) mounted inside. This structure has the function of reflecting the solar radiation that does not affect directly the absorber pipe, optimizing the plant total optical efficiency. Moreover, it also acts as pipe protection.

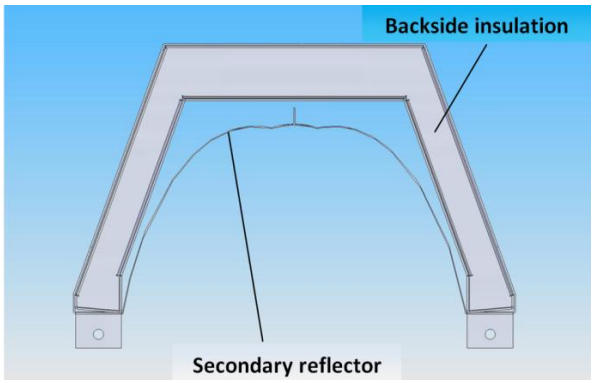

Figure 3-7 The secondary reflector with the backside insulation.

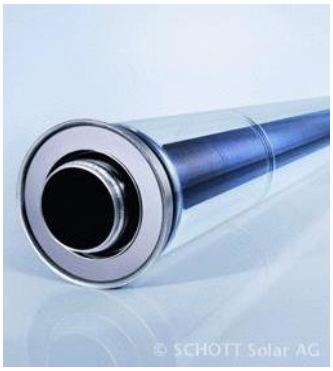

Figure 3-8 Absorber pipe and glass cover.

The receiver is formed by an absorber pipe and a glass cover. The absorber pipe is a welded pipe, , with a nominal absorptivity of 0.94. In both ends of the pipe there are flanges, model DN 50(DIN 2633, PN 16), to connect it with the hydraulic circuit. The temperature in the hydraulic circuit is limited to a maximum of 200^{o} Celsius and the pressure to a maximum value of 16 bars. However, for the normal operation, the maximum operating temperature was limited to 180^{o} Celsius and a pressure of 13 bar, with the pressure release valve limited to 16 bar in order not to force the system components (pump, valves) working at their maximum temperature limit for a long period. The absorber pipe is surrounded by a glass cover, to ensure the vacuum between them, to minimize thermal losses (Figure 3-8).

3.1.1.4. Drive and Control

In LFR collectors each row of mirrors moves independently of the adjacent ones. The drive actuator is an electrical engine that rotates mirrors of an angle that permits at each row to reflect sunlight and concentrate it on the receiver. Engine rotation is transmitted to mirrors through a transmission belt with a ratio speed reduction of 2.8: 1 on the output pulley (see Figure 3-9). To determine the current position of the mirror rows, each mirror row is equipped with a potentiometer (the sensors are positioned near the drive mechanisms).

The mirror tracking of the Fresnel collector is based on a solar position algorithm. The position of the sun is calculated according to the current time and the geographic position of the collector. Based on this information and the geometry of the collector, the optimal angle of each mirror line is determined. If the deviation of the current position taken from the inclination sensor to the optimal angle exceeds a certain threshold, the position of the mirror line is adjusted.

Figure 3-9 Drive mechanism

To calculate the optimal angle of the mirror lines the geometry of the plant is considered. This includes the following information:

- The direction of the mirror axes.
- The position of the mirror axes relative to the focus point.
- The distance of the mirror surface relative to the mirror rotation axis.

In addition to the standard tracking mode of the mirrors of the collector, two operation modes are programmed for the operation of the collector:

1. Mirrors in stow position: in this mode all mirrors are upside down to protect the mirrors from dust and to make sure that no concentrated irradiance occurs. (see Figure 3-10)
2. Maintenance mode: For mirror cleaning and maintenance of drive mechanism parts the collector must be set to maintenance mode (see Figure 3-11Figure 3-11).

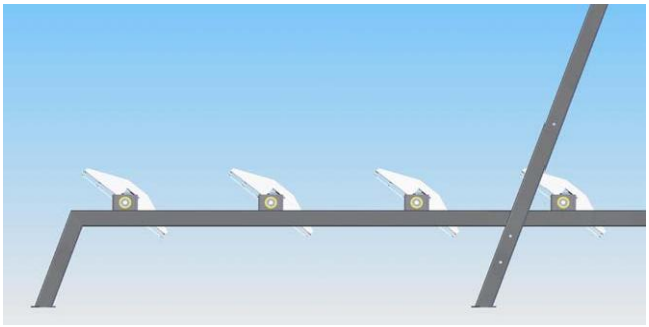

Figure 3-10 Mirrors in stow position.

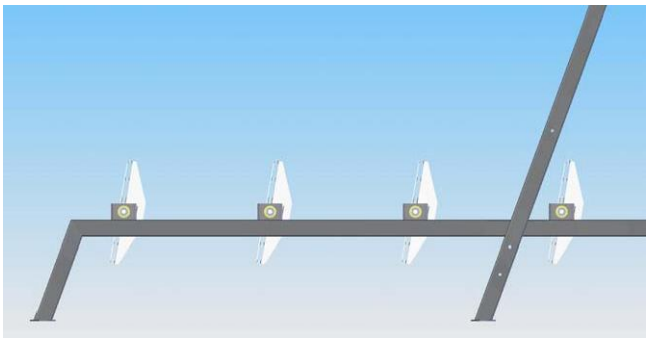

Figure 3-11 Mirrors in maintenance position.

3.1.2. Cold storage

The cold storage used in this installation is a three cubic meters of water-glycol storage with glycol presenting 30% of the mixture volume to guarantee the ability of the storage to work down to -10^{o} C with no freezing risk. This kind of storages use the sensible heat capacity of water to store cooling energy. In order to ensure high stratification in the cold storage, it is preferable to mount the storage vertically. However, in order to avoid creating shadow on the LFR collector, in our facility it was installed horizontally. The schematic diagram of the storage presenting its connections with the load is presented in (**Error! Reference source not found.**), and the photo of the installed storage is presented in (Figure 3-13 & Figure 3-14).

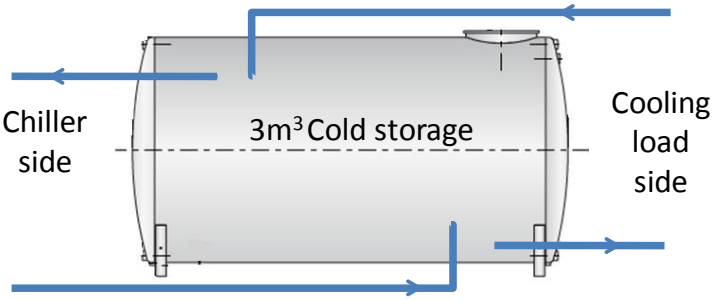

Figure 3-12 Schematic of the cold storage connections.

Figure 3-13 The installed cold storage.

Figure 3-14 The first experimental setup, the solar collector, absorption chiller and cold storage.

3.2. The second experimental setup in Morocco

The plant serves as industrial refrigerator for a dairy factory in Marrakech, Morocco (Figure 3-15 and Figure 3-16). According to the food processing standards, the milk has to be cooled after the first milking to 7.3°C or less within 4 hours of the start of the first milking. In the existing plant, the fresh milk arriving from dairy farms is cooled via two plate heat exchangers, supplied on their cold side with chilled water at about 2 °C (Figure 2-17). The cooled milk is then stored in insulated storage tanks to be processed in the factory facilities to produce yogurt, cheese, butter and other products.

Figure 3-15 Parabolic trough collectors on the roof of the plant in Marrakech, Morocco.

Figure 3-16 Heat exchanger used to cool the fresh milk arriving in the factory.

The system (Figure 3-17) consists of a roof mounted parabolic trough collector. Heat absorbed by the collector is supplied to the generator of a single-effect water-ammonia absorption chiller which can deliver its cold to the cooling load, or to the PCM ice storage to be used when there is a cooling load and no solar radiation.

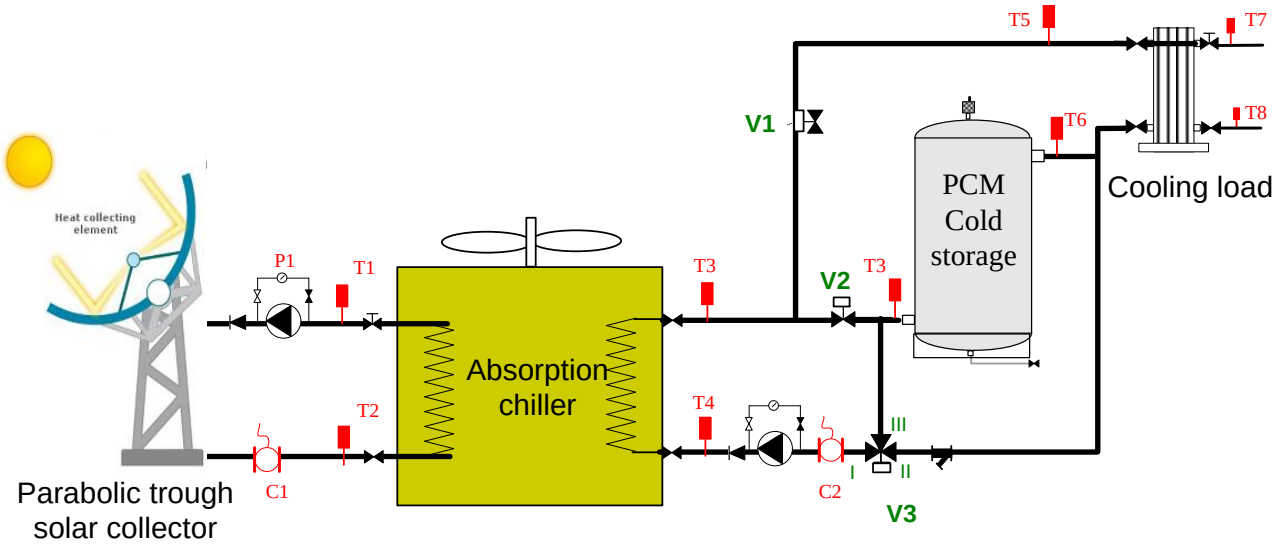

Figure 3-17 General scheme of the second experimental setup in Morocco.

The technical data of the main system components are presented in Table 3-2. These components are; the solar collector, the absorption chiller and the cold storage. In the following sections, a detailed description of solar field and the cold storage is presented.

Table 3-2 Technical data of the second experimental setup in Morocco.

Thermally driven cooling systems	Technology	Ammonia-water Absorption chiller
	Nominal capacity	12.8 kW_{cold}
	Heat rejection system	Integrated Air Cooled Condenser
Solar thermal collectors fields	Technology	Concentrating parabolic trough collector
	Gross area	63.4 m^2 gross area/ 58.5 m^2 aperture area
	Tilt angle, orientation	Single axis tracking, 32 ^{o} to North-South
	Typical operation temperature	110 - 180°C
Storage system	Cold storage	2 m^3 PCM ice storage
	Heat storage	None

3.2.1. Solar field: Roof mounted parabolic trough collector (PTC)

The roof mounted parabolic trough (RMT) concentrating collectors used in this project is from IST Abengoa company. This collector is a compact design of the ground mounted collector PT1 which was developed by IST and tested by Sandia national laboratories. The concentrator is built according to a patented design that makes it light, which is a requirement for the roof installations, yet exceedingly strong.

The solar field consisted of 18 modules of (3067 mm length x 1148 mm width) arranged in four rows as presented in Figure 3-18. It can be seen that the rows on the left have more collector modules (six) compared to the ones on the right (three); this unbalanced configuration was opposed due to the fact that two chimneys of the factory existed on the right southern part of the roof. And in order to avoid their emissions which could reach the collector surface and deteriorates its reflectivity dramatically it was decided not to install collectors in that zone.

3.2.1.1. Steel structure

The PTC collectors are subject to higher wind loads than LFR collector due to their shape, and thus wind load analysis was carried out to design the supporting steel structure of the collectors. This load profile required the use of HEB steel beams with a Depth of 100 mm and having a Nominal Weight per length of 10 20.4 kg/m (Figure 3-19). Moreover, an anemometer was considered as an essential part of the solar field control in order to drive the collectors to a stow position in case of very high wind velocities Figure 3-20.

3.2.1.2. Concentrator

The reflector is enhanced-polished aluminum which is coated to ensure a higher resistance, and the frame is made of aluminum as well which is resistant to corrosion.

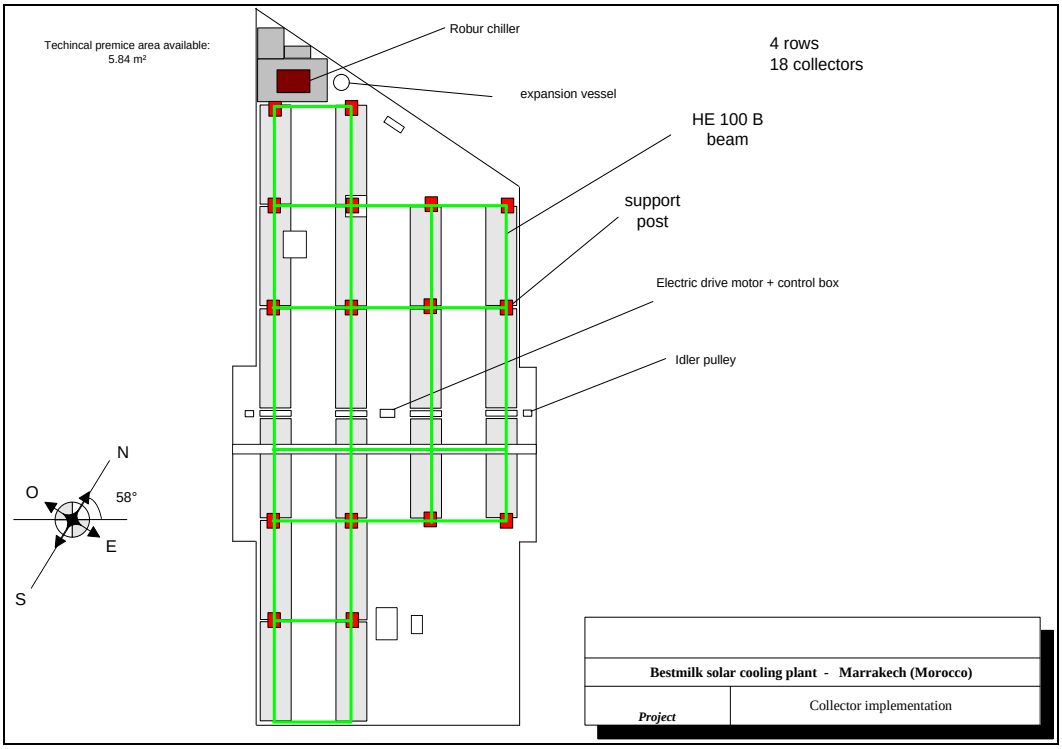

Figure 3-18 Solar field configuration on the roof of the dairy factory.

Figure 3-19 The supporting steel structure installed on the roof of the dairy factory.

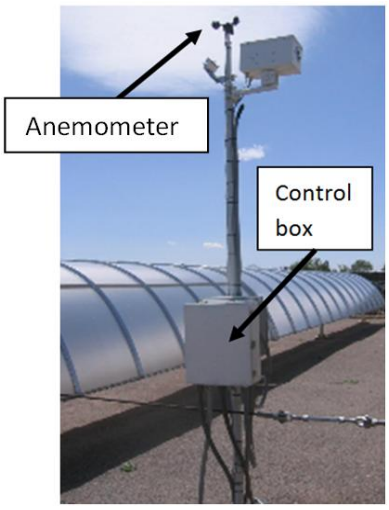

Figure 3-20 The anemometer connected to control box.

3.2.1.3. Receiver

The receiver/absorber is a black nickel-coated (optionally black-chrome-coated) steel absorber pipe surrounded by a non-evacuated glass enveloped with sol–gel anti-reflective coating that increases light transmission to the absorber. It has an aluminum rib support structure.

Figure 3-21 The PTC receiver/absorber.

3.2.1.4. Flexible Hoses

It was mentioned that it is an advantage of the LFR collector that the absorber is fixed, on the contrary for the PTC the absorber moves with the concentrator, thus a flexible hoses deliver and receive thermal heat transfer fluid from the receiver and connect to the fixed field piping are

required. The proven flex design accommodates the tracking motion of the receiver and has a life expectancy greater than 15 years.

3.2.1.5. Drive and Controls

Controlled by an Honeywell Fluxline Control System, the collectors track the sun continuously during the day. A single drive motor operates the four rows of RMT modules. The microprocessor monitors safety devices that measure sun, wind, fluid flow, and system temperatures. System operating data can also be recorded for local or remote computer access. The system stows the concentrators upside down in high winds and at night to protect the reflective surface and receivers.

3.2.2. Cold storage

The cold thermal energy storage (CTES) system that was selected for the second installation is the ice-encapsulated type. Compared to other static ice-making systems, such as the ice-on-coil type, the ice-encapsulated type offers the advantages of the relatively low cost, simplicity and wider heat exchange area. The phase change material (PCM), in this case de-ionized water, is encapsulated in spherical capsules of relatively small diameter of 77 mm (Figure 3-23). The capsules are packed into a conventional tank (Figure 3-22) and the void volume around the capsules is filled with refrigerant fluid (water glycol) (Figure 3-25).

Figure 3-22 The PCM cold storage.

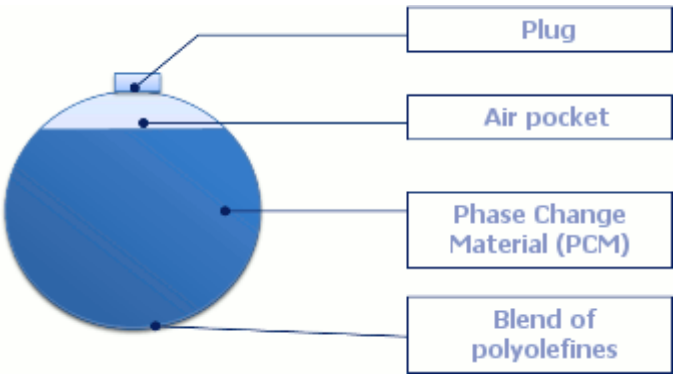

Figure 3-23 PCM capsule

During the charging phase, cool refrigerant flows around the capsules and ice starts forming from the internal surface towards the centre of the capsules (see Figure 3-24). The capsules are conceived to allow for expansion of the PCM during the solidification process of water. During the discharge phase, the same refrigerant circulates around the capsules and gets chilled by the ice contained in the capsules. The ice starts melting, again from the internal surface towards the centre of the capsules (see Figure 3-26).

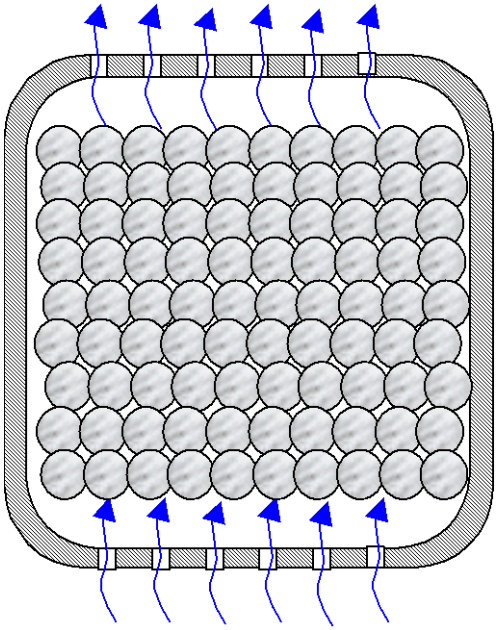

Figure 3-25 Ice-encapsulated storage.

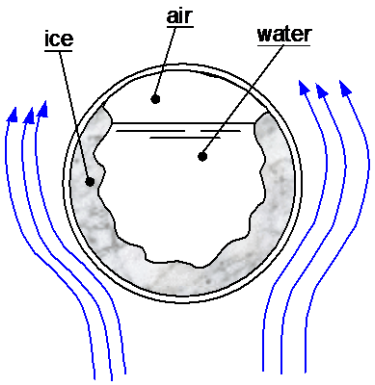

Figure 3-24 Capsule charge phase

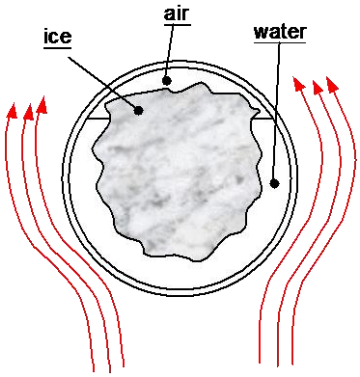

Figure 3-26 Capsule discharge phase

The capsules are made of polymeric materials (polyolefine), which allows for good thermal conduction, high mechanical resistance to repeated charge-discharge cycles and low cost.

Figure 3-27 The parabolic trough collectors installed on the roof of the plant in Morocco.

4. Chapter Four: Performance Figures and Monitoring Systems

Monitoring of installed solar assisted cooling systems represents a fundamental tool in order to optimize the monitored system itself and to draw conclusions for the optimization of the design and control for future installations. This is especially true for a technology in an early stage of application as it is the case for solar assisted cooling systems.

In order to allow a clear comparison between monitoring results of different installed systems, and as well between measured and simulated values, a comprehensive and unified monitoring procedure is required. Such a monitoring procedure which has been developed within the framework of the international perennial years project – Task 38 Solar Air-conditioning and Refrigeration – under the umbrella of the International Energy Agency (IEA) Solar Heating and Cooling Programme has been applied in this project (Sparber, Thuer, Besana, Streicher, & Henning, 2008).

The discussion about which performance figures to be considered is basically based on the fact that the main reason to use solar energy for air-conditioning and refrigeration is to reduce the consumption of conventional energy sources (i.e., fossil fuels and electricity). Therefore, energy performance is a key issue when designing solar-assisted air-conditioning systems. Of course, economic parameters are equally important and a combined analysis of energy and economic performance can help to select the configuration which leads to the highest energy savings for a given investment. (H.-M. Henning, 2004).

The performance figures developed by the unified monitoring procedure were mainly primary energy oriented, other interesting performance figures used in the literature are considered in this chapter as well, such as the solar cooling ratio (SCR) which will be defined later in this chapter.

4.1. Monitoring objectives

It is crucial to define the monitoring activities objectives before any sensor or hardware is selected; this was done to avoid that hardware and monitoring conception may be inappropriate for the particular monitoring task, or critical data points may be overlooked.

4.1.1. System level

Figure 4-1 presents the overall system scheme for the first installation in Tunisia, the energy inputs and outputs to the solar cooling system -surrounded by the red rectangle- is the main focus and not the performance of each single component, and thus the main objectives for monitoring on system level are:

- Identify the system contribution to end user's energy demand and the total primary energy savings.
- Identify inefficiencies or improper design at a system level.
- Verify design goals achievement at a system level.

- Investigate the influence of various control strategies on the system performance.
- Identify maintenance needs required at a system level.
- Provide accurate performance data to feed the system simulation model.
- Provide experimental data to identify possible modifications to be implemented on the plant in order to improve the system performance.

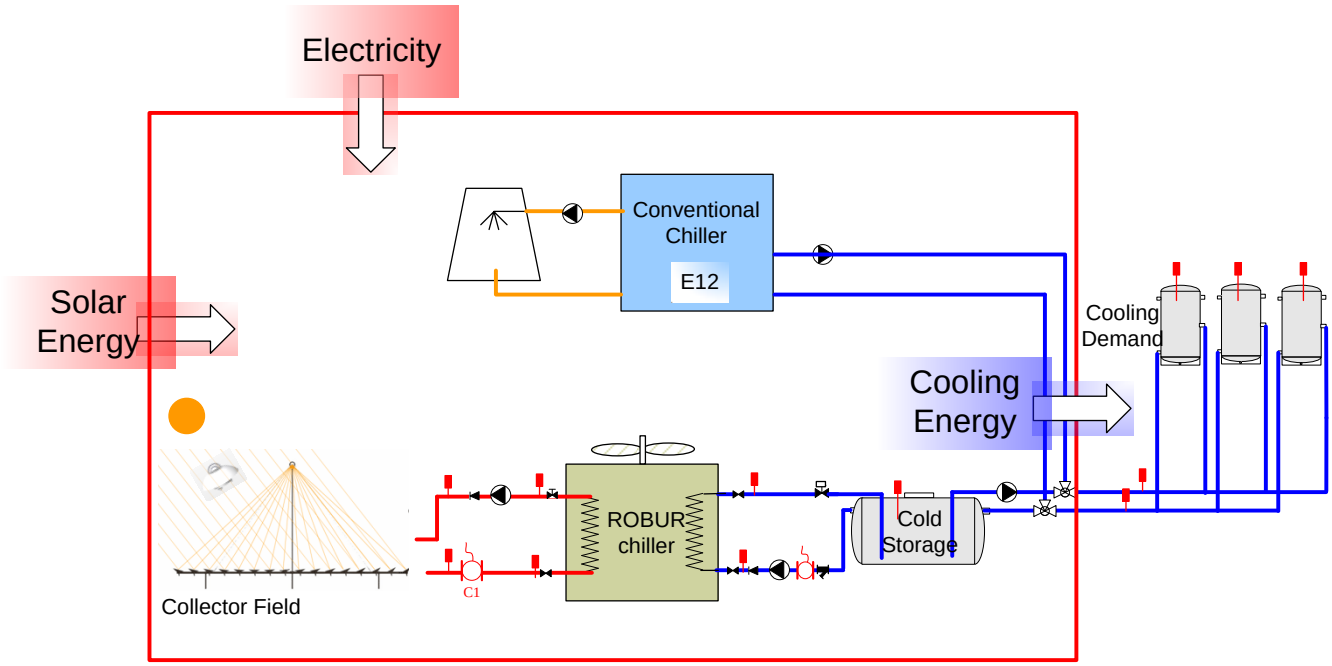

Figure 4-1 Input and output energy flows to the system.

4.1.2. Component level

The main monitoring objectives for the analysis at component level are:

- Verify the performance of the system components compared to the manufacturer data.
- Profile the energy performance of the main system components:
  - The concentrating solar collector.
  - The thermally driven chiller.
  - The cold storage.
- Provide experimental data to feed the parameter identification and model validation process.

4.2. Unified monitoring procedure

During my frequent participation in the experts sessions related to data monitoring and analysis of Task 38, I contributed to the development of a comprehensive and unified monitoring procedure. The latter, in order to allow a clear comparison between monitoring results of different installed systems, evaluating the primary energy ratio and other energy performance figures. The procedure describes the sensors required to evaluate a specific performance factor, and also it put constrains on the acceptable uncertainty of the sensors and the monitoring system to ensure the quality of the analysis.

In this section, the unified monitoring procedure developed within Task 38 is described; as well as its utilization for the analysis of the performance data of the monitored system in this project is explained.

In order to have a common starting point for the single monitoring levels a basic scheme and a reference system had to be defined. Figure 4-2 and Figure 4-3 present respectively the proposed reference solar assisted heating and cooling (SHC) system and the conventional reference system.

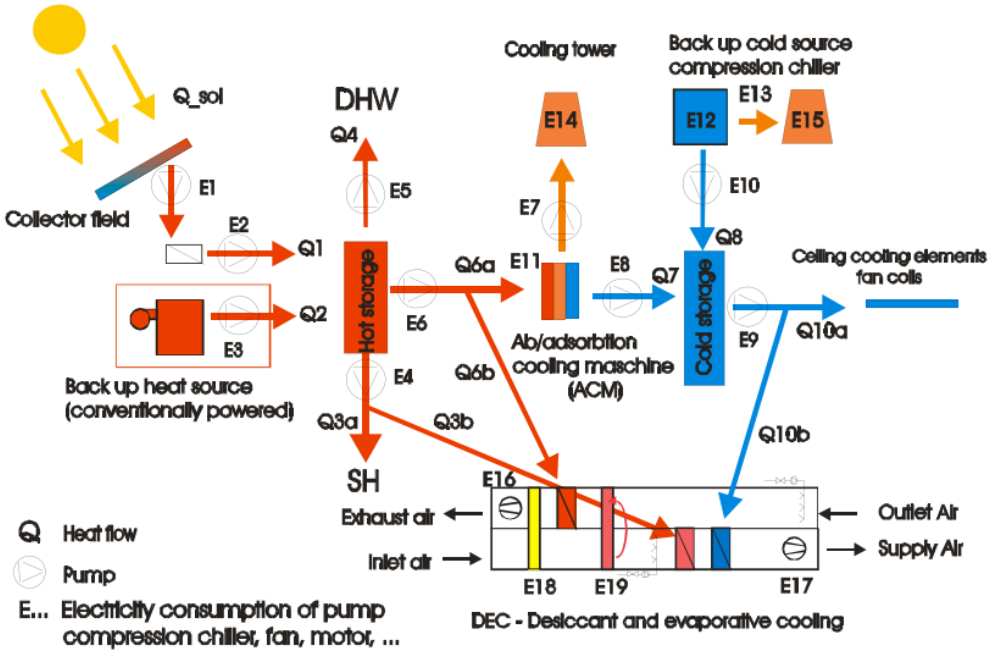

Figure 4-2 Proposed reference solar heating and cooling system including the single energy fluxes (SHC Max System)

The main energy fluxes presented in the Figure 4-2Figure 4-2 are the heat delivered for space heating SH (Q3), the heat delivered for domestic hot water DHW (Q4), the cold supplied to the end user SC (Q10) and the heat supplied to the system by the backup heat source (Q2).

The proposed schematic of the conventional reference system (Figure 4-3) consists of a compression chiller for the cooling application and a conventionally powered backup heat source for SH and DHW applications.

For the elaboration of the unified monitoring procedure several boundary conditions have been considered. On one hand the procedure defines minimum requirements to be respected by all running monitoring projects, on the other hand detailed data and single energy flows should be measured where feasible in order to acquire a possibly complete picture of the functioning and to allow detailed analysis. The procedure should allow a comparison between different systems and as

well permit to draw (with the results) a learning curve over the coming years on the cost development of installed solar assisted heating and cooling systems.

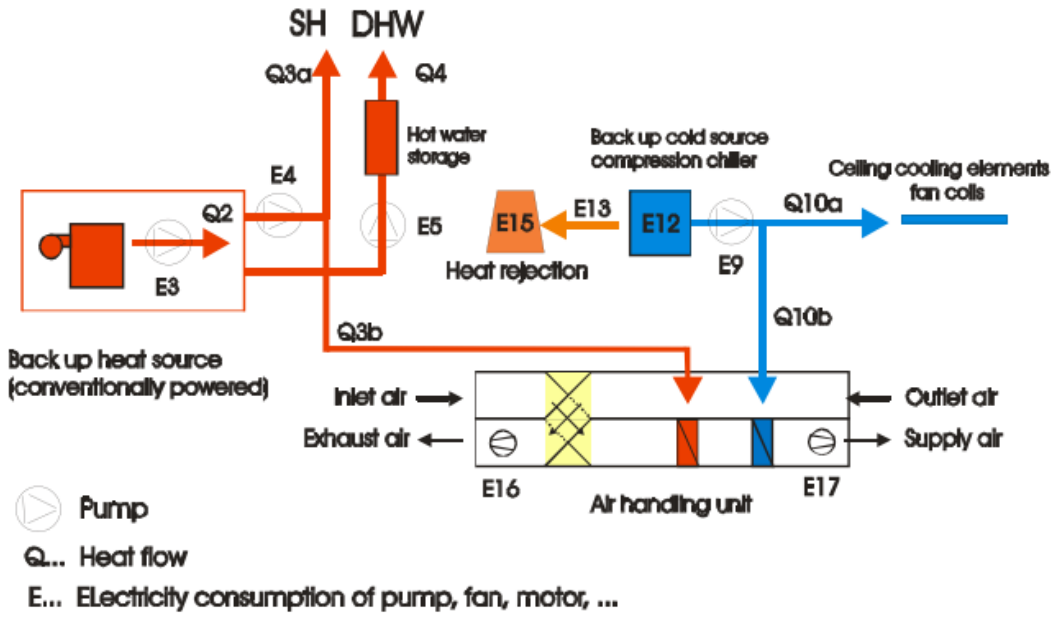

Figure 4-3 Proposed schematics of the conventional reference systems including the single energy fluxes

The procedure is subdivided in three different levels of complexity, allowing a first evaluation with a limited set of sensors or a precise evaluation with a full monitoring system. Further a short explanation of the three levels is given.

First level: The first level of the procedure permits to acquire basic information on cost and performance (on primary energy level) of the system with a limited number of sensors. Within this level, four heat meters and the electricity counters for the measurement of the electricity consumption of the overall system are required. In Figure 4-4 the scheme with the measured energy fluxes is presented.

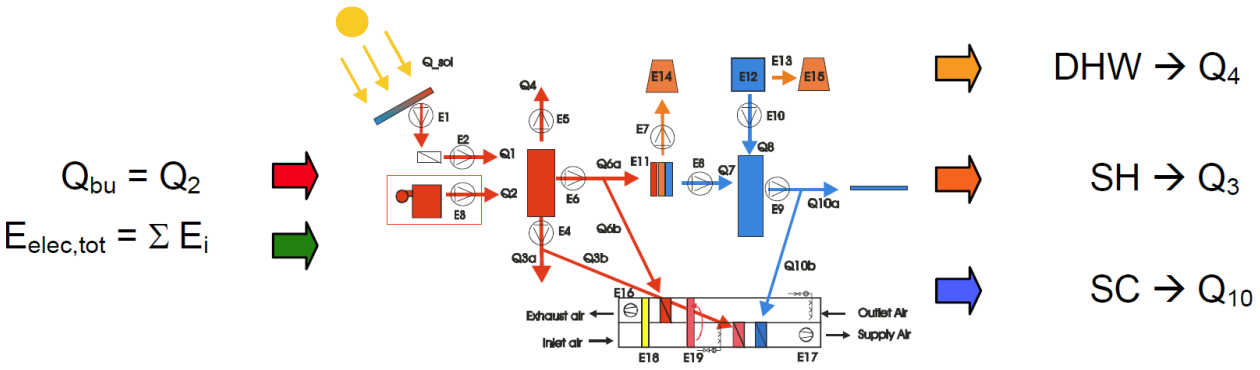

Figure 4-4 Energy Flux measured in the first level.

The Primary Energy Ratio (PER) of the solar assisted cooling system is defined as the cooling and heating energy delivered by the system and the consumption of primary energy, it can be calculated as shown in Equation 1:

$$PER = \frac{(Q_3 + Q_4 + Q_{10})}{\frac{Q_2}{\varepsilon_{fossil} . \eta_{boiler}} + \frac{E_{elec,tot}}{\varepsilon_{elec}}} \qquad \text{Equation 1}$$

Where the heat and electricity fluxes are measured and the primary energy conversion factors for heat and electricity from fossil fuels have been considered as the following values (based on European Directives (European Parliament, 2006), Task 25 and Task 32):

- ε_{elec}= 0.4 (The primary energy conversion of electricity: kWh of electricity per kWh of primary energy)
- ε_{fossil} = 0.9 (The primary energy conversion of fossil fuel: kWh of heat per kWh of primary energy)
- η_{boiler}= 0.95 (boiler efficiency)

In general it has to be stated that the conversion and performance factors given in the European directives are based on literature and discussion agreements but have to be considered only as proposals for calculation and comparison; as they depend on different aspects such us country specifications, technology and component size. The PER of a reference system (see Figure 4-3) can be calculated as shown in Equation 2:

$$PER_{ref} = \frac{(Q_3 + Q_4 + Q_{10})}{\frac{Q_3 + Q_4}{\varepsilon_{fossil} . \eta_{boiler}} + \frac{Q_{10}}{SPF_{ref} . \varepsilon_{elec}} + \frac{E_{elec,tot\_ref}}{\varepsilon_{elec}}} \qquad \text{Equation 2}$$

In this equation the heat and electricity fluxes are again the measured values. Within the calculation of the electricity consumption of the reference system the consumption of the pumps of solar circuit loop and of the absorption chiller have to be subtracted as shown in Equation 3:

$$E_{elec,tot\_ref} = E_{elec,tot} - (E_1 + E_2 + E_6 + E_7 + E_8 + E_{10} + E_{11} + E_{14} + E_{18} + E_{19}) \qquad \text{Equation 3}$$

The Seasonal Performance Factor (SPF) of the reference compression chiller has been set to:

- SPF_{ref} = 2.8 (compression chiller efficiency of the reference system)
- $\eta_{boiler,\ ref}$ = 0.95 (reference boiler efficiency)

Based on the proposed reference solar assisted heating and cooling (SHC Max system) shown in Figure 4-2 and the actual configuration of the first solar cooling system installed in Tunisia (dedicated to cooling only rather than heating and domestic hot water preparation) the scheme have less energy fluxes. The monitoring scheme of the solar cooling system in Tunisia with the energy fluxes to be measured are presented in Figure 4-5.

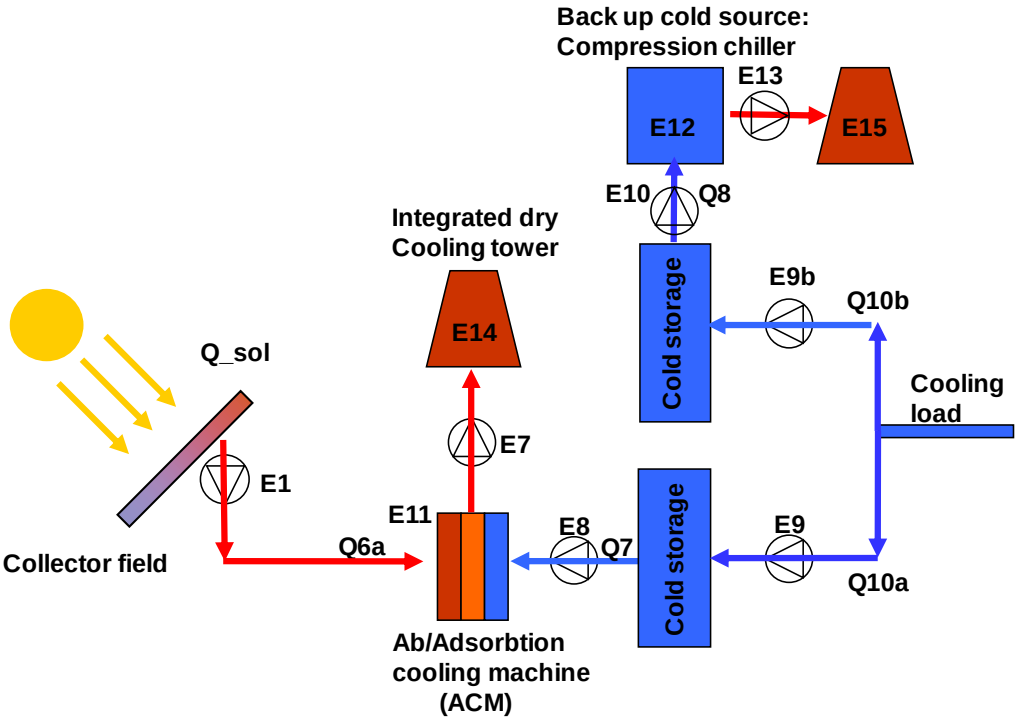

Figure 4-5 Monitoring scheme of the solar cooling system installed in Tunisia based on the unified monitoring procedure.

Based on the scheme of Figure 4-5, the primary energy ratio of the solar assisted cooling system shown in Equation 1 is reduced to Equation 4:

$$PER = \frac{Q_{10}}{\frac{E_{elec\,,tot}}{\varepsilon_{elec}}}$$ Equation 4

Where $E_{elec,tot}$ is the total electricity consumption of the solar cooling system components (absorption chiller, heat rejection system and circulating pumps). And the PER of a corresponding reference system can be calculated as shown in Equation 5:

$$PER_{ref} = \frac{Q_{10}}{\frac{Q_{10}}{SPF_{ref}\,.\,\varepsilon_{elec}} + \frac{E_{elec\,,tot\,\_ref}}{\varepsilon_{elec}}}$$ Equation 5

Where $E_{elec,tot,ref}$ is the total electricity consumption of the reference system components (compression chiller, heat rejection system and circulating pumps).

From the financial point of view the overall cost per installed cooling capacity can be calculated as following:

$$\text{Specific solar assisted cooling installation cost} = \frac{Cost\ (€)}{kW_{cold}}$$ Equation 6

The cost term (€) includes the costs of all components shown in Figure 4-2 minus the appliances deployed in the corresponding conventional reference system Figure 4-3; such as back up heating / cooling system and eventually installed cogeneration systems.

Second level: The second level requires an increased number of sensors with respect to the 1st level. In fact, two heat counters and a pyranometer have to be added to the 4 heat counters and the total electricity counters already present in the previous section. The monitoring for this level is mainly focused on the solar thermal energy management (see Figure 4-6).

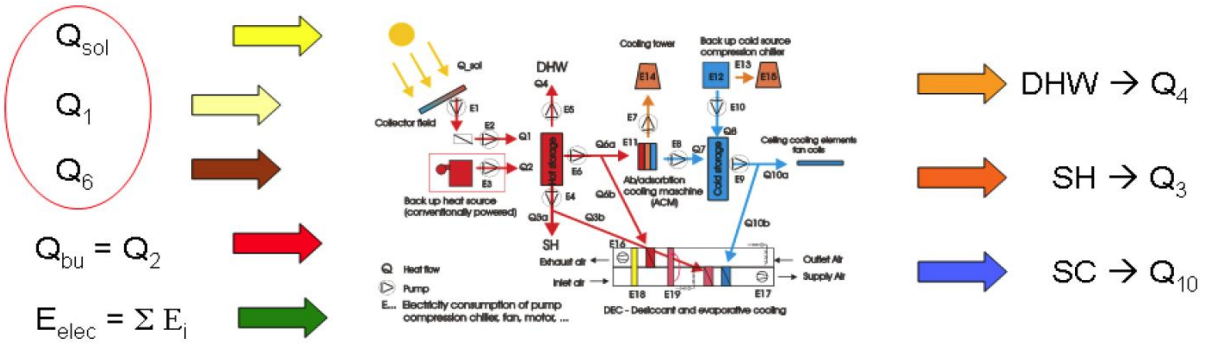

Figure 4-6 Second level monitoring scheme including the measured inputs and outputs of the solar assisted

Based on the monitoring output of the sensor in this monitoring level, the collector efficiency can be calculated according to Equation 7:

$$\eta_{\text{coll ,net}} = \frac{Q_1}{Q_{sol}} \qquad \text{Equation 7}$$

Where Q_1 is the useful gain of the solar collector, and Q_{sol} is the beam solar irradiance that hits the solar collector aperture area. The absorption chiller's thermal coefficient of performance COP_{th} can be calculated as follows:

$$\text{COP}_{\text{th}} = \frac{Q_7}{Q_6} = \frac{Heat\ flux\ extracted\ at\ low\ temperature}{Driving\ Heatflux\ supplied\ to\ the\ generator\ of\ the\ chiller} \qquad \text{Equation 8}$$

The electrical COP of the solar cooling system represents the ratio of the cooling power produced by the system in [kWh] to the total electricity consumption of the system components (absorption chiller, heat rejection system and circulating pumps) in [kWh]. The COP_{elec} of the solar cooling system has been calculated based on equation 9 below:

$$\text{COP}_{\text{elec}} = \frac{Q_7}{E_{elec\ ,tot}} \qquad \text{Equation 9}$$

4.3. Monitoring system

The monitoring system consisted of global and diffused pyranometers, thermometers and electromagnetic and ultrasonic flow meters. All these sensors have been connected to a data acquisition system that is connected to a computer. A data acquisition application was developed using the platform LabView and installed on the computer onsite, the computer was connected to internet so that it would be remotely accessible from anywhere by means of credentials accounts. The monitoring system made possible the assessment of the system´s performance both on system level and on component level. The monitoring system acquires data from the three loops; the solar loop, the absorption chiller and the cold storage circuit. The main monitoring parameters of each circuit are summarized in Table 4-1 and on the scheme in Figure 4-7Figure 4-7 .

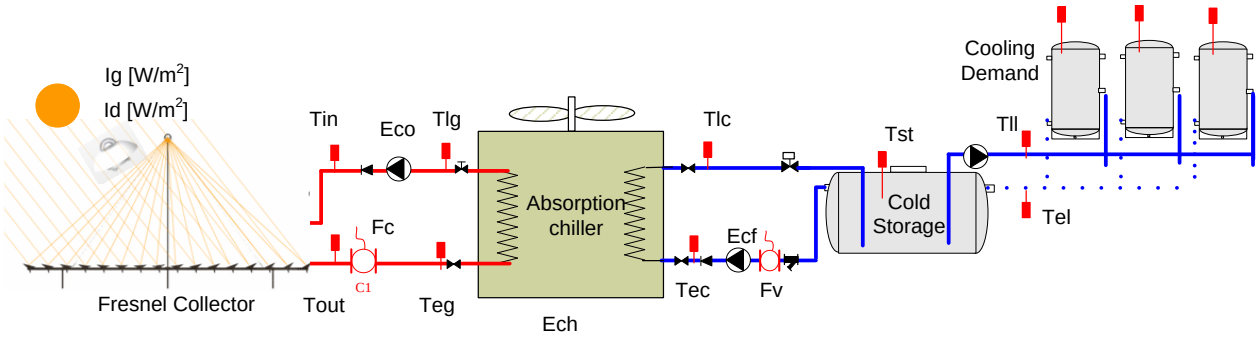

Figure 4-7 Monitoring system indicating monitored parameters.

Table 4-1 Main monitored parameters in the three loops of the system.

Circuit	*Monitored Parameters*	*Nomenclature*	*Unit*
	Global radiation on horizontal	G	W/m²
Solar Loop	Diffused radiation on horizontal	Gd	W/m²
	entering collector temperature	Tin	°C
	leaving collector temperature	Tout	°C
	Collector flow rate	Fc	m^3/s
	Electricity consumption of primary pump	Eco	W
Absorption	Entering generator temperature	Teg	°C
Chiller	Leaving generator temperature	Tlg	°C
	Generator flow rate	Fg	m^3/s
	Entering evaporator temperature	Tev	°C
	Leaving evaporator temperature	Tlv	°C
	evaporator flow rate	Fv	m^3/s
	Electricity consumption of secondary pump	Ecf	W
	Electricity consumption of the absorption chiller and the condenser´s fan.	Ech	W
	Entering from chiller temperature	Tlv	°C
Cold Storage	Leaving to chiller temperature	Tev	°C
	Chiller flow rate	Fv	m^3/s
	Entering from load temperature	Tel	°C
	Leaving to load temperature	Ell	°C
	Load flow rate	Fl	m^3/s
	Storage temperature	Tst	°C

4.4. Measuring Devices

In the following sections, the sensors used for the monitoring system are described in details regarding technical and practical aspects.

Two pyranometers were used to measure the global and diffused radiation on the horizontal surface. The beam radiation on horizontal surface was calculated by subtracting the diffused radiation (global

pyranometer with shadow band) from the global radiation. The DNI direct normal radiation was calculated by considering the beam radiation on horizontal surface and the incident angle.

The resistance temperature detectors (PT100) that have been used were calibrated within their temperature operation range using a calibration bath with the capability of working at temperature range from (-50 – 200) °C. These sensors were installed in a way to be countering the fluid flow in order to achieve a sufficiently good heat transfer between the fluid and the sensor and hence better response to temperature variance.

An ultrasonic flow meter was used in the solar loop, which in addition to its high accuracy can withstand the high temperatures in the solar loop (up to 200 °C). In the other two circuits electromagnetic flow meters were used. The list of sensors used in the monitoring system is presented in Table 4-2.

Table 4-2 Summary of sensors used in the monitoring system.

Measurement type	***Sensor type***	***Signal***	***Unit***	***Uncertainty***
Temperature in fluid loop	Thermometers PT100 Class 1/10 DIN	4-wire resistance Ω	°C	±0.03 °C @ 0 °C
Volume flow	▪ Ultrasonic flow meter ▪ Electromagnetic flow meter	0-20 mA	m^3/s	± 0.5% of measured value
Solar radiation ▪ Global ▪ Diffused	▪ Pyranometer ▪ Pyranometer with a shadow band	1-5 V	W/m^2	< 5% Daily uncertainty First class

4.4.1. Solar radiation measurements

Measuring the solar radiation is certainly of high importance for the estimation of the performance of a solar cooling system. Moreover, when using concentrating solar collectors, it is important not only to measure the total horizontal irradiance, but also the direct beam irradiance that hits the solar collectors.

For measuring the total solar radiation a pyranometer device was selected.

For measuring the direct solar radiation, two options were possible, the first which is to use a pyrheliometer that tracks the sun continuously and measures only the direct solar radiation as required, and the second is to use another pyranometer with a shadow band in order to allow it to

measure the diffused radiation only. Then the direct radiation can be calculated as the difference between the total solar radiation and the diffused solar radiation. (See Figure 4-8)

Even though the first option seems more straightforward solution, the high cost of the pyrheliometer with its tracking system compared to the pyranometer with a shadow band favored the second option. And hence, two pyranometers were installed on a horizontal surface; one of them is equipped with a shadow band that is adjusted manually each two weeks.

Pyranometers from the manufacturer LSI LASTEM s.r.l. were used for the first plant in Tunisia, and pyranometers from the manufacturer Kipp and zonen were installed at the second plant in Morocco. Both pyarnometers satisfy the first class accuracy requirements. The main characteristics of both pyranometers are presented in Table 4-3.

Table 4-3 Characterestics of used pyranometers.

	Kipp & Zonen	***LSI LASTEM s.r.l***
Spectral range	285 to 2800 nm	300 to 3000 nm
Sensitivity	7 to 14 µV/W/m²	30 to 45 µV/W/m²
Response time	< 5 s	27 s
Temperature dependence of sensitivity (-10 ºC to +40 ºC)	< 1 %	< 4 %
Operating temperature range	-40 °C to +80 °C	-40 °C to +80 °C
Maximum solar irradiance	4000 W/m²	2000 W/m²
Field of view	180 °	180 °

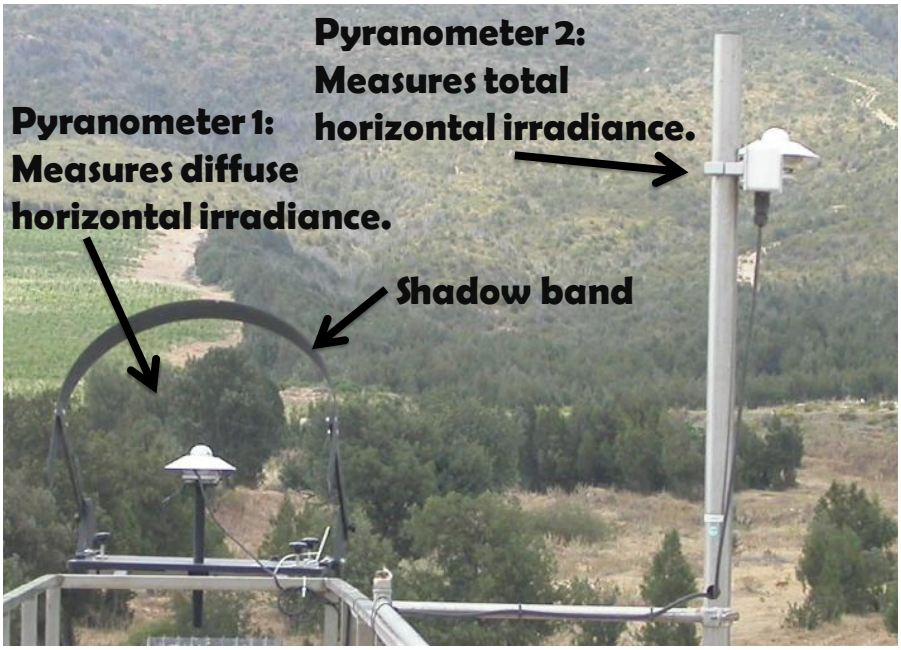

Figure 4-8 Total and diffused irradiance measuring pyranometers.

All radiometers were supplied with a calibration report produced by comparison, under the sun (ISO 9847), with a radiometer calibrated at the World Radiation Center WRC-PMOD in Davos.

4.4.2. Temperature Measurements

Temperature measurements were carried out using resistance temperature detector (RTD) thermometers. The selected RTD thermometers are industrial platinum resistance thermometers (IPRT) of the type PT100 (Figure 4-9).

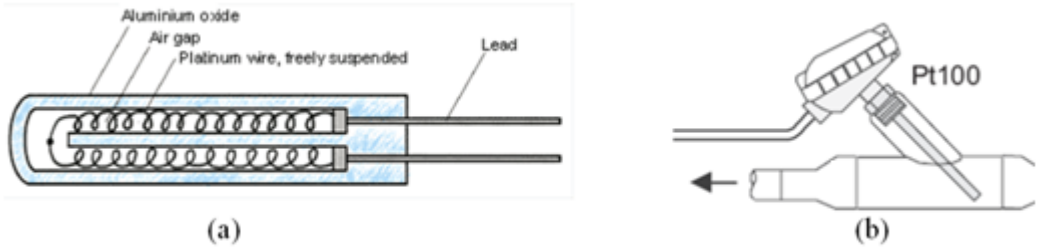

Figure 4-9 RTD sensor internal structure (a), and installation in the pipe (b).

Regarding the uncertainty of the used sensors, the majority of the used sensors are of class A, However it was required to use some sensors of class 1/10 DIN which are more accurate for a specific measuring points. The uncertainties of classes A and 1/10 DIN is presented in Table 4-4.

Table 4-4 Uncertainty of PRT of class 1/10 DIN and class A.

Class A	*Class 1/10 DIN*	*At temperature [°C]*
±0.19 °C	±0.04 °C	-20 °C
±0.15 °C	±0.03 °C	0 °C
±0.35 °C	±0.12 °C	100 °C
±0.55 °C	±0.22 °C	200 °C

The sensors diameter is 6mm, and the length of the proofs ranges from 200-600mm, depends on whether it is used to measure the temperature inside a pipe or a tank. (See Figure 4-10)

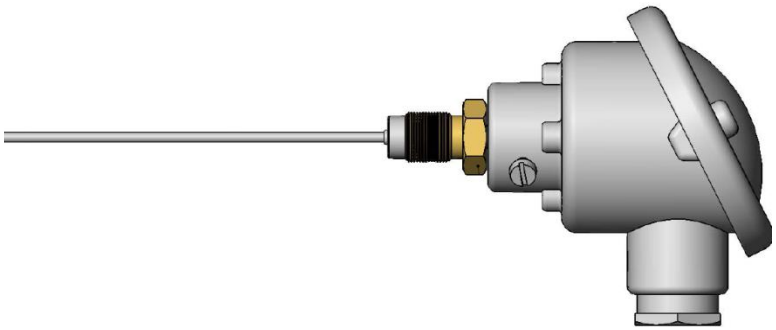

Figure 4-10 Pt100-detector mounted in protection tube.

These thermometers are manufactured to withstand temperatures up to 250°C, which is higher than the maximum temperature within the system. However, specially manufactured types of IPRT can withstand temperatures up to 650°C.

Sensors used in the plants are used for both the monitoring and the control of the plant, and terminal heads of the sensors could be either a probe mounted terminal block or a probe mounted transmitter based on the required functionality of the sensor:

4.4.2.1. Probe mounted terminal block. (Figure 4-11)

This type of connection was used for sensors connected to the data acquisition system, were the signal was transmitted to the data acquisition system and analyzed in the terminal block as will be explained in the data acquisition system description.

Figure 4-11 Probe-mounted terminal block.

4.4.2.2. Probe mounted transmitter. (Figure 4-12)

This type of connection was used for sensors connected to the control system, where a digital output is required, and the measured value is converted and transmitted.

Figure 4-12 Probe-mounted transmitter.

Pt100 sensors can have two, three or four wires. The main advantage of the four-wire connection is that it reduces the error result from the leads resistance, and thus the measured values have a better accuracy. Thus the four-wire connection was used for the monitoring system. The electrical current

and the signal are separated into two circuits, which render the unbalance in the resistances of the wires insignificant.

4.4.3. Flow rate measurements:

The number of relevant factors to be considered when specifying a flowmeter for a particular application is very large. These include the temperature and pressure of the fluid, its density, viscosity, chemical properties and abrasiveness and whether it contains particles. The required performance factors of accuracy, measurement range, acceptable pressure drop, output signal characteristics, reliability and service life must also be addressed. (Morris, 1996)

Based on the aforementioned factors, Electromagnetic flow meters have been chosen to measure the flow rate in the system loops. However, due to the high temperatures in the solar loop that the line of a standard electromagnetic flowmeter can not withstand, it was decided to use an ultrasonic flowmeter.

4.4.3.1. Electromagnetic Flow meter

The electromagnetic flow meters used are form the producer Krohne, called OPTIFLUX 4040 C which is a 2-wire technology electromagnetic flowmeter. The operational temperature of the thermal fluid is in the range (-10 to 30°). The technical data of the flowmeter are presented in Table 4-5.

It has to be mentioned that the flowmeters were installed outdoors, and due to the high solar radiation and ambient temperature they were covered for protection from direct solar radiation as shown in Figure 4-13.

Table 4-5 Electromagnetic Flow meter characteristic.

Measuring range	0,3...12 m/s (1...40 ft/s)
Process conditions	Liquids with maximum solid particle / gas content < 3% (by volume)
Inaccuracy (under reference conditions)	± 0,5 % of measured value
Conductivity	Non-water ≥ 5 µS/cm Water ≥ 20 µS/cm
Power supply	Mains supply 100…240 V AC (48...63Hz) +10% / -15%

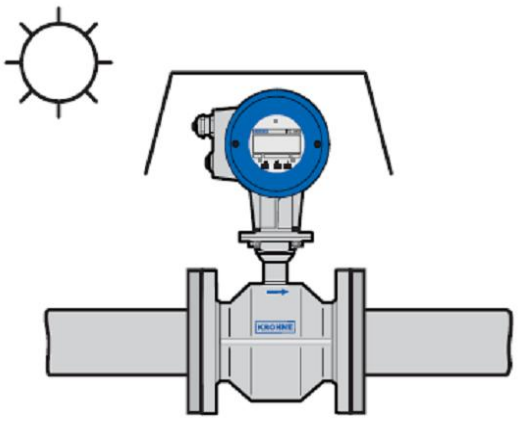

Figure 4-13 The electromagnetic flow meter installed and shaded from the sun.

4.4.3.2. Ultrasonic flowmeters

The ultrasonic flow meter used is UFM 3030 liquid process flow meter from the producer "Krohne" consists of a UFS 3000 flow sensor and a flow converter, UFC030. The flow sensor was built together with the flow converter as a compact flow meter (see Figure 4-14).

The main characteristics of the ultrasonic flow meters are:

- Independent of conductivity, viscosity, temperature, density and pressure of the fluid.
- No moving or intruding parts, therefore no pressure loss or wear
- Three beams generate a measurement effectively independent of flow profile
- No material build-up as unobstructed flow sensor with smooth surface finish.

The technical data of the flowmeter are presented in Table 4-6.

Table 4-6 Ultrasonic Flow meter characteristic.

Measuring range	v = 0 to 20 m/s (0 ft/s to 66 ft/s)
Measuring error (under reference conditions)	v = 0,5 to 20 m/s (1.5 to 60 ft/s): < ± 0.5% of measured value
Repeatability (under reference conditions)	± 0,2% of measured value
Process conditions	Maximum solid particle content < 5% (by volume)

Figure 4-14 Ultrasonic flowmeter, consists of a flow sensor and a flow converter.

4.4.4. Electricity meter

A three phase electrical supply provides the power required by the solar cooling system components; pumps, absorption chiller, control valves and control system. The total electrical consumption of the system was measured using an electronic wattmeter that measures the instantaneous current in the load and the voltage across the load, and based on this instantaneous power the wattmeter calculates the average power in watts.

Figure 4-15 The electricity meter used.

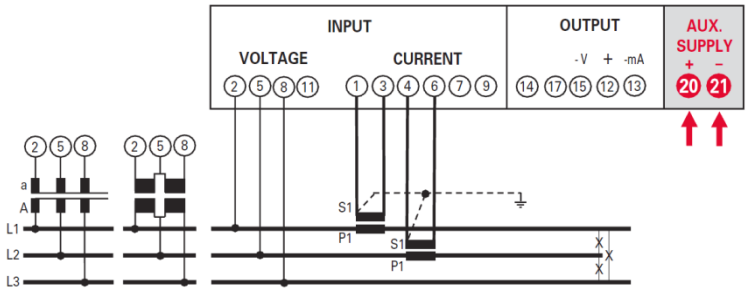

Figure 4-16 Connection of the electrical supply to the electrical meter.

The selected wattmeter is Tema fp from the Italian manufacturer IME corresponds to The International Electrotechnical Commission (IEC) standard IEC *60688* which recommends a transducer of *class 0.5* or better (which means a maximum error of 0.5 percent at rated power) (See Figure 4-15 and Figure 4-16).

4.4.5. Data Acquisition:

In order to analyse, visualize and store the measured data by the four types of sensors (thermometers, pyranometers, flowmeteters and wattmeter) it is necessary to use a data acquisition system.

Data acquisition DAQ is the sampling of the real world to generate data that can be manipulated by a computer. Data acquisition typically involves acquisition of signals and waveforms and processing the signals to obtain desired information. A DAQ system consists of sensors, DAQ measurement hardware, and a computer with programmable software. A simplified scheme of data acquisition system is shown in Figure 4-17.

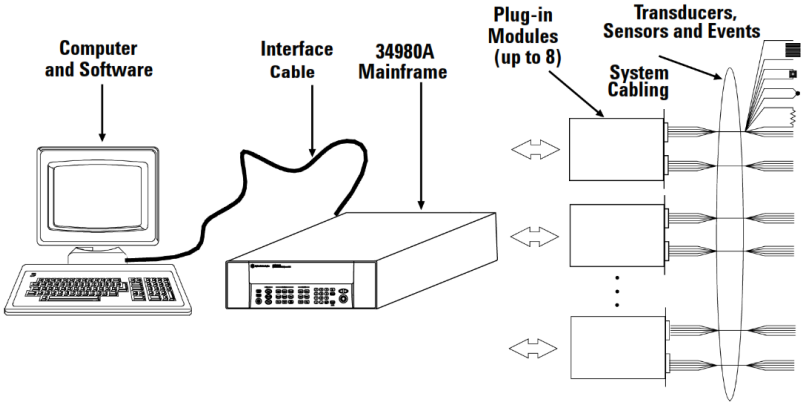

Figure 4-17 A simplified scheme of the data acquisition system.

Cables of the sensors were collected in a junction box in the centre of the plant, from which a single cable was extended to the office room where the data logger and the PC are located. The distance between the plant and the office room is about 60m.

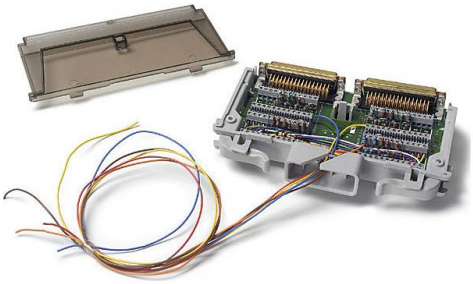

Figure 4-18 (Agilent 34921T) Terminal block.

Figure 4-19 (Agilent 34980A) multifunction switch, and different plug-in modules.

All the sensors cables were connected to (Agilent 34921T) terminal block (Figure 4-18) , which is connected to the (Agilent 34921A 40-channel multiplexer) (see Figure 4-19) which is a multiplexer for general purpose scanning. This plug-in module is plugged in the switching and data acquisition platform (Agilent 34980A Multifunction Switch/Measure Unit) (see Figure 4-19). The uncertainty of the data acquisition system (Agilent 34980A) accounts for 0.06 °C when using an RTD thermometer.

The data acquisition, processing and storing, are achieved through a virtual instrument VI developed with the help of the graphic programming software LabVIEW (see Figure 4-20). The data are stored in the computer hard disk in a universal format, allowing for its subsequent processing with a datasheet software. The computer was connected to internet so that it would be remotely accessible from anywhere by means of credentials accounts.

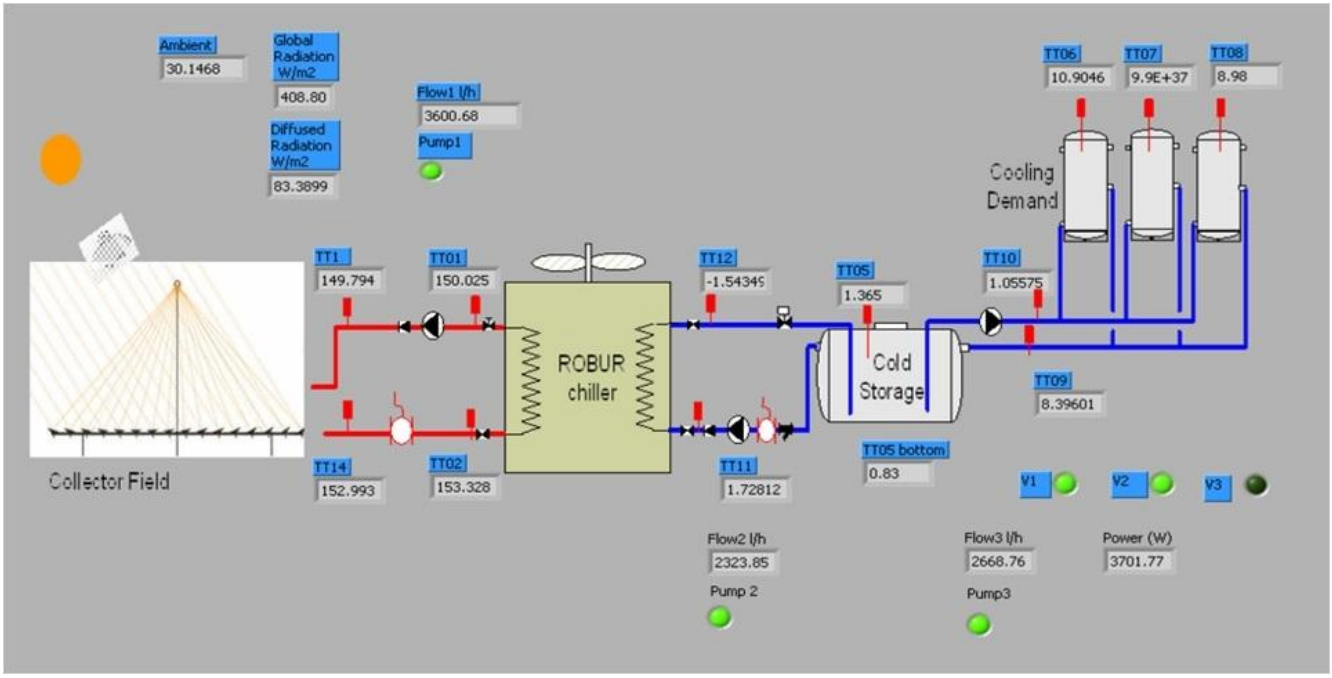

Figure 4-20 The graphical user interface of the virtual instrument programmed using LabVIEW software platform.

4.5. Measuring devices calibration (Thermometers)

Instrument calibration consists of comparing the output of the instrument under test against an instrument of known accuracy when the same input is applied to both instruments. This procedure is carried out for a range of inputs covering the whole measurement range of the instrument. Calibration insures the measuring inaccuracy of all instruments used in a measurements system is known over the whole measurement range, provided that the instruments are used in environmental conditions which are the same as those under which they were calibrated.

Basically the thermometer consists of the detector, the connecting chain and the readout instrument. Thermometers were calibrated by the comparison method which is performed in four basic steps:

1. The reference probe and the Unit Under Test (UUTs) were placed in the temperature source (calibration bath) in close proximity to one another at the same depth in the calibration bath, it has be mentioned also that the calibration bath should have some kind of a stirrer that moves the fluid and ensure a homogenous temperature in the bath.
The reference probe is a RTD sensor that was calibrated certified by the (Calibration center 104) in Italy. The temperature source is the calibration bath (Micro-baths 7103) from Hartscientific company which works in the range between -30 to 150 °C (see Figure 4-21 and Figure 4-22).

2. The leads of the thermometers to the DAQ were connected using to proper 4-wire connections.
Both the reference probe and the UUTs were connected to the same DAQ to ensure that the calibration process takes into consideration all the error sources associated with the measurements chain.

3. The DAQ Measures the reference probe and the UUTs resistances and determines the temperatures. This procedure was repeated for each temperature point.

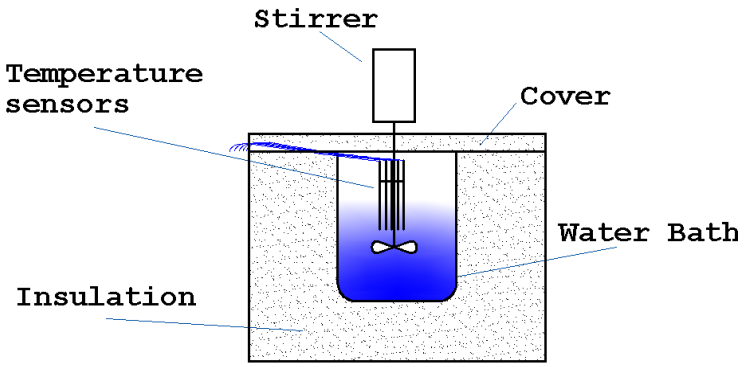

Figure 4-21 The setup of oil bath used for thermometers calibration.

Figure 4-22 The calibration bath.

4. Data fitting.

The temperature measured by the UUT is corrected using equation 10. Then, the difference between the reference temperature and the corrected temperature is calculated for each calibration point.

$$T_{corrected} = T_{measured} + k_0 + k_1 \times T_{measured} + k_2 \times T_{measured}^{\ 2} \qquad \text{Equation 10}$$

This difference is then raised to the power 2, and the summation of the squared error is minimized by varying the fitting coefficients k_0, k_1 and k_2 using the solver function in the excel software. A sample of the fitting procedure tables is presented for the sensor TT12 which measures the cold output temperature of the absorption chiller.

Table 4-7 Sample of the thermometer data fitting for one probe (TT12).

Measured Temperature	Reference Temperature	Error in measurements	Corrected Temperature	Error in corrected temperature	Square of error in corrected temperature
[°C]	[°C]	[°C]	[°C]	[°C]	
-19.89182	-19.941	0.050	-19.9411	3.15E-04	9.94E-08
-9.919857	-9.956	0.036	-9.95658	-0.00101	1.02E-06
0.056	0.025	0.031	0.026232	0.00118	1.39E-06

7.4859	7.458	0.028	7.457664	-0.00049	2.43E-07
20.03032	20.013	0.018	20.03032	1.76E-02	0.000309
Summation					0.000312

Based on the calculations above, the coefficients were determined as k_0= -0.298, k_1 = 0.00042 and k_2=-2.82E-05.

4.6. References

European Parliament. (2006). *Directive 2006/32/EC of the European Parliament and of the Council of 5 April 2006 on energy end-use efficiency and energy services and repealing Council Directive 93/76/EEC, L114/76, Annex II, footnote 3*.

Henning, H.-M. (Ed.). (2004). *Solar Assisted Air-Conditioning in Buildings A Handbook for Planners* (p. 150). SpringerWienNewYork.

Morris, A. S. (1996). *The Essence of Measurements* (p. 221). Prentice Hall Europe.

Sparber, W., Thuer, A., Besana, F., Streicher, W., & Henning, H. M. (2008). Unified Monitoring Procedure and Performance Assessment for Solar Assisted Heating and Cooling Systems. *Eurosun 2008, 1st International Congress on Heating, Cooling and Building* (pp. 1-8).

5. Chapter Five: Monitoring Results

The activities related to this chapter refer to the Tunisian pilot plant, which has been running since 2008. The results reported here were obtained in the period (2009-2011). Here, the typical daily performance of the system is described, followed by a more detailed description of the system's main components performance: the collector and the chiller.

The electrical consumption of the system components is discussed afterwards, and the energy analysis and the performance figures developed in the previous chapter are applied for the analysis of the plant performance data.

5.1. Daily analysis

Figure 5-1 presents the operation of the system in a typical sunny day (1 May 2010). It can be seen that in the morning, as soon as the solar radiation level measured by the pyranometer reaches the set point (300W/m2) the solar pump and the collector tracking system start, this had happened at 7:00 am; as a result the temperature of the fluid in the solar loop is increased.

The thermal capacitance of the solar loop pipes and expansion vessel absorbs some of the useful energy gain of the collector at the beginning of the operation of the system during the warming up period.

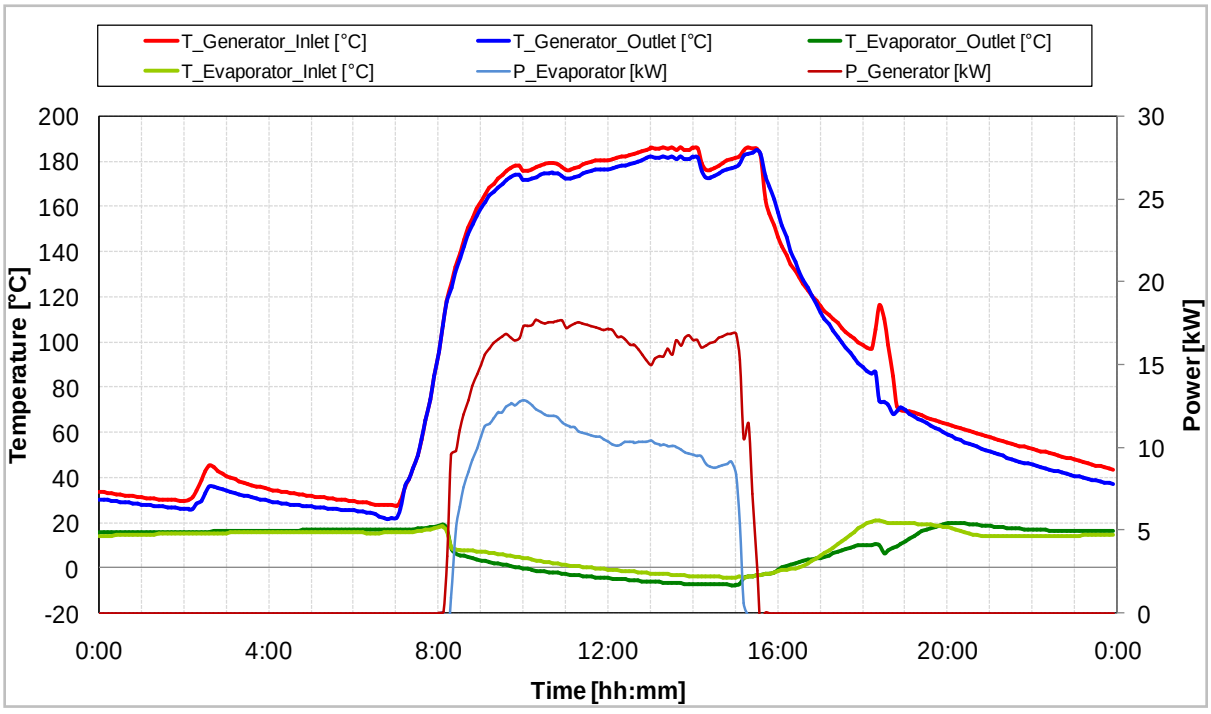

Figure 5-1 Useful gain and inlet/outlet temperatures of the collector and the chiller. (1 May 2010)

The absorption chiller starts when the input temperature to the generator reached the required set temperature (120°C), this had happened at 8:20 am. And both the collector and the chiller continued their normal operation till the output temperature of the chiller reached -8 ^{o}C, where the chiller's control switched both the chiller and solar loop's pump off. In order to ensure the complete dissipation of the cooling energy produced by the chiller, the circulation pump continues to circulate for ten minutes after the chiller is switched off.

It can be seen that at 1:40 pm the output temperature of the collector reached 185°C, and hence part of mirrors of Linear Fresnel Reflector LFR collector turned into defocus position in order to avoid overheating of the system. This automatic partial defocus function of the LFR collector tracking system continued to regulate the output temperature of the collector until 2:00 pm when some clouds partially blocked a part of the solar radiation and thus the collector output temperature was reduced due to the reduction of the solar radiation intensity. Afterwards, the output temperature starts to increase again.

It can also be seen that the cold output temperature from the chillers went down from about 8 °C at the beginning of the operation of the system to about -8°C after the chiller worked for 7 hours for that day.

5.2.Solar radiation analysis

The total solar radiation (G), which is the sum of the beam and the diffuse solar radiation on a horizontal surface, often referred to as global radiation on the surface, was measured using a pyranometer installed on a horizontal surface as mentioned in the monitoring section. The diffused radiation (Gd) is the solar radiation received from the sun after its direction has been changed by scattering by the atmosphere. It was measured using a pyranometer with a shadow band installed on a horizontal surface. The beam solar radiation (Gb), which is the solar radiation received from the sun without having been scattered by the atmosphere (beam radiation is often referred to as direct solar radiation) was calculated by subtracting the diffused solar radiation from the total solar radiation as shown in equation 1:

$$G_b = G - G_d \qquad \text{Equation 1}$$

The direct normal solar radiation (G_{bn}) is then calculated by considering the incident angle (θ) using equation 2:

$$G_{bn} = G_b / \cos\theta \qquad \text{Equation 2}$$

The incident angle (θ) for a horizontal surface is the same as the zenith angle of the sun (θz), Its value must be between 0 and 90 when the sun is above the horizon, equation 3 presents the calculation of the zenith angle.

$$\cos\theta_z = \cos\phi\cos\delta\cos\omega + \sin\phi\sin\delta \qquad \text{Equation 3}$$

Where:

ϕ is the latitude of the location where the measurements were taken.

δ is the declination angle for the specific day of measurements.
And ω is the hour angle at the measurement time.

Figure 5-2 presents the measured total and diffuse solar radiation on a horizontal surface in addition to the calculated direct solar radiation both on horizontal surface and on a surface normal to the direction of solar radiation on a winter day (5th February 2009).

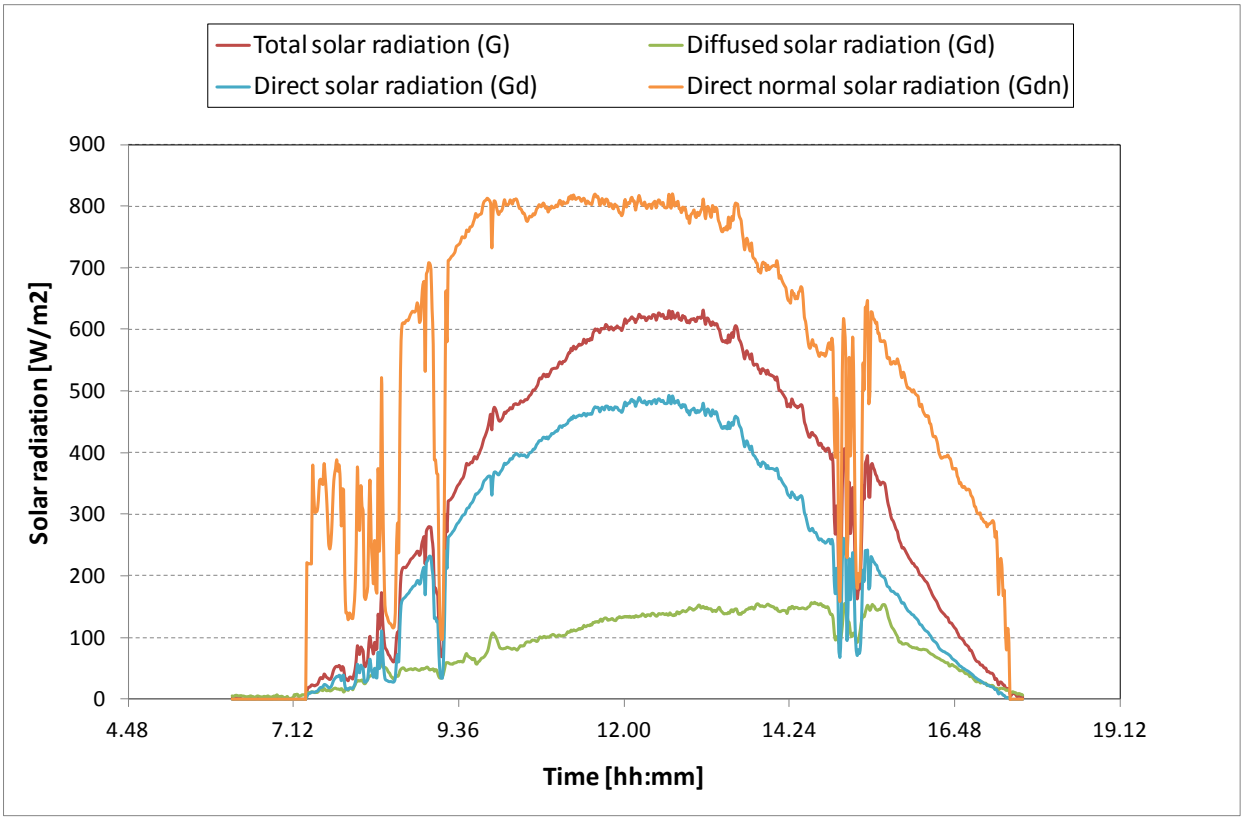

Figure 5-2 Solar radiation components for the 5th of February 2009.

5.3.Solar collector performance

The main parameters used to describe the thermal performance of the collector are the useful gain and the thermal efficiency. Basically the useful gain is estimated by measuring the fluid inlet and outlet temperatures and the fluid flow rate. The useful gain is calculated using Equation 4:

$$Q_{collector} = \rho F_C C_P (T_{out} - T_{in}) \qquad \text{Equation 4}$$

Where F_C is the volumetric flow rate of the heat transfer fluid (pressurized water or thermal oil) in the collector [m^3/s], ρ is the fluid density [kg/m^3], C_p is the specific heat capacity of heat transfer fluid [kJ/kg.K] and T_{out} and T_{in} are the inlet and outlet temperatures of the collector. The temperature dependency of ρ and C_p has been considered in the calculations.

The sun tracking collector's efficiency can be expressed as the ratio between the net heat absorbed by the thermal-fluid and the direct insolation on the solar collector field:

$$\eta_{th} = \frac{Q_{collector}}{Q_{direct\ ,solar}} = \frac{\rho F_C C_P (T_{out} - T_{in})}{G_{bn} \times A_{collecto\ r}} \qquad \text{Equation 5}$$

Where $A_{Collector}$ is the aperture area of the collector [m^2].

The performance of the collector during a typical summer day [1 May 2009] is presented in Figure 5-3, this figure shows the input and output temperatures of the pressurized water in the collector, the total solar radiation received by one square meter of the collector's plane, the collector useful output and the collector efficiency.

In this day the collector's useful gain was in the range of 20 kW during the period between 9:30 am and 4:00 pm. It has to be mentioned that this output corresponds to the operation of only 9 out of the 11 rows of the Fresnel mirrors with an aperture area of 72 m^2 instead of 88 m^2. And the average collector's efficiency during the day is 0.3 based on the direct radiation normal to surface G_{bn}.

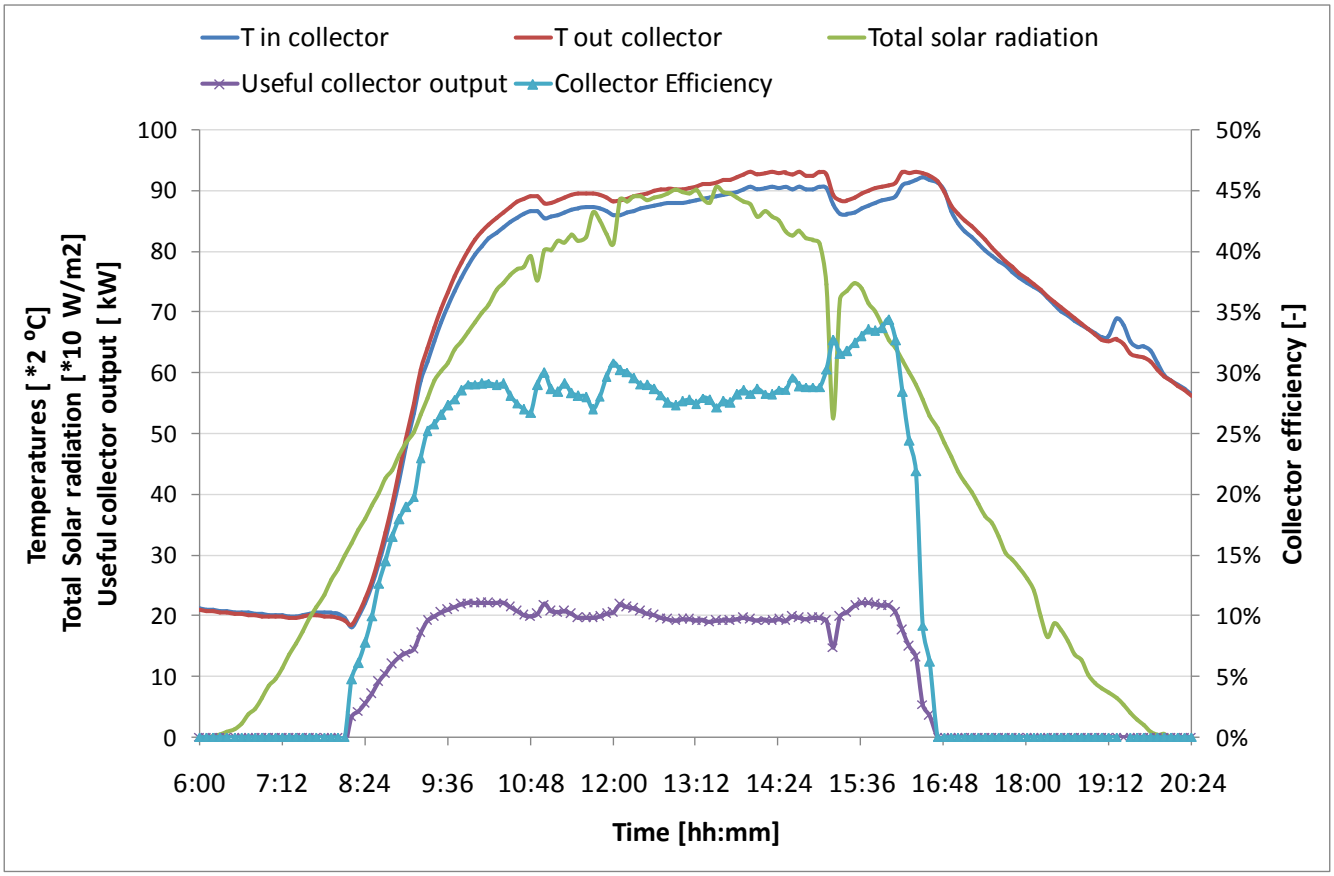

Figure 5-3 Collector performance during a typical summer day. [1 May 2009]

5.4.Absorption chiller performance

Two key figures characterize the energy performance of the absorption refrigeration machine; the cooling capacity and the thermal coefficient of performance COP_{th}. While the nominal cooling capacity of the chiller is 12.8 kW both the cooling capacity and the COP_{th} of the chiller are dependent on the inlet flow rate and temperature to the generator, the input flow rate and temperature to the evaporator and the ambient temperature.

The cooling capacity of the chiller was calculated by equation 6:

$$\dot{Q}_{chiller} = \rho F_V C_P (T_{ev} - T_{iv}) \qquad \text{Equation 6}$$

Where ρ is the heat carrier fluid density in the loop external to the chiller on the evaporator side. C_p is the specific heat capacity of the same fluid, in this case a mixture of water-glycol. The temperature dependency of ρ and C_p was considered in the calculations.

The thermal COP, defined as the ratio between the useful cooling and the thermal energy flux to the generator of the chiller; in this case, from a solar hot water flow, was calculated based on equation 7:

$$COP_{th} = \frac{\dot{Q}_{evaporator}}{\dot{Q}_{generator}} = \frac{\rho F_V C_P (T_{ev} - T_{iv})}{\rho F_g C_P (T_{ig} - T_{\mathrm{eg}})} \qquad \text{Equation 7}$$

The electrical COP was calculated by the equation 8:

$$COP_{elec} = \frac{\dot{Q}_{evaporator}}{E_{elec\,,solar}} = \frac{Heat\ flux\ extracted\ at\ low\ temperature\ level}{Electricity\ consumption\ of\ the\ solar\ system} \qquad \text{Equation 8}$$

Where the $E_{elec,solar}$ is the electrical consumption of the solar cooling system including the solar loop pump, the absorption chiller, the heat rejection system and the control system.

Figure 5-4 presents the thermal energy to the chiller, the cooling capacity provided by the chiller and the thermal and electrical COP of the chiller during its operation in a summer day (29 May 2009),

The COPth value of the chiller was varying from 0.55-0.7 for the operating conditions of this day. Referring to the long term operation of the chiller., The COP_{elec} value of the chiller was varying from 4-6 for the operating conditions of the considered day.

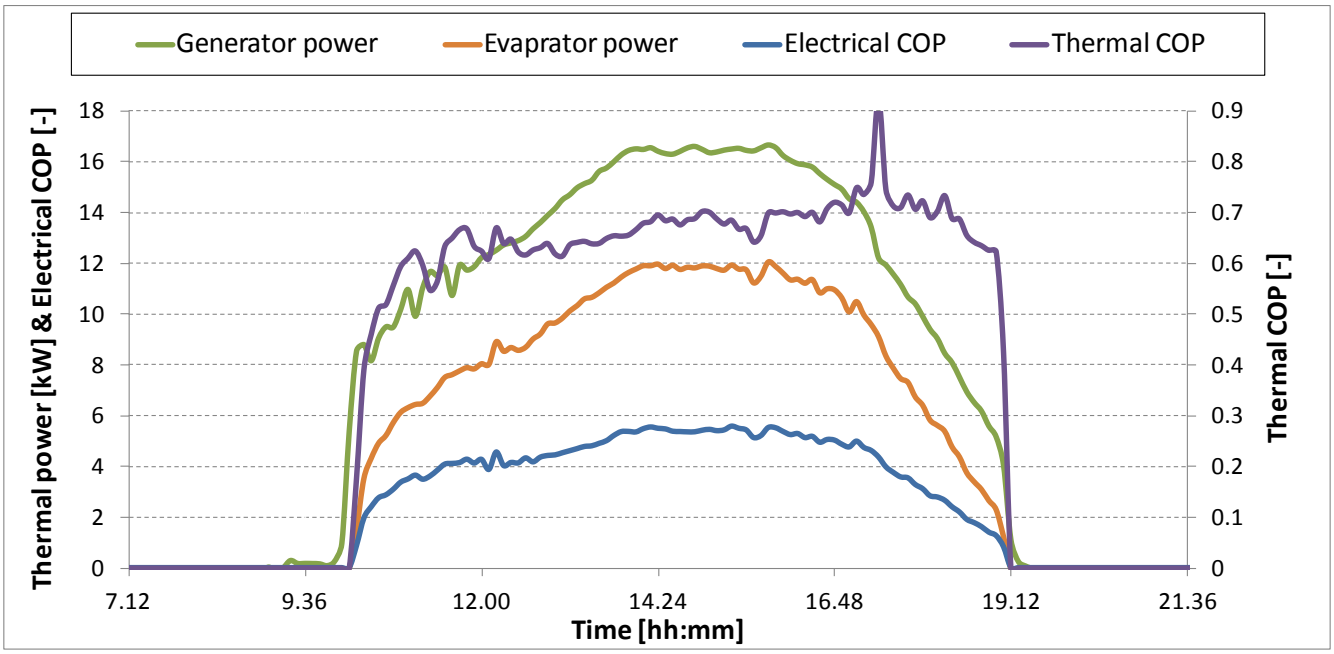

Figure 5-4 The thermal power of the generator and evaporator, and the thermal and electrical COPs of the chiller. for the day [29 May 2009].

The statistical analysis of the performance showed that the chiller worked most frequent with a thermal COP of 0.6 as shown in the histogram of Figure 5-5.

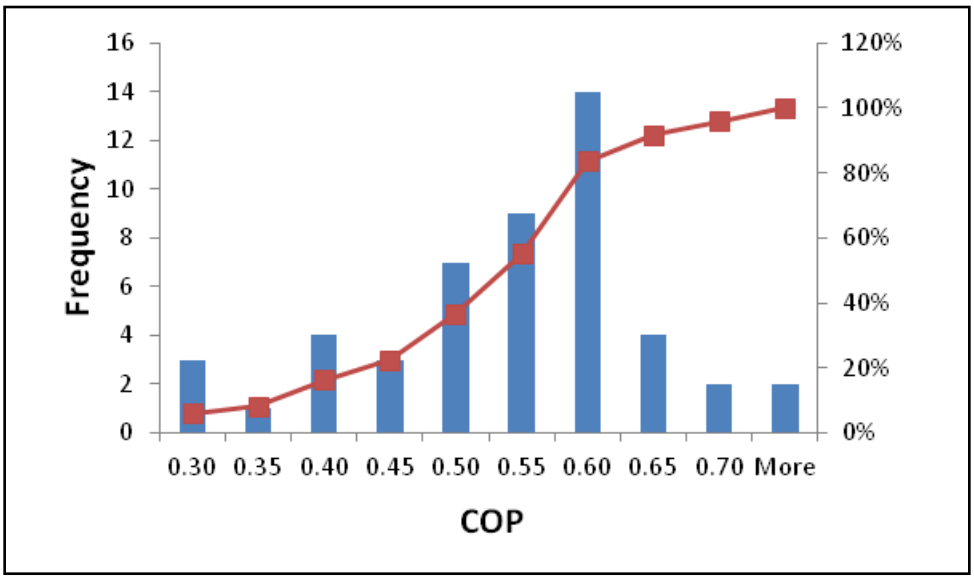

Figure 5-5 The frequency of the performance of the operation of the chiller.

The performance of the chiller is dependent on the water inlet temperatures at the generator and evaporator, and to the air inlet temperature at the condenser. Both the chillers cooling power and COP_{th} are increasing with increasing the input temperature to the generator and the input temperature to the evaporator as can be seen in Figure 5-6 & Figure 5-7.

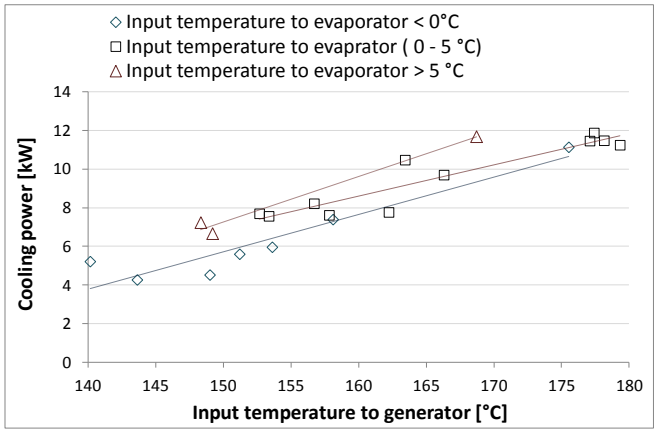

Figure 5-6 Cooling power of the chiller in [kW] as a function of the input temperature to generator [°C] at different input temperatures to the evaporator.

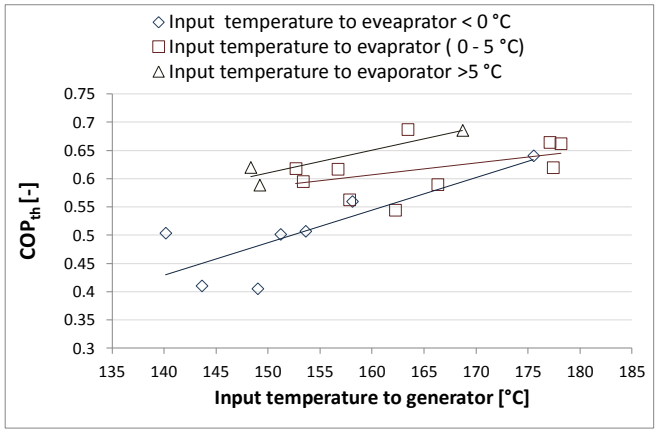

Figure 5-7 Thermal COP [-] as a function of the input temperature to generator [°C] at different input temperatures to the evaporator.

The ambient temperature at which the chiller rejects its heat have a high influence on the chiller's performance as can be seen in Figure 5-8 and Figure 5-9. The higher the ambient temperature the lower the cooling power and the thermal COP of the chiller.

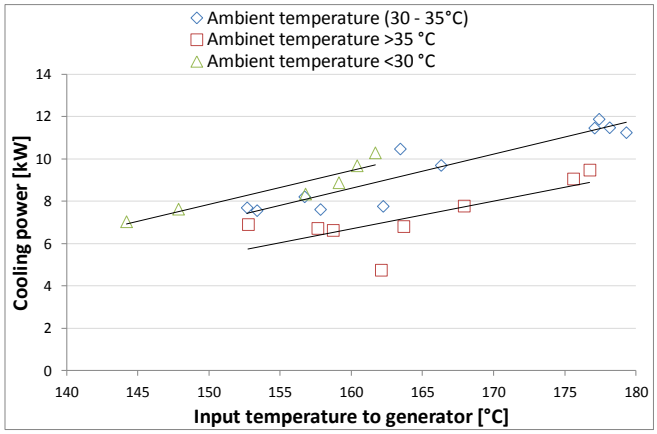

Figure 5-8 Cooling power of the chiller in [kW] as a function of the input temperature to generator [°C] at different levels of ambient temperature.

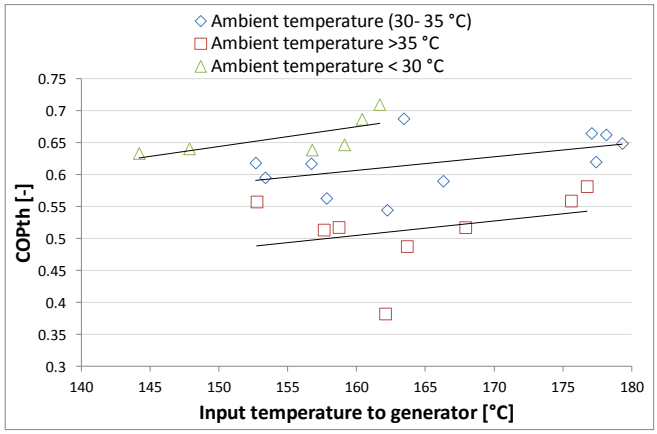

Figure 5-9 Thermal COP [-] as a function of the input temperature to generator [°C] at different levels of ambient temperature.

A detailed analysis of the chiller's performance data was done, and chiller's data were fitted using a parametric-empirical approach to relate the thermal COP and the cooling power of the thermally driven absorption chiller to its operating conditions. This is explained in details in the next modeling chapter.

5.5.Energy and economic performance of the system

In this section, the global energy balance of the system is described, the electrical consumption of the system compared to a conventional system and the economical figures are discussed as well.

5.5.1. Global energy balance

The daily energy flows diagram in Figure 5-10 contains all energy flows in the solar cooling plant on a typical sunny day. In this typical condition, the total direct solar radiation on the horizontal surface is 545 kWh; the collector absorbs 200 kWh with a daily average efficiency of 0.36. The pipeline heat loss represents 43 kWh which accounts for 17% of the solar energy absorbed. The COP of the absorption chiller is 0.56, and the Solar Cooling Ration SCR is 0.16.

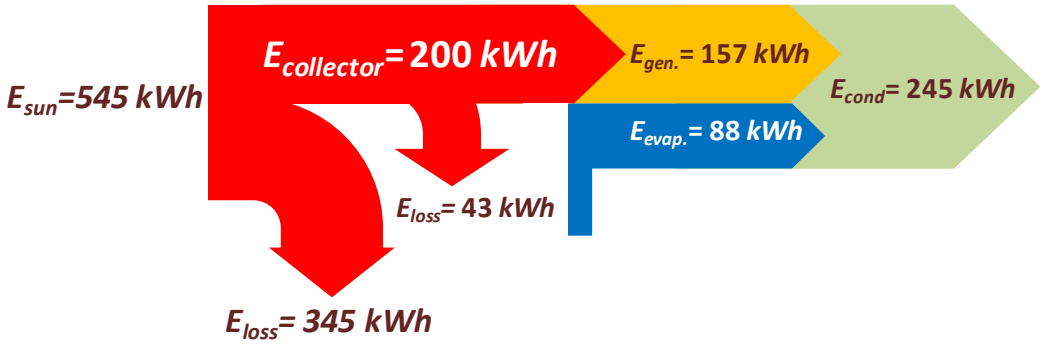

Figure 5-10 Energy flow diagram. (8 July 2010)

5.5.2. Electricity consumption of the system

Thermally driven chillers are characterized by their low electricity consumption compared to a conventional compression chiller. However, the solar the cooling system includes other components that participate to the electricity consumption of the system; pumps, control and tracking systems and the heat rejection components.

A wattmeter was installed to measure the electrical consumption of the system as a whole. This wattmeter was also used to evaluate the contribution to the electrical consumption of each single component; by running components one after the other and measuring the electrical consumption of each component alone. The electrical consumption, which can vary slightly during the operation, of the different components of the system is presented in Table 5-1.

Table 5-1 Electrical consumption of system components. [W]

Components	Electrical consumption [W]
Fresnel Collector tracking system	100
Solar loop pump	800
Absorption chiller + dry cooler	900
Pump chiller to cold storage	850

The electrical consumption shares of the system components are presented in Figure 5-11. The electrical consumption of the chiller and the dry cooling system alone (900 W) is relatively small compared to the cooling power of the absorption chiller (12800 W). The same can be said about the electrical consumption of the LFR collector tracking system (100 W). However, the electrical

consumption of the solar loop pump (800 W) is definitely high; this is due to the fact that the pressure drop to circulation of the thermal fluid (pressurized water) inside the collector absorber and the chiller's generator is significantly high. The latter since the chiller's generator is a prototype which is optimized from neither the hydraulic nor the heat transfer point of view. That requires the pump to overcome a high pressure drop and thus consumes a lot of electricity in the pump's motor.

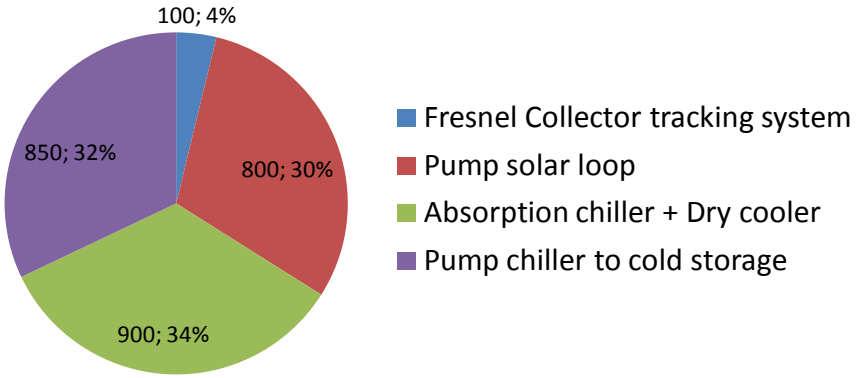

Figure 5-11 Shares of electricity consumption of each component of the system. (Power [W]; consumption share [%])

5.5.3. Primary Energy Savings

In order to estimate the savings associated with the introduction of the solar cooling system, it is required to measure the electrical consumption of the solar cooling system and compare it to a reference system of vapor compression chiller using electrical energy. The electrical consumption of the solar cooling system includes the LFR collector tracking system, the solar loop pump, and the absorption chiller with its air-cooled condenser (which is highlighted in Figure 5-12).

The secondary circulation pump connecting the chiller to the cold storage is not included in the electrical consumption of the solar cooling system. This is due to the fact that this pump is not an auxiliary component that is required by the solar cooling system, but it is also used by the conventional system connecting the compression chiller to its respective cold storage.

For a reference system operating in conditions similar to that of the solar cooling plant, i.e. low evaporator temperature (down to -10 °C) and high ambient temperature (up to 45 °C) with being air-cooled, the typical SPF of this reference system working in full load would be in the range of 2.5 (Yu & Chan, 2005) and the primary energy conversion of electricity ε_{elec} isr 0.32 in Tunisia which was calculated based on the energy mix of the country.

Substituting these values in the equation of Primary energy ratio for a reference system (equation 5 of chapter 4) results in a PER_{ref} value of 0.8 [kWh cold/kWh primary energy]. The primary energy ratio of the solar assisted cooling system was calculated based on (equation 4 of chapter 4).

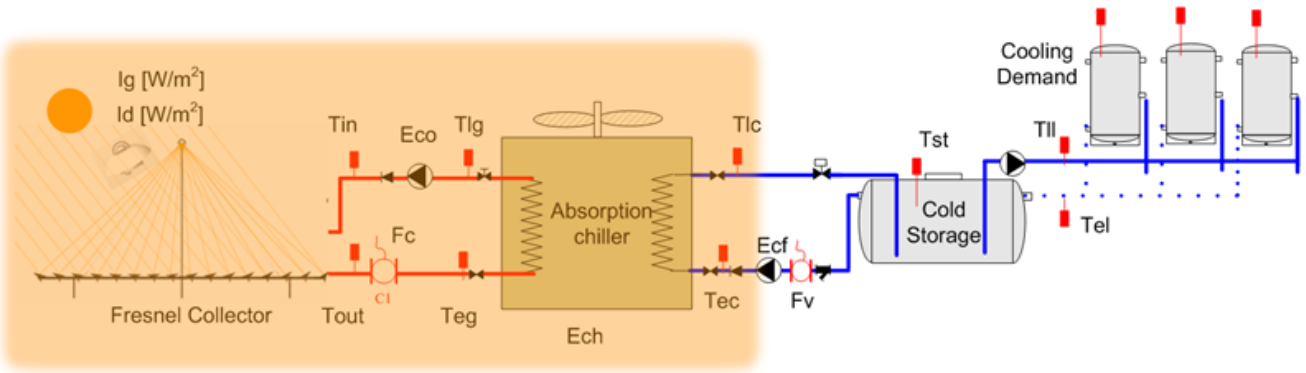

Figure 5-12 Solar cooling system scheme, highlighting the components considered for the primary energy consumption assessment.

The Primary Energy Ratio (PER) is the ratio between the cold produced by the system [kWh] and the primary energy consumed by the system. The average of the PER improved from 1.13 during the months of (May-July) 2009 to reach a value of 1.62 during the same months of the year 2010 with an improvement of 44 %.

The electrical COP of the solar cooling system represents the ratio of the cooling power produced by the system in [kWh] to the total electricity consumption of the system components (absorption chiller, heat rejection system and circulating pump) in [kWh]. Figure 5-13 represents the COP_{ele} of the system, it can be noticed that while the value was 2.8 during the months of (May to July) 2009, the value has been improved to 4.05 during the same months of 2010.

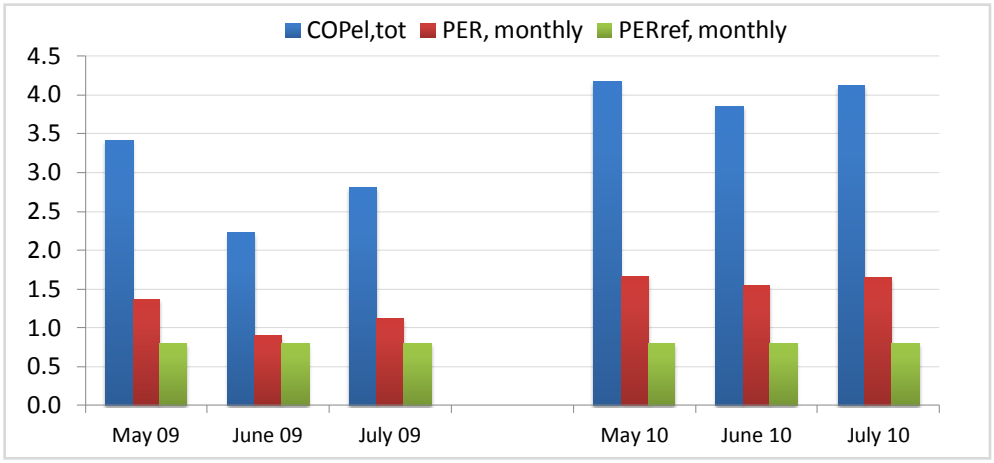

Figure 5-13 Energy consumption and PRE for the months of May, June and July for the years of 2009 and 2010.

During the year 2009 the PER for the month of May is the highest with a value of 1.4, whereas for the months of June and July there was a problem with two of the eleven mirrors of the LFR collector, and this resulted in a reduction of the system production, together with higher ambient temperatures during these two month, a lower PER value achieved compared to that for the month of May.

Optimization of the performance parameters of the control system were applied in April 2010 which explain the improvement of the system performance in the summer months of 2010. These modifications are explained in more details in the optimization chapter.

5.6. References

Yu, F. W., & Chan, K. T. (2005). Advanced control of condensing temperature for enhancing the operating efficiency of air-cooled chillers. *Building and Environment*, *40*(6), 727-737. Retrieved from http://www.sciencedirect.com/science/article/pii/S0360132304002562

6. Chapter Six: Modeling and Simulation

Numerical simulation offers the possibility to study virtually physical systems and to test rapidly the proposed solutions. Simulation is then the most adapted method to understand the behavior of a system in order to optimize it. The enhancement and the development of a technology are essentially based on the capacity to simulate accurately its behavior in order to optimize it. This reality applies to solar cooling technologies. (Bourdoukan, 2009).

To design and optimize thermally driven solar cooling systems, the solar thermal supply with or without storage, the energy conversion by the chiller system and the demand must be closely matched to obtain high solar fractions and thus significant primary energy savings. As there is very limited experience with solar cooling systems and since the cooling loads strongly depend on the internal load and external gain profile of the buildings or the industrial cooling process, simulation tools are essential to avoid over-sizing the solar thermal system. During the operation of the solar cooling plants, simulation tools can be very useful to analyze and improve control strategies. (Schumacher, Cotrado, Pietruschka, & Eicker, 2011).

While a lot of research activities are focused toward modeling and validating single components models, such as concentrating collectors, absorption chillers, cooling towers, etc. The work done in this thesis project was targeted at system concept development and optimization. However, in order to ensure a reasonable accuracy of the new system concept models, it was necessary to develop the simulation models of the components and to validate these models based on the acquired monitoring data.

6.1. Simulation tool selection

In general, simulation tools can be classified according to their degree of complexity. The basic of all simulation tools are algorithmic programming languages like Fortran or C and/or object-oriented languages like C++, C#, Java etc. However, the ability to use a programming language for the purpose of simulating solar cooling systems requires fundamental knowledge in modeling, programming and numerical methods.

Since practically most physical system models use differential algebraic equations (DAE) these must be solved for every time step over the time interval of interest. Several programs exist which release users from having to solve the set of DAEs. Two examples with support for heating and cooling systems are EES (Engineering Equation Solver) developed at the University of Wisconsin and SPARK (Simulation Program Analysis and Research Kernel) developed at the Lawrence Berkley National Laboratory. In the framework of IEA Task 38 (Solar Air-Conditioning and Refrigeration) several components for absorption chiller simulation have been developed for SPARK.

Graphical programming languages (GPLs) partly "hide" the formulation of DAEs from the user via a graphical user interface (GUI). Instead of having to formulate the model equations directly these tools provide graphical elements, which can be compiled and interconnected by computer-mouse operations. A large number of special purpose Graphical Programming Languages (GPLs) exist. From the renewable energy sector examples are TRNSYS (Transient System Simulation Tool), originally designed for solar heating and building simulation at the University of Wisconsin, INSEL (Integrated Simulation Environment Language), originally designed for photovoltaic systems at the University of Oldenburg, ColSim, primarily designed for the development of controllers in thermal systems at the Fraunhofer Institute for Solar Energy Systems, and Polysun, which recently included models for absorption chillers to be used in the simulation of solar cooling systems.

TRNSYS: The TRaNsient SYstem Simulation software (TRNSYS) (Klein et al., 2006) is a widely used modular thermal process simulation program (John A. Duffie & Beckman, 2006).It is a flexible graphically based software environment used to simulate the behavior of transient systems. TRNSYS is made up of two parts. The first is an engine (called the kernel) that reads and processes the input file, iteratively solves the system, determines convergence, and plots system variables. The kernel also provides utilities that (among other things) determine thermophysical properties, invert matrices, perform linear regressions, and interpolate external data files. The second part of TRNSYS is an extensive library of components, each of which models the performance of one part of the system. The standard library includes approximately 150 models ranging from pumps to multizone buildings, wind turbines to electrolyzers, weather data processors to economics routines, and basic HVAC equipment to cutting edge emerging technologies. Models are constructed in such a way that users can modify existing components or write their own, extending the capabilities of the environment.

INSEL: (Integrated Simulation Environment Language), originally designed for photovoltaic systems at the University of Oldenburg, it is a commercial simulation tool which allows modeling and simulation of photovoltaic and thermal systems by creating the desired system out of a comprehensive component library. For solar thermal air-conditioning systems, component models like thermally driven chillers are available as well. Similar to TRNSYS, the system is designed using a graphical user interface. Building simulation is not integrated yet.

COLSIM:A non-commercial open source simulation tool, applicable under Linux operating software. COLSIM is modular like TRNSYS, but allows more sophisticated control strategies in the short time range. Concerning cooling and air-conditioning equipment, few components are available so far and thus, more composition of the types by the user is required.

Polysun: is a simulation tool has been developed at the Solar Energy Institute SPF at the Technical University of Rapperswil HSR in Switzerland. The Spin-Off company Vela Solaris has taken over the Polysun development and forcefully advances usability and versatility. With Polysun 5.0 (spring 2009),

the Polysun functionality has been extended to cover heat pump, geo-thermal, photovoltaics, PVT and solar cooling.

Based on the literature review, TRNSYS is gaining popularity and the performance of solar absorption systems have been simulated using TRNSYS by several researchers (Florides, Kalogirou, Tassou, & Wrobel, 2002)(Joudi & Abdul-Ghafour, 2003)(Assilzadeh, Kalogirou, Ali, & Sopian, 2005)(Balghouthi, Chahbani, & Guizani, 2005)(Xavier, 2006). Some researchers include economical analysis of their proposed systems since cost plays an important role in decision making (Ghaddar, Shihab, & Bdeir, 1997)(Eicker & Pietruschka, 2009). Moreover, within the International Energy Agency IEA Tasks 25 and 38, components for thermally driven chillers have been developed. These reasons in addition to the capabilities of TRNSYS simulation software answered the requirements of the simulation activities planned and thus it was selected for this project.

6.2.Simulation models

The main simulation models used to simulate the system components are: Absorption chiller model; Linear Fresnel collector model; Parabolic trough collector model; Phase change material (PCM) Cold Storage.

6.2.1. Absorption chiller modeling

In the complete thermodynamic models of heat driven chillers, many equations have a non-linear structure that have hindered the development of reliable programmed solver modules of absorption machines for simulating performance in detailed energy optimization programs. For this reason, several attempts have been made in order to reduce the operating characteristics of absorption chillers into easier ones to handle simple algebraic equations. (Puig-Arnavat, López-Villada, Bruno, & Coronas, 2010)

In order to propagate the installation of solar cooling systems, dimensioning and system design have to be optimized. Even though the transient simulation software TRNSYS is well established for this purpose, considerable deviations to measured values are possible, when components are not correctly used or designed for the simulation.(Witte et al., 2008).

The standard TRNSYS Type 107 models a single-effect hot-water driven chiller using a lookup approach from a performance data file to predict the part load performance. With the release of TRNSYS 16 this Type was made a standard TRNSYS component. Although originally adapted to the operation and control of large scale absorption chillers (e.g. Cooling power >~ 200 kW), this type and – as often expected – also the available example performance data file can be used for small capacity chillers also, since its data are normalized. Nevertheless some difficulties occurred when applying Type 107 in combination with the example performance file to the Robur absorption chiller. For example, this type is designed for a chiller working with a cooling tower, and thus expecting cooling water temperature and flow rate, which is not the case with the air cooled chiller used in this project. To overcome the drawbacks of the type 107 mentioned above, a new type called 207 was developed.

This absorption chiller model is a static "black box" model (Figure 6-1), in which manufacturer experimental data are correlated to predict the chiller response for specific operating conditions. The mathematical model is described by (Aprile, 2006). The cited model has the following parameters (constants which characterize the operation), inputs and output.

- The chiller main parameters are: specific heat of the heat carrier (Cp_{hot}), specific heat of refrigerant (Cp_{cold}), auxiliary power for pumps and fans operation (E_{ch}), minimum refrigerant outlet temperature ($T_{set,point}$).
- The chiller inputs are: heat carrier volume flow rate (F_g), heat carrier inlet temperature (T_{eg}), ambient temperature (T_{amb}), refrigerant volume flow rate (F_v), refrigerant inlet temperature (T_{ev}).
- The calculated outputs are: refrigerant outlet temperature (T_{lv}), heat carrier outlet temperature (T_{lg}), heat rate released to ambient (Q_{amb}), heat rate driving the chiller and subtracted from the heat carrier (Q_g), the chilling power (Q_v), the chiller coefficient of performance (COP) and the part-load fraction (PL).

It has to be mentioned that within the experimental activities described in the results chapter, all of the chiller model's inputs and outputs were monitored (Table 6-1) in order to evaluate the performance of the chiller and to validate the simulation model for future simulations.

Table 6-1 Monitored parameters of the absorption chiller.

Monitored Parameters	***Nomenclature***	***Unit***
Entering generator temperature	T_{eg}	°C
Leaving generator temperature	T_{lg}	°C
Generator flow rate	F_g	m^3/s
Entering evaporator temperature	T_{ev}	°C
Leaving evaporator temperature	T_{lv}	°C
evaporator flow rate	F_v	m^3/s
Electricity consumption of secondary pump	E_{cf}	W
Electricity consumption of the absorption chiller and the condenser´s fan.	E_{ch}	W

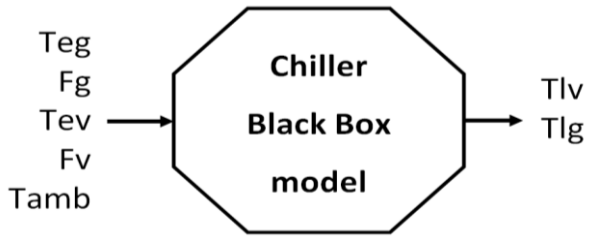

Figure 6-1 Absorption chiller static model inputs and outputs.

6.2.1.1. Inputs - outputs dependency table

The dependency table (Table 6-2) between the set of outputs (COP, Normalized Cooling power $Qv_{nor.}$) and the set of inputs (F_g, T_{eg}, T_{amb},T_{ev}) is derived from the manufacturer experimental curves of COP and $Qv_{nor.}$.

Table 6-2 Sample of the experimental data dependency between (COP, Normalized Qv) and the set of inputs (Fg, Teg, Tamb,Tev) from the manufacturer.

$Qv_{nor.}$	COP	Fg	Teg	Tev	Tamb
.	.	.	.	.	.
0.72	0.69	1760	190	-5	20
0.49	0.52	1760	190	-5	25
0.32	0.38	1760	190	-5	30
0.21	0.27	1760	190	-5	35
0.15	0.18	1760	190	-5	40
.	.	.	.	.	.

The data from the manufacture cover the input domain presented in Table 6-3. Two constrains are related to the manufacturer provided experimental data, the first is that the heat carrier fluid is thermal oil and not pressurized water "which was used in our first experimental setups" and the second is the limited range of input temperatures to the chiller.

Table 6-3 Input data domain for chiller COP and cooling power.

Input	Unit	Lower limit	Upper limit	Experimental values
Fg	l/h	1760	3080	1760, 3080
Teg	°C	190	240	190, 215, 240
Tev	°C	-5	0	-5, 0
Tamb	°C	0	45	0, 5, 10, 15, 20, 25, 30, 35, 40, 45

During the first phase of the project, "system simulation for concept development", it was necessary to extend the range of input temperatures to be able to simulate the chiller according to the perspective operating conditions. The assumptions taken by (Aprile, 2006) which are supported by numerical simulations (Joudi & Lafta, 2001) were followed and the input data domain was extended as shown in Table 6-4.

Table 6-4Extended input data domain for chiller COP and cooling power.

Input	Unit	Lower limit	Upper limit	Experimental values
Fg	l/h	1760	3080	1760,3080
Teg	°C	190	240	**100,130,160**,190,215,240,**270,300**

Tev	°C	-5	0	**-20,-10**,-5,0,**5**
Tamb	°C	0	45	0,5,10,15,20,25,30,35,40,45

Both experimental and extrapolated data were grouped together and saved in an external file. The file structure was made in accordance to the specifications for DYNAMICDATA, a TRNSYS library function(Klein et al., 2006). This function is used for output data interpolation.

6.2.1.2. Absorption chiller performance data fitting

The chiller performance data acquired during the quasi-steady state operation of the system during 2009 and 2010 were analyzed in order to correlate the chiller's cooling power and thermal COP to the chiller's operating parameters; the inlet and outlet temperatures flow rates as well as the ambient temperature.

Several authors have proposed approaches based on the characteristic equation model to describe the performance characteristics of absorption chillers. This model uses the characteristic equation approach developed by(Hellmann, Schweigler, & Ziegler, 1999) that has been used to fit both catalogue data (Hellmann & Ziegler, 1999)and experimental data (Kühn & Ziegler, 2005). With this approach, both the cooling capacity and the COP of the chiller are expressed as functions of the external heat exchanger fluid temperatures combined in the so-called characteristic temperature difference (ΔΔt). The characteristic equation predicts the part load behavior of absorption chillers and avoids the need for extensive numerical simulations of the internal thermodynamic cycle.

(Puig-Arnavat et al., 2010) compared two of these approaches of utilizing the characteristic equation method in order to find a simple model that best describes the performance of thermal chillers. And after comparing the results obtained using experimental data from a single-effect absorption chiller, It was concluded that the adaptation of the characteristic equation method developed by (Kühn & Ziegler, 2005) is the simplest .And that it provides similar or better accuracy than the other approach, hence, as a first attempt, this approach has been selected to fit the experimental data gained during the measurement phase of this project. In this approach described by (Kühn & Ziegler, 2005) a numerical fit was carried out to improve the results of the characteristic equation method. These authors used the following arbitrary characteristic temperature function $\Delta\Delta t'$ presented in Equation 1:

$$\Delta\Delta t' = t_g - a.t_{AC} + e.t_E \qquad \text{Equation 1}$$

They also defined a linear characteristic Equation 2.

$$\dot{Q_E} = s'.\acute{\Delta}\Delta t' + r \qquad \text{Equation 2}$$

Insertion of ΔΔt′ in the characteristic equation yields Equation 3.

$$\dot{Q_E} = s'.t_g - s'.a.\acute{t}_{AC} + s'.e.t_E + r \qquad \text{Equation 3}$$

A multi-regression fit was carried out with Microsoft Excel (2007) to calculate the value of the four parameters: s', a, e and r in Equation 3. The multiple linear regression algorithm determines regression coefficients to minimize the residual sum of squares as can be seen in Table 6-5. The numerical fit of the four parameters resulted in Equation 4.

$$\dot{Q}_E = \begin{matrix}(0.0067529).t_g - (0.0067529).(14.964916).t_{AC} \\ +(0.0067529).(58.721279).t_E + 12.574092\end{matrix} \qquad \text{Equation 4}$$

Table 6-5 Sample of the data sheet used to calculate the parameters for the cooling power fitting equation.

T_g	T_E	Q,chiller measured	T_{AC}	Q,chiller fitted	Error	Error^2
162.15	-0.30	9.79	30.10	10.51	-0.72	0.52
162.61	-0.73	9.61	30.30	10.32	-0.71	0.50
162.83	-1.17	9.59	29.38	10.24	-0.65	0.42
.	.	.	.	.	.	.
						Σ (error^2)

The fitted cooling capacity versus the measured cooling capacity is presented in Figure 6-2. A high deviation of the fitted values can be seen with respect to the measured ones especially for cooling power values above 10 kW, which makes this model unsatisfactory, and thus a further investigation of correlations has been carried out.

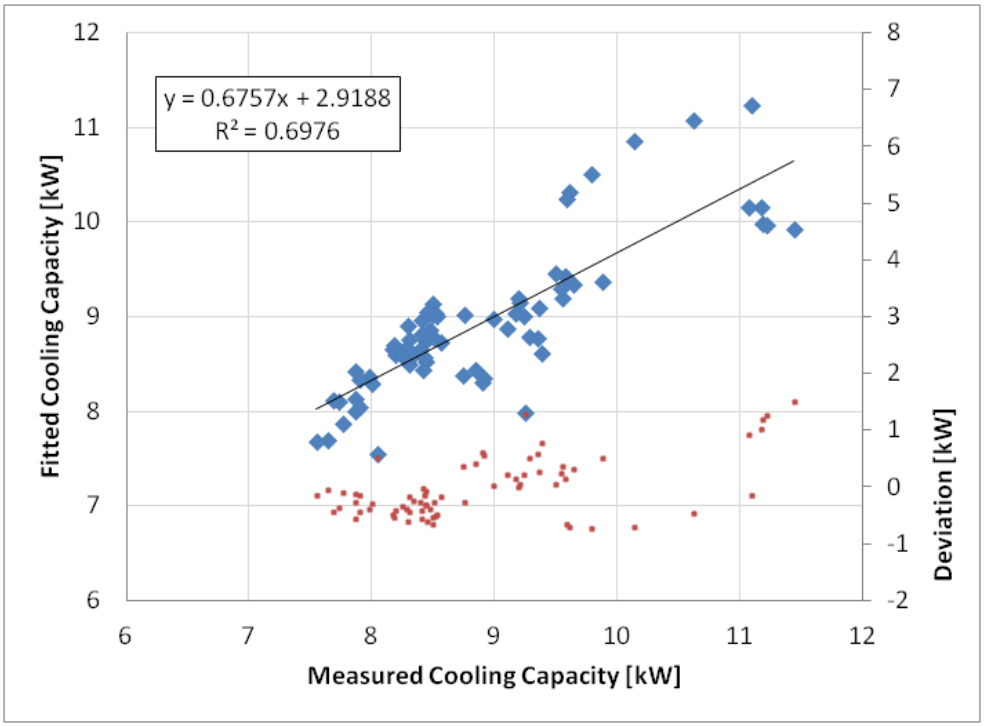

Figure 6-2 Fitted versus measured cooling capacity usingcharacteristic equation model.

The second data fitting attempt was done by using the model created by (Beausoleil-Morrison, Mottillo, Brandon, Sears, & Ferguson, 2004) and used by (Edwards, 2011) and (Johnson, 2011).

This model is a three nodes model (Figure 6-3): the water-side of the generator, the water-side of the evaporator, and the air-side of the condenser. The model was created to use an experimentally obtained COP_{th} characteristic equation based on experimentally derived relationships for the generator and evaporator heat transfers.

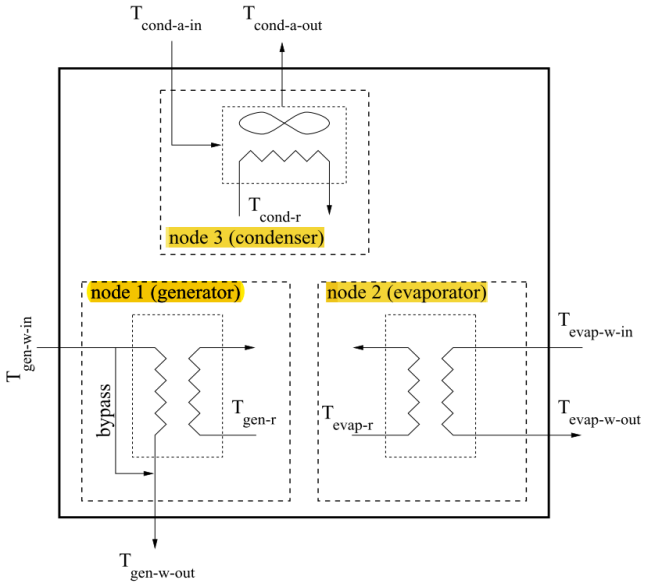

Figure 6-3 Three-node representation of thermally driven absorption chiller. (Beausoleil-Morrison et al., 2004)

The parametric-empirical approach of the model is used to relate the thermal COP to the thermally driven absorption chiller unit's operating conditions, Equation 5. Specifically, it determines the performance in response to the water inlet temperatures at the generator and evaporator, and to the air inlet temperature at the condenser.

The equation was structured to facilitate the determination of the coefficients from laboratory experiments, in this equation; T is the temperature (°C), the subscripts for gen,$_{in}$, evap,$_{in}$, and con,$_{in}$ are the inlet conditions for the generator, evaporator, and condenser, respectively. Tgen$_{,ref}$, Tcond$_{,ref}$, and Tevap$_{,ref}$ are reference temperatures and represent the "standard" operating conditions for the unit, and the remaining variables are coefficients to be determined.

$$\begin{aligned} COP = a &+ b_1.\left(T_{gen-w-in} - T_{gen-ref}\right) + b_2.\left(T_{cond-a-in} - T_{cond-ref}\right) \\ &+ b_3.\left(T_{evap-w-in} - T_{evap-ref}\right) + c_1.\left(T_{gen-w-in} - T_{gen-ref}\right)^2 \\ &+ c_2.\left(T_{con-a-in} - T_{con-ref}\right)^2 + c_3.\left(T_{evap-w-in} - T_{evap-ref}\right)^2 \\ &+ d_1.\left(T_{gen-w-in} - T_{gen-ref}\right).\left(T_{cond-a-in} - T_{cond-ref}\right) \\ &+ d_2.\left(T_{gen-w-in} - T_{gen-ref}\right).\left(T_{evap-w-in} - T_{evap-ref}\right) \\ &+ d_3.\left(T_{cond-a-in} - T_{cond-ref}\right).\left(T_{evap-w-in} - T_{evap-ref}\right) \end{aligned}$$

Equation 5

The fitting achieved by this equation was satisfactory, however, a new parameter was added to the equation to cope with the variation of the flow rates of the generator and the evaporator regarding their nominal flow rates, Equation 6, and it was seen the resulted fitting became even better.

$$
\begin{aligned}
COP = a &+ b_1.\left(T_{gen-w-in} - T_{gen-ref}\right) + b_2.\left(T_{cond-a-in} - T_{cond-ref}\right) \\
&+ b_3.\left(T_{evap-w-in} - T_{evap-ref}\right) + c_1.\left(T_{gen-w-in} - T_{gen-ref}\right)^2 \\
&+ c_2.\left(T_{con-a-in} - T_{con-ref}\right)^2 + c_3.\left(T_{evap-w-in} - T_{evap-ref}\right)^2 \\
&+ d_1.\left(T_{gen-w-in} - T_{gen-ref}\right).\left(T_{cond-a-in} - T_{cond-ref}\right) \\
&+ d_2.\left(T_{gen-w-in} - T_{gen-ref}\right).\left(T_{evap-w-in} - T_{evap-ref}\right) \\
&+ d_3.\left(T_{cond-a-in} - T_{cond-ref}\right).\left(T_{evap-w-in} - T_{evap-ref}\right) \\
&+ f_1.\left(\frac{F_g}{F_{g-nominal}}\right).\left(\frac{F_v}{F_{v-nominal}}\right)
\end{aligned}
$$

Equation 6

As previously was done with the characteristic equation, the quasi steady-state data were fitted using Equation 6, and results presented in Figure 6-4 showed a good agreement between the fitted and the measured thermal COP of the chiller.

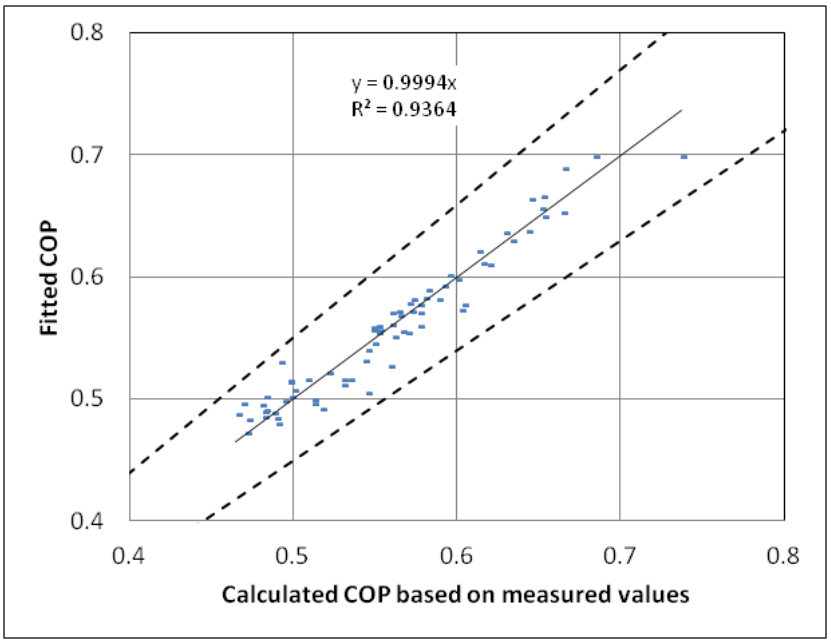

Figure 6-4Fitted Vs. Measured thermal COP during quasi-steady state operation, with ±10% deviation lines.

The list of the reference values used for the fitting procedure and the fitting coefficients resulted from this process are presented in Table 6-6**Error! Reference source not found.**.

Table 6-6 The reference values used for the fitting procedure and the fitting coefficients resulted from the process.

reference values		***coefficient***	***Qch***	***COP***
Tgen,ref	200	*a1*	10.25318307	0.56338
Tev,ref	0	*b1*	-0.14096533	-0.0329
Tcond,ref	50	*b2*	-0.23763632	-0.23763632
Mdot,oil	3500	*b3*	0.348104908	0.08508
Mdot,water	2600	*c1*	-0.01790811	-0.01790811
Cp,oil @ 180 °C	2.12	*c2*	0.002494226	0.002494226

Cp,chw @ 0 °C	3.52	*c3*	-0.00621841	-0.00621841
		d1	0.007696709	0.00039
		d2	0.003498518	-9E-05
		d3	-0.03458663	0.0031
		f1	0.595555792	0.595555792

The main constrain of using the quasi-steady state data only is that the data acquired during this state covers a very narrow range of the input temperatures to the generator and the evaporator of the chiller as can be seen in Table 6-7.

Table 6-7Domain of inputs for the quasi-steady state operation ofthe chiller.

Input temperature	***Min: Max Temperature [°C]***
Input to the generator	162 : 185
Input to the evaporator	-5.15 : 1.64
Ambient air temperature	29.38 : 41.87

Analysis of the chiller performance data showed that the input temperature to the generator for many operating hours is less than that found in the quasi steady state conditions presented in Table 6-7. And thus in order to extrapolate the fitting results of the quasi-steady state conditions to other operating conditions which could result in unexpected results, it was decided to fit all the performance data acquired for the chiller performance which should cover the complete range of the operation of the chiller. The result of this fitting is presented in Figure 6-5 and shows a high agreement between the fitted and the measure thermal COP of the chiller.

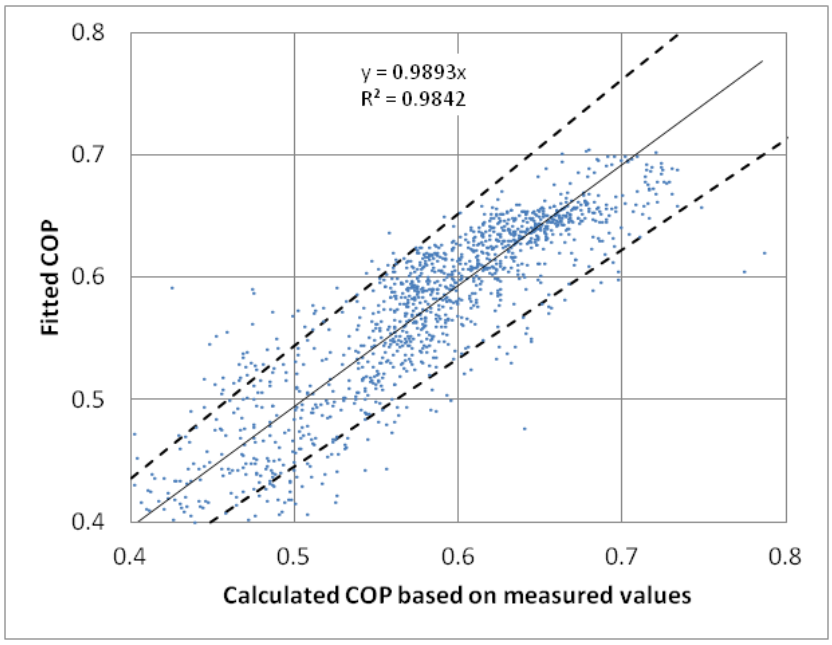

Figure 6-5Fitted Vs. Measured thermal COP during, with ±10% deviation lines.

The same procedure applied for fitting the thermal COP of the chiller to its operating conditions was done to fit the evaporator heat rate "cooling power" in [kW] to the chiller operating conditions, Equation 7.

$$\begin{aligned}\dot{Q}_{ev} = a &+ b_1.\left(T_{gen-w-in} - T_{gen-ref}\right) + b_2.\left(T_{cond-a-in} - T_{cond-ref}\right) \\ &+ b_3.\left(T_{evap-w-in} - T_{evap-ref}\right) + c_1.\left(T_{gen-w-in} - T_{gen-ref}\right)^2 \\ &+ c_2.\left(T_{con-a-in} - T_{con-ref}\right)^2 + c_3.\left(T_{evap-w-in} - T_{evap-ref}\right)^2 \\ &+ d_1.\left(T_{gen-w-in} - T_{gen-ref}\right).\left(T_{cond-a-in} - T_{cond-ref}\right) \\ &+ d_2.\left(T_{gen-w-in} - T_{gen-ref}\right).\left(T_{evap-w-in} - T_{evap-ref}\right) \\ &+ d_3.\left(T_{cond-a-in} - T_{cond-ref}\right).\left(T_{evap-w-in} - T_{evap-ref}\right) \\ &+ f_1.\left(\frac{F_g}{F_{g-nominal}}\right).\left(\frac{F_v}{F_{v-nomin\ al}}\right)\end{aligned}$$

Equation 7

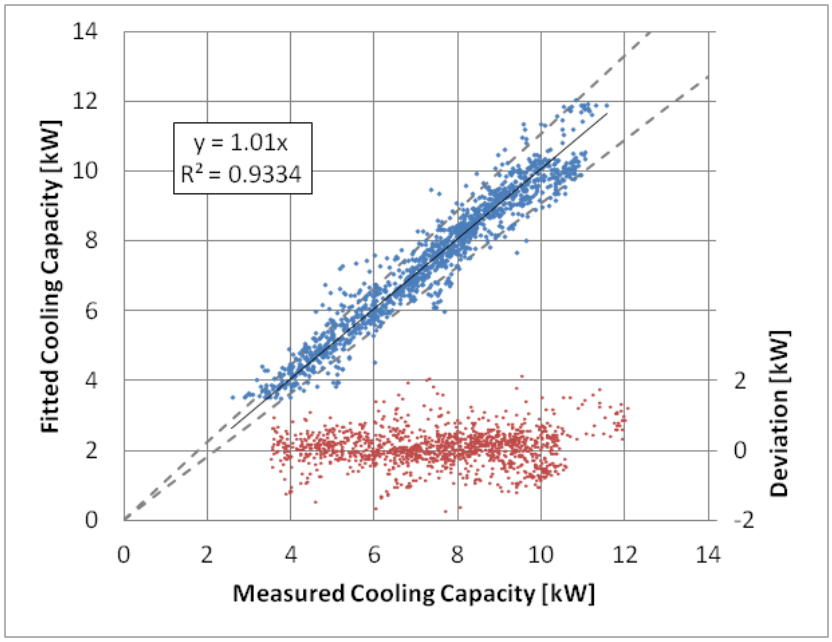

Figure 6-6 Fitted versus measured cooling of the absorption chiller, with ±10% deviation lines.

Results obtained of the fitting of the data showed a high agreement between the fitted and the measured data (Figure 6-6). However, it have to be noticed that for cooling power above 11 kW, the fitting model values tend to be slightly higher than the measured ones, but with less than 10% deviation from the measured values.

The list of the reference values used for the fitting procedure and the fitting coefficients resulted from this process are presented in Table 6-8.

Table 6-8 The reference values used for the fitting procedure and the fitting coefficients resulted from the process.

reference values		***coefficient***	***Qch***	***COP***
Tgen,ref	200	*a1*	7.034743	0.298463

Tev,ref	0	*b1*	-0.03314	-0.00837
Tcond,ref	50	*b2*	-0.01168	0.004708
Mdot,oil	3500	*b3*	0.705833	0.043823
Mdot,water	2600	*c1*	-0.00042	-0.00013
Cp,oil @ 180 °C	2.12	*c2*	0.016094	0.000536
Cp,chw @ 0 °C	3.52	*c3*	-0.01872	-0.0016
		d1	-0.00678	6.29E-05
		d2	0.004736	4.92E-05
		d3	0.007326	0.00091
		f1	-0.41073	0.025952

Based on the correlations of the cooling power and the COP_{th} of the chiller with respect to its operating conditions, a new characteristic map of the performance of the chiller was created considering the full range of possible operating conditions. The aim of creating this file was to use it as an input file for the TRNSYS model 207. The range of the input temperatures and flow rates to the generator, evaporator and the ambient temperature to the model are described in Table 6-9.

Table 6-9 Range of inputs for the input file for TRNSYS model 270 of the absorption chiller.

Input	***Values***	***No. of values***	***Unit***
Tin_hot	110:10:180	8	°C
Tin_cold	-9:3:21	11	°C
Tamb	15:5:45	7	°C
Vdot_hot	2000:1000:4000	3	l/h
Vdot_cold	2500	1	l/h

The predicted cooling power of the chiller is presented in Figure 6-7 based on the fitted correlations of the chiller working at different ambient temperatures and inlet temperatures to the evaporator at a constant input flow rate and temperature to the generator.

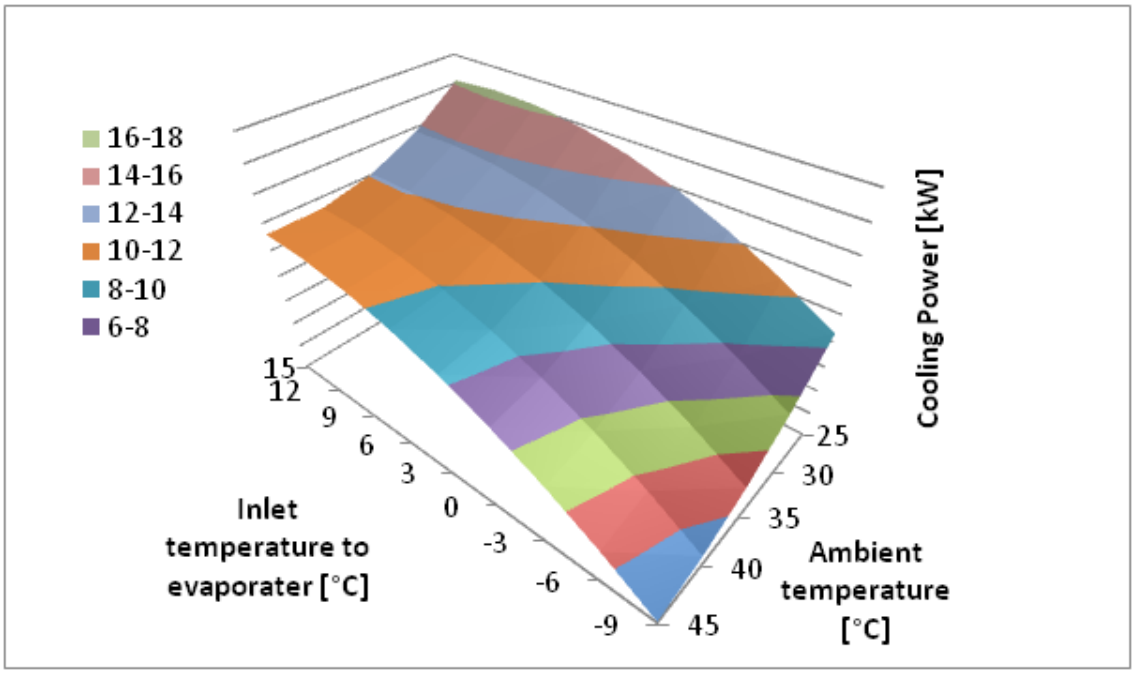

Figure 6-7 Cooling power of the chiller at different ambient temperatures and inlet temperatures to the evaporator.

6.2.2. Solar collectors modeling

The solar collector model is composed of the optical and the thermal parts. In order to describe the optical model for the PTC and LFR collectors, it is necessary to describe the direction of beam radiation. The geometric relationship between a plane of any particular orientation relative to the earth at any time and the incoming beam solar radiation, that is, the position of the sun relative to that plane, can be described in terms of several angles; some of these angles are indicated in Figure 6-8. (John A. Duffie & Beckman, 2006)

Angle of incidence (θi): the angle between the beam radiation on a surface and the normal to the surface.

Zenith angle (θz): the angle between the vertical and the line to the sun, that is, the angle of incidence of beam radiation on a horizontal surface.

Solar azimuth angle (γ_s): the angular displacement from south of the projection of beam radiation on the horizontal plane.

Surface azimuth angle (γ): the deviation of the projection on a horizontal plane of the normal to the surface from the local meridian, with zero due south.

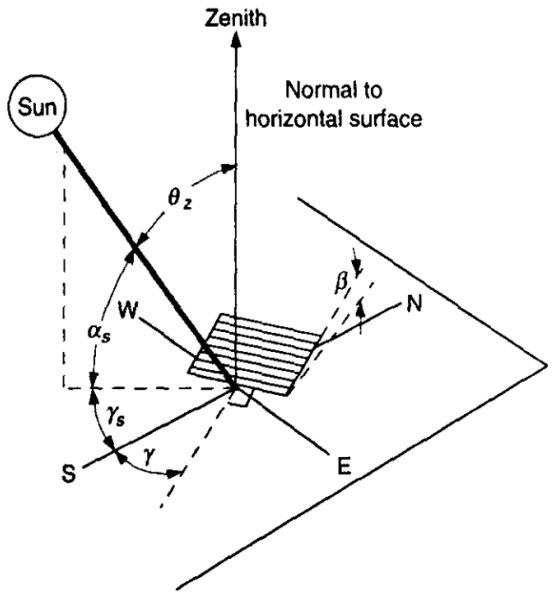

Figure 6-8 Zenith angle, slope, surface azimuth angle, and solar azimuth angle for a tilted surface. (John A. Duffie & Beckman, 2006)

6.2.2.1. Linear Fresnel reflector modeling

The efficiency η of a linear Fresnel collector depends on the operation temperature of the collector, the direct normal irradiation $G_{bn}$and the incidence angle θ_i of the solar radiation. The efficiency is defined as the ratio of the thermal power, absorbed by the heat transfer fluid, to the direct normal irradiation on the aperture area:

$$\eta = \frac{\dot{m} \,.\, (h_{out} - h_{in})}{A_{col} \cdot G_{bn}} \qquad \text{Equation 8}$$

Where $\dot{m}$ is the mass flow rate of the heat transfer fluid , and h_{in} and h_{out} are the enthalpies of the entering and exiting heat transfer fluid. The collector area A_{col} is defined as the cumulative area of the primary mirrors. In practice the efficiency is determined by experiments and the results are approximated by a polynomial fit.

$$\eta = \frac{\dot{m} \,.\, (h_{out} - h_{in})}{A_{col} \,.\, G_{bn}} = \eta_{opt,0} - a_1 \cdot T_m^* - a_2 \cdot G_{bn} \cdot T_m^{*\,2} \qquad \text{Equation 9}$$

The optical efficiency $\eta_{opt,0}$ is the collector efficiency for a perpendicular irradiation and no heat loss ($T_m = 0$). Where the reduced mean temperature T_m^* is defined as:

$$T_m^* = \frac{T_m - T_{amb}}{G_{bn}} \qquad \text{Equation 10}$$

Where T_{amb} is the ambient temperature. The mean fluid temperature T_m is the average of the inlet and outlet temperatures of the collector. The coefficients a_1 and a_2 are particular for each collector.

The optical analysis of Fresnel reflectors is fairly complicated. Since the location of the reflectors is fixed, the angle of incidence of the sun on the reflector varies with time. This causes shading and blocking. Shading occurs if direct sunlight fails to reach a mirror because the mirror is in the shadow of another mirror; blocking occurs if light reflected by a mirror fails to reach the absorber because it is intercepted by the backside of another mirror (see Figure 6-9).

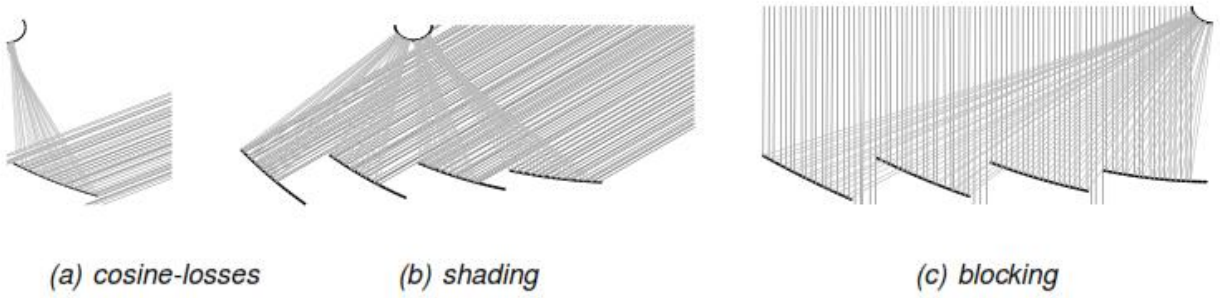

Figure 6-9 Geometric losses of Fresnel type collectors (Mertins, Lerchenmüller, & Häberle, 2004)

Overall, only part of the total incident solar radiation is effectively absorbed by the absorber tube. It is common practice to calculate the optical efficiency at 0° angle of incidence and express the variation of optical efficiency as respect to this value (the so called Incident Angle Modifier, IAM):

$$IAM = \frac{\eta_{opt}(\theta_z, \gamma)}{\eta_{opt,0}} \qquad \text{Equation 11}$$

Usually the incident angle modifier IAM(ϑ) is determined in experiments. It describes the angular dependent losses of the collector. These losses are mainly caused by the increasing beam expansion and the increasing end losses. Furthermore the effect of the cosine of the irradiation angle is considered. The measured data are approximated by mathematical functions or stored in tables.
Moreover, Linear Fresnel-collectors change their relative sun position not only in one but in two dimensions. Therefore two independent angles are required to define the position of the sun in relation to the collector. The two angles are the longitudinal angle $\vartheta_{||}$ and the transversal angle $\vartheta\perp$(see Figure 6-10). Accordingly the incidence angle modifier depends on two independent angles. In practice a transversal $IAM\perp$ and a longitudinal $IAM_{||}$ are determined by experiments or ray-tracing. The final *IAM* as a function of zenith angle ϑ_z and azimuth angle γ $IAM(\vartheta_z,\gamma)$ or respectively of longitudinal and transversal sun position $IAM(\vartheta_{||},\vartheta\perp)$ is calculated by factorization.

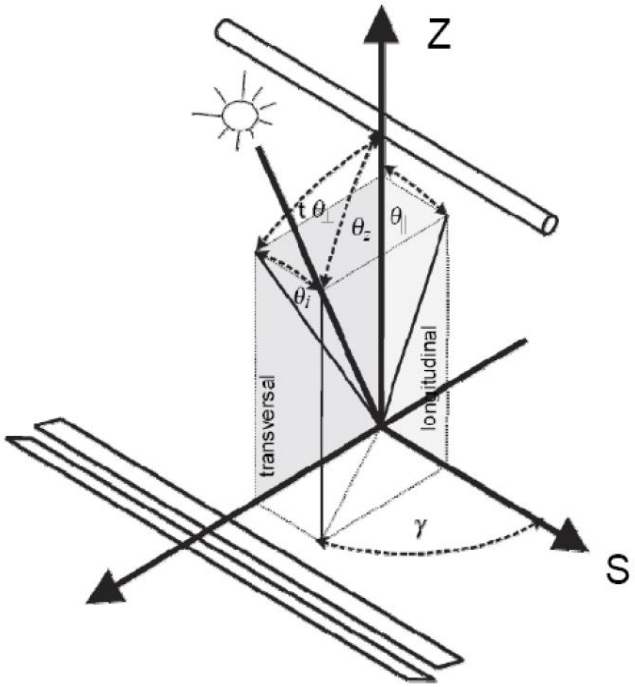

Figure 6-10 Angle definition for a linear Fresnel collector oriented north-south.

In simple geometries, like flat plate and CPC collectors, the IAM can be expressed according to the following formula (McIntire, 1982):

$$IAM(\theta_\perp, \theta_\parallel) = IAM(\theta_\perp, 0) \cdot IAM(0, \theta_\parallel) \qquad \text{Equation 12}$$

The complex behavior of the Fresnel collector IAM imposes to define a different mathematical model for the calculation of the IAM. In particular, according to (Mertins et al., 2004), the IAM can be always expressed as a factorization of longitudinal IAM and the transversal IAM, but taking into account a modified expression of the longitudinal angle. Instead of $\vartheta_\parallel$ in equation 12, the angle θ_i, which is the angle between the transversal and the sun-vector, is used in the model in order to get higher accuracy:

$$\theta_i = \arcsin(\cos(\gamma)\sin(\theta_z)) \qquad \text{Equation 13}$$

Longitudinal and transversal IAM of the Fresnel collector are plotted in Figure 6-11. The calculations were repeated for a collector with different length but otherwise identical geometry. The transversal IAM (blue line) remains the same, while the longitudinal IAMs differ due to end losses. The transversal IAM oscillates at zenith angles below 45° because of the receiver shadow, which moves over the primary mirrors and the gaps between them. (Häberle et al., 2007)

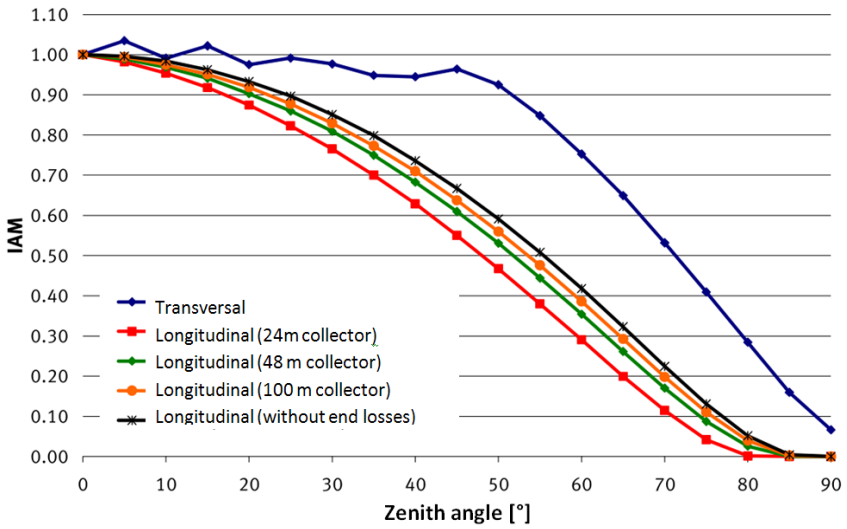

Figure 6-11 Incidence angle modifier IAM for a linear Fresnel collector, the longitudinal IAM is shown for one collector with different lengths, with and without end losses. (Häberle et al., 2007)

Regarding the thermal part of the model, since the receiver of the LFR is and evacuated tube, the thermal behavior of the linear Fresnel reflector does not represent an issue as it was simulated using the evacuated tube collector model in TRNSYS type 71. Thermal models for evacuated tube collector have been already implemented: they rely on a quadratic form of the thermal losses as respect to the average temperature difference in the collector to the external environment.
Finally, the efficiency equation and its parameters of the model are:

$$\eta = \eta_{opt,0} \cdot IAM - a_1 \cdot T_m^* - a_2 \cdot G_{bn} \cdot T_m^{*\,2} \qquad \text{Equation 14}$$

Where, for the LFR collector installed in this project, the data provided by the manufacturer are:

η=collector efficiency based on aperture area.
η_o=0.58 IAM: incident angle modifier
a_1 = 0.1W/m^2K
a_2 = 0.00043 W/m^2K^2
G_{bn} = Incident beam radiation on horizontal W/m^2
T^*=reduced mean temperature

Combining the new model of optical losses with the existing model of thermal losses, a new mathematical model has been developed in order to better describe the behavior of the linear Fresnel reflector. The model algorithm logic is the following:

1) Calculate the modified transversal angle according to the angle of incidence and geometry of the collector;

2) Type 71 reads the biaxial incidence angle modifier (IAM) data from an external data file. These data are read and interpolated by subroutine DYNAMICDATA. The data consists of between 2 and 10 values of incidence angles (in both directions) and modifiers.
3) Calculate IAM as factorization of transversal and longitudinal IAM;
4) Calculate optical efficiency and absorbed radiation;
5) Calculate thermal efficiency;
6) Calculate heat gain and outlet temperature.

6.2.2.2. Linear Parabolic trough collector modeling

The roof mounted parabolic trough collectors from the companyIndustrial Solar Technology ISTused in this project has thoroughly been tested and evaluated by Sandia (Dudley, 1995) and the German Aerospace Centre (DLR) (Kruger, Heller, Hennecke, & Duer, 2000)for efficiency and durability. The simulations are based on the measurements at the Sandia laboratory.

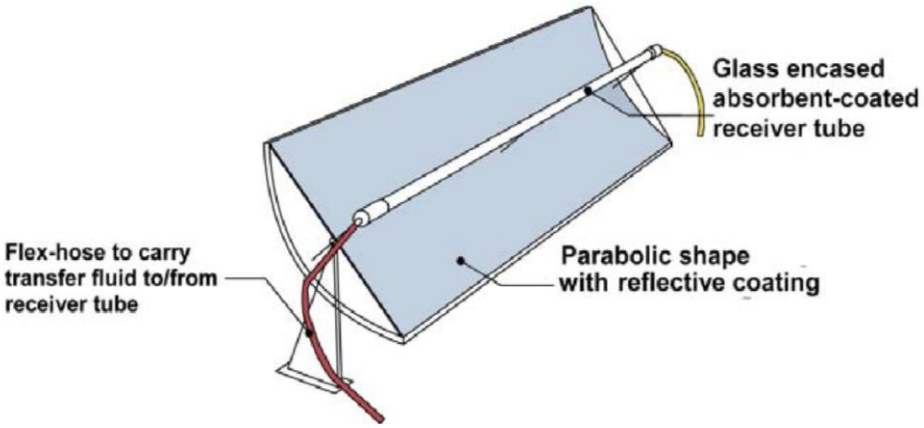

Figure 6-12 Sketch of a parabolic trough collector (picture source: AEE INTEC, Austria)

The performance equation of the IST collector (obtained by the Sandia tests) as given by the manufacturer is:

$$\eta = 0.762 - 0.2125 \cdot T_m^* - 0.001672 \cdot G_{bn} \cdot T_m^{*\,2} \qquad \text{Equation 15}$$

The incidence angle modifier IAM of the collector, given by the manufacturer, is:

$$IAM = \cos(\theta) + 0.0003178(\theta) - 0.000003985\,(\theta)^2 \qquad \text{Equation 16}$$

In the standard TRNSYS component library there is no model to simulate a parabolic trough collector. Therefore, to simulate the selected collectors, type 536 from the TESS library was used. This type is based on the theoretical equations developed in(John A. Duffie & Beckman, 2006), see also(Thermal Energy System Specialists, 2004)This model basically follows the equation:

$$Q = \mathrm{R}_1\,\mathrm{R}_2 A_{col}\,N_{parallel} - \left[F_1\,IAM\,G_{bn}\,\frac{F_2}{CR}\,(T_{in} - T_{amb})\right] \qquad \text{Equation 17}$$

Where R_1 and R_2 as modifiers for flow correction different from the tested flow rate.

$N_{parallel}$ is the number of collectors in parallel.

F_1 and F_2 are the intercept and slope of the collector efficiency curve.

CR as the concentration ratio of the trough.

Since the collector had physically four parallel rows, $N_{parallel}$was set to 4. The one-dimensional IAM-values as well as both F_1 and F_2 (0,76 and 4,17) wherecalculated from data provided by the manufacturer (Equations 8 and 9). The concentration ratio of the RMT is 7.165 (ratio of the net aperture area to the receiver area). By using an equation to reduce the incident beam radiation, the possible effect of soiling of the coated polished aluminium reflector caused by the weather conditions was taken into account. The shading of parallel rows was simulated with a shading mask (type 30) of the TRNSYS standard component library, for precise description see(Klein et al., 2006)

6.2.3. PCM cold storage modeling

An ice-making storage was selected as the cold thermal energy storage system. Compared to other static ice-making systems, such as the ice-on-coil type, the ice-encapsulated type offers the advantages of low cost, simplicity and wider heat exchange area. The phase change material (PCM), e.g., deionized water, is encapsulated in spherical capsules of relatively small diameter, usually in the range 50 to 100 mm. The capsules are packed into a conventional tank and the void volume around the capsules is filled with refrigerant fluid, such as water glycol solution. The phase change process is described in (Eames & Adref, 2002). During charging, cool refrigerant flows around the capsules and ice starts forming from the internal surface towards the centre of the capsules (see Figure 6-13.). The capsules are conceived to allow for ice expansion. During discharge, refrigerant circulates around the capsules and gets chilled by the frozen capsules. The ice starts melting, again from the internal surface towards the centre of the capsules (see Figure 6-14).

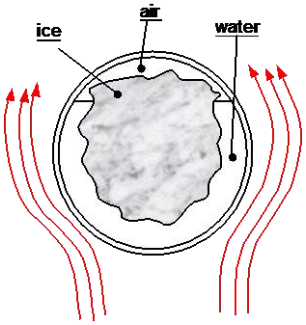

Figure 6-13 Capsule discharge phase

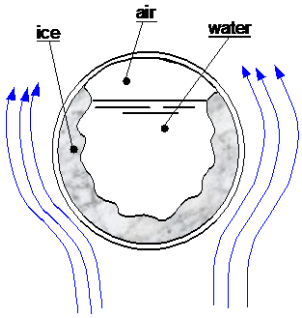

Figure 6-14 Capsule charge phase

A user-defined TRNSYS type was developed by (Aprile, 2006)to describe the behaviour of an ice-making ice-encapsulated cold storage. The storage can be represented like a stack of layers (nodes),

each one containing a certain number of capsules. The number of capsules in each layer is directly calculated as follows:

$$\mathrm{N}_{\text{capsul es}} = \frac{V_{tank}\,(1-\varepsilon)}{V_{capsule}\ \cdot N_{layers}} \qquad \text{Equation 18}$$

Where V_{tank} is the tank volume, $V_{capsule}$ is the capsule volume and ε is the void fraction around the capsule, typically in the range 0.4 to 0.5 depending on the capsule shape. Heat balance equations over each layer yields the following:

$$\delta_{ref} V_{ref} Cp_{ref} \frac{dT_j}{dt} = \dot{m}_{ref} Cp_{ref} \left(T_{j-1} - T_j\right) - N_{capsules} Q_{ref \to capsule} \qquad \textit{when } m_{ref} \textit{ is downward} \qquad \text{Equation 19}$$

$$\delta_{ref} V_{ref} Cp_{ref} \frac{dT_j}{dt} = \dot{m}_{ref} Cp_{ref} \left(T_{j+1} - T_j\right) - N_{capsules} Q_{ref \to capsule} \qquad \textit{when } m_{ref} \textit{ is upward} \qquad \text{Equation 20}$$

where δ_{ref}, V_{ref} and Cp_{ref} are the refrigerant density, volume and specific heat respectively, m_{ref} is the refrigerant mass flow rate, T_j is the refrigerant temperature within the j layer and $Q_{ref \to capsule}$ is the heat transferred from refrigerant to capsule.

The expression for $Q_{ref \to capsule}$ depends on the particular state of the PCM inside the capsule. Four conditions are possible:PCM liquid; PCM in transition from liquid to solid; PCM in transition from solid to liquid and PCM solid.

When the PCM is completely liquid or solid, the lumped capacity model is used, assuming the PCM temperature is uniform in the capsule and equal to the temperature of the layer. During PCM phase transition inside the capsule, the following experimental equations, as described in (Eames & Adref, 2002), have been used:

$$Q_{ref \to capsule} = 1.44 \cdot k_{ice} \left(T_j - T_{pc}\right) \cdot \left(0.12 \frac{t^*}{R_o} - 1\right)^2 \qquad \textit{when } T_j < T_{pc} \qquad \text{Equation 21}$$

$$t^* = \frac{\left(T_{pc} - T_j\right)}{L \cdot R_o^{\,2}} \frac{k_{ice}}{\delta_{ice}} t$$

$$Q_{ref \to capsule} = 4.00 \cdot k_{wat} \left(T_j - T_{pc}\right) \cdot \left(0.30 \frac{t^*}{R_o} - 1\right)^2 \qquad \textit{when } T_j > T_{pc} \qquad \text{Equation 22}$$

$$t^* = \frac{\left(T_j - T_{pc}\right)}{L \cdot R_o^{\,2}} \frac{k_{wat}}{\delta_{wat}} t$$

where L is the latent heat of water, $V_{capsule}$ is the capsule volume, R_o is the capsule radius, δ_{wat} and k_{wat} are the density and thermal conductivity of water, δ_{ice} and k_{ice} are the density and thermal

conductivity of ice, T_{pc} is the phase change temperature, *t* is the time since phase change has started, and *t** is the dimensionless time.

6.3.Models validation

6.3.1. Procedure

The system designed as explained in experimental setup chapter, has been installed in March 2008. The prolonged experimental activities carried out on the solar cooling system resulted in sufficient spectrum of data that have been used to calibrate and validate the TRNSYS simulation models.

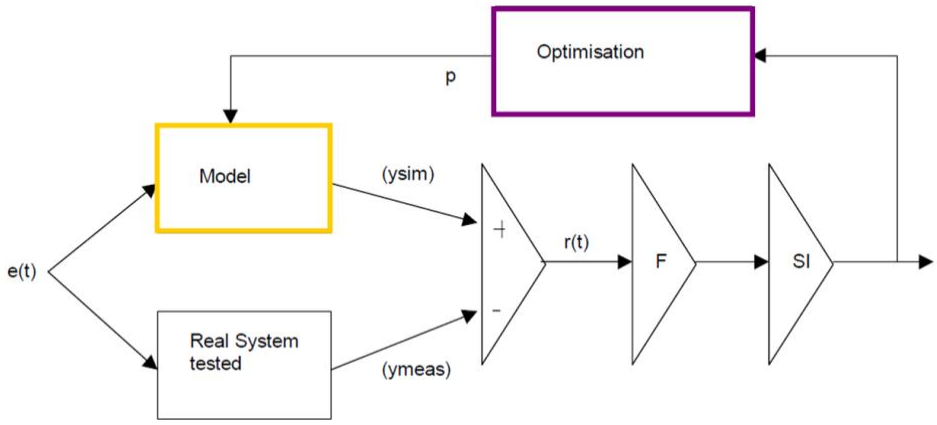

Figure 6-15The dynamic fitting procedure. Adapted from (Bales, 2001)

The validation procedure presented in Figure 6-15 based on the procedure of "Parameter identification manual for TRNSYS models"(Bales, 2001)has been applied as follows:

- The input e(t) in the Fresnel collector testing corresponds to the solar radiation, input temperature and flow rate. These inputs were measured in the real system operation.
- The same measured inputs are used as input signals applied to the TRNSYS model. Measured data for input solar radiation, temperatures and flows are read from a data file created by the measurement program.
- The measured output (y_{meas}) is compared to the simulated output (y_{sim}), which is dependent on the parameters set (p). The measured output, output temperature of the collector, is read directly from the same data file as the input data. The simulated values come directly from the simulation models themselves.
- The deviation (r(t)) is first filtered (F) to remove "noise" in the data, then squared and integrated (SI). The resulting signal gives a measure of the goodness of fit.
- An optimisation procedure is used to derive the best parameter set p –i.e., to minimize r(t) and hence the difference between the simulated and measured output temperatures.

6.3.2. Parameter identification (PI) tools

The dynamic fitting procedure presented in the previous section requires in addition to the simulation software an optimization algorithm and a proper interface between them. The simulation software TRNSYS have been selected for the simulation activities in this project. The TRNSYS potential of printing out the simulation results in an output data file allows for an easy connection with an optimization software. Several optimization software tools are able to be connected with TRNSYS. In literature are reported other experiences in this sense: (Bales, 2001) and (Ayadi, 2007) coupled TRNSYS with the optimization software "Dynamic Fitting Program" DF for the parameter identification of a hot storage and absorption chiller models respectively, for the coupling a third software called FITTRN was used.(Al-Alili, Hwang, Radermacher, & Kubo, 2010) created a user developed interface that coupled TRNSYS with the MATLAB for optimizing the performance of a solar cooling system model. A third option was the generic optimization software GenOpt. GenOpt is an optimization program for the minimization of a cost function that is evaluated by an external simulation program. It has been developed for optimization problems where the cost function is computationally expensive and its derivatives are not available or may not even exist. (Wetter, 2009). GenOpt can be coupled to any simulation program that reads its input from text files and writes its output to text files. The independent variables can be continuous variables (possibly with lower and upper bounds), discrete variables, or both, continuous sand discrete variables. Constraints on dependent variables can be implemented using penalty or barrier functions. GenOpt uses parallel computing to evaluate the simulations.

In this project the optimization software GenOpt was used and coupled to TRNSYS. GENOPT can open TNRSYS's input file and alter the design variables. Then, GENOPT calls TRNSYS engine to simulate the system and reads the out- put file to find the value of the objective function as can be seen in Figure 6-16.

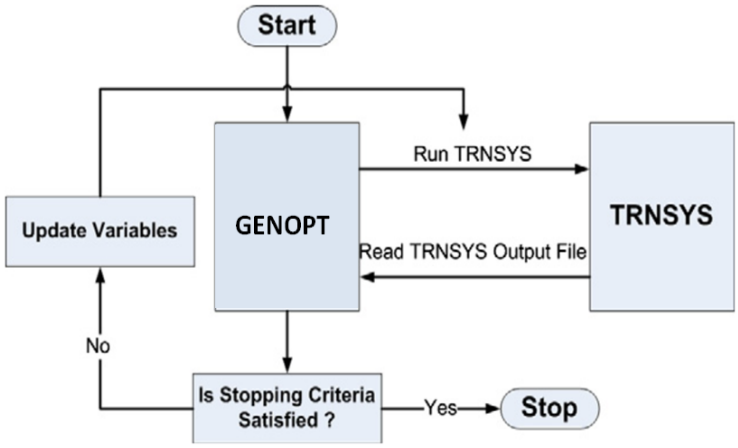

Figure 6-16 Optimization flow diagram. Adapted from (Al-Alili et al., 2010)

In order to couple TRNSYS with GenOpt it is necessary to create four input files that indicate all the required information by the optimization software to start its processing (see Figure 6-17):

1. Initialization: Specification of file location, (input files, output files, log files, etc.)
2. Command: Specification of parameter names, initial values, upper/lower bounds, optimization algorithm, etc.
3. Configuration: Configuration of simulation program (error indicators, start command, etc.)
4. Simulation input template: Templates of simulation input files.

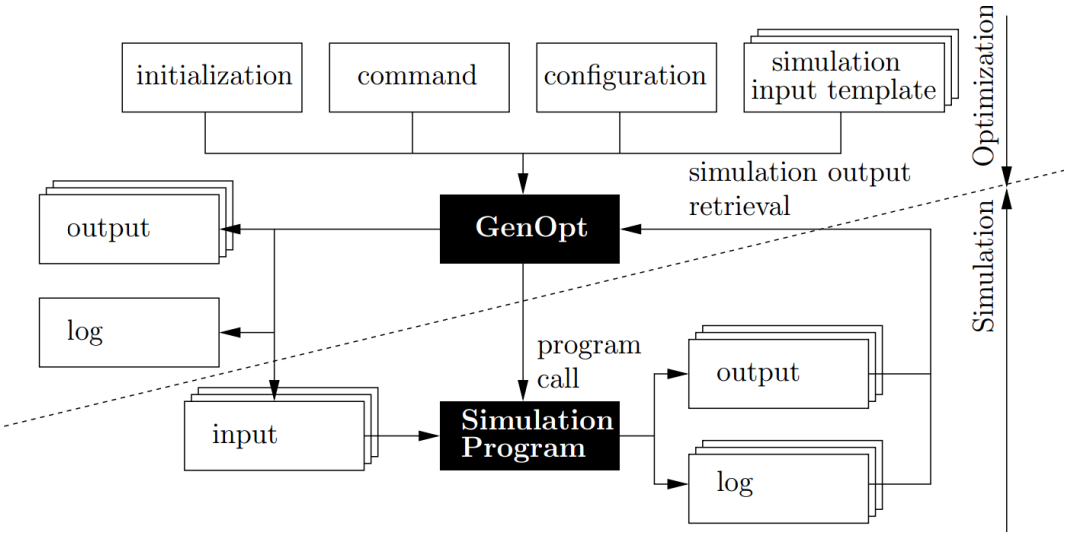

Figure 6-17Interface between GenOpt and the simulation program that evaluates the cost function.

6.3.1. Results of the parameter identification of the LFR collector

The efficiency curve for a solar collector, determines the collector's performance at different radiation and temperature levels, given a set of boundary conditions. For a single axis-tracking collector the efficiency curve equation and parameters can be expressed as follows:

$$\eta = \eta_0 * IAM - a_1 * \frac{\Delta T}{G_{bn}} - a_2 * \frac{(\Delta T)^2}{G_{bn}}$$ Equation 23

Where, for the collector technology used in the installation mentioned, the data provided by the technology provider for a 180 m^2 LFR collector are:

η=collector efficiency based on gross area.

η_0=0.567 for a gross area of a 180 m^2

IAM: incident angle modifier

a_1=0 W/m^2K

a_2 = 0.00034 W/m^2K^2

G_{bn}= Incident beam radiation on horizontal W/m^2

ΔT=average receiver fluid temperature above ambient

air temperature The LFR collector model's parameters were identified based on the experimental data of the first experimental setup in Tunisia and found to be: $\eta_0=0.5,\ a_1 = 3.9 * 10^{-7}, a_2 = 0$.

Considering that the end losses from a 120m^2,16 m length collector are 5% more than those from a 180 m^2, 24m length collector.(Häberle et al., 2007)The optical efficiency of the system analysed could be corrected to $\eta_0=0.538$ which matches fairly well (i.e., error of 7.5 %) with the value derived from the parameter identification procedure.

The evacuated tube collector absorber is designed to work at high temperatures up to 400 °C. Thus for the moderate temperature range of operation used in this plant (below 185°C) the heat losses are relatively low, and the collector performance showed to be less sensitive to the loss coefficient a_1 and a_2.

6.4. Systems simulation

For the two installed systems, the model of the whole system is developed in TRNSYS 16(Klein et al., 2006) (see Figure 6-18). The system is divided into three main subsystems:the solar collector subsystem. (LFR or PTC collector), the refrigeration subsystem (the absorption chiller with the cold storage) and the cooling load (Hourly load profile input file).

The calculation of ambient temperatures and the solar radiation of the selected sites in this simulation is based on climatic data from Meteonorm 4.10.(METEOTEST, 1999)

Regarding the first experimental setup in Tunisia, both (Aprile & Motta, 2007) and (Döll & Núñez, 2007) carried out parametric simulations that lead to the sizing of the system components.

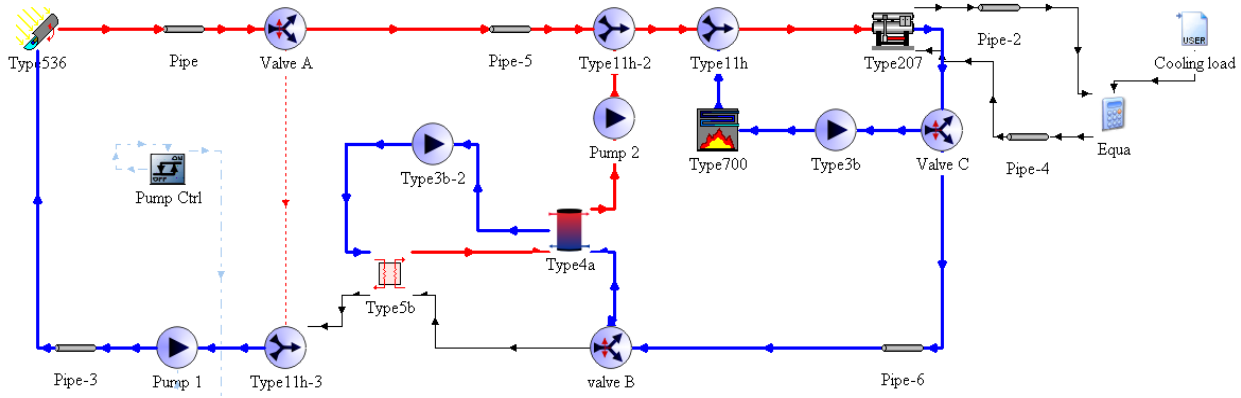

Figure 6-18 TRNSYS studio representation of the second system model.

Regarding the second experimental setup in Morocco, (Ayadi, Motta, Aprile, Doll, & Nunez, 2008) carried out a parametric study to investigate the influences of the collector field area, size of the latent heat storage, the chilled mass flow rate that is to be cooled and the possible effect of dust on the reflector area. Some results are presented below.

6.4.1. Evaluated Parameters

To evaluate the system, two performance figures were calculated: the extracted heat per incident beam radiation defined as the total efficiency (η_{total}) and the ratio between the cooling energy

provided by the solar cooling system and the total cooling energy required by the given process defined as the Solar fraction (SF).

$$\eta_{total} = \frac{Q_{extracted,solar}}{I_{beam,incident}} \quad [\%]$$ Equation 24

$$SF = \frac{Q_{extracted,solar}}{Q_{total}} \quad [\%]$$ Equation 25

6.4.2. Variation of collector field area and storage size

The system was simulated with different numbers of collectors and varying sizes of the ice storage. The parameters variations are shown in Table 6-10.

Table 6-10 Simulated collector's area [m²], storage volume [m³] and capacity [kWh]

Number of collectors	11	13	15	18	20
Net aperture area [m²]	35,75	42,25	48,75	58,50	65,00

Size of storage vessel [m³]	1,5	2,0	2,5	3,0
Latent capacity [kWh]	70,4	93,9	117,4	140,8

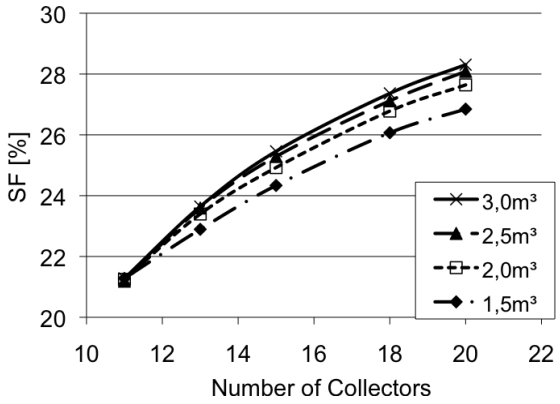

Figure 6-19 Solar Fraction of the system with different storage volume

The results of the simulation (time step = 1 min) are presented in the form of diagrams. The simulations highlighted that the system's solar fraction for the given process rises with the collector field size, ranging from approximately 21 to 28% depending on the storage size. (See Figure 6-19).

Moreover the influence of the cold storage size shows a lower impact on the solar fraction and system efficiency than the size of the collector field. Nevertheless it is to mention, that the influence of the cold storage size increases with larger collector field's areas due to the fact that part of the additional heat delivered by the larger collector field can be stored on the "cold side" of the system. With smaller collector fields a large cold storage is not needed, since in most cases the smaller amount of produced cold will be extracted from the solar cooling system before the cold storage will be completely charged (avoiding collector defocus).

6.4.3. Investigation of the effect of dust

Due to the conditions on the site, some degrading of the collector reflectivity could occur due to the effect of dust as well as particles exhausted by nearby chimneys. This effect is presented in Figure 6-20 for a system with varying number of collectors, a 2 m³ cold storage and mass flow in the cold heat exchanger of 3000 kg/hr.

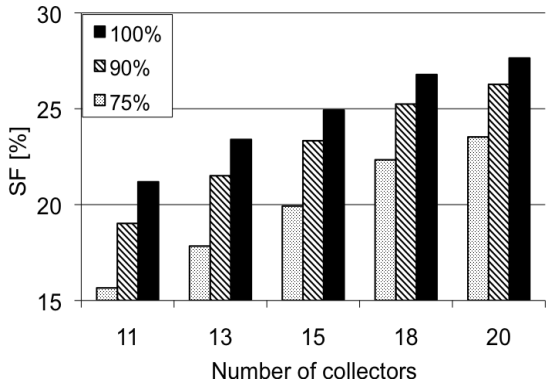

Figure 6-20 Solar Fraction of the system with different fractions of cleanliness

In systems with a small collector field the effect of dust has a higher influence on the solar fraction. Because a greater amount of heat is dumped due to overheating in systems with bigger collector fields, only part of the radiation lost by the effect of dust is "missing" in the system. For systems with smaller solar fields, which dump less energy, they are more affected by the effect of dust, and these losses reduce the total system efficiency with about 5%. As a conclusion, the collector field should be designed in an appropriate way to produce the expected useful heat, and at the same time frequent cleaning should be done for the collector mirrors.

6.4.4. Simulation outcomes

Regarding the collectors' field area, its increase resulted in a growth of both, the solar fraction and the dumped energy. The latter is due to defocusing of the collectors when the input energy exceeds the demand of the absorption chiller; which can be significant for large collectors´ areas. As a result, 18 modules of parabolic through collectors were selected for the given application, in order to guarantee enough thermal energy with an acceptable amount of dumped energy.

The optimum size of the PCM storage, for the selected collector area, is 2 m^3. Three percent of the solar fraction depends on the cleanliness of the collector field, and this was taken into consideration during the sizing process as well as for the planned frequent maintenance of the system.

6.5.References

Al-Alili, A., Hwang, Y., Radermacher, R., & Kubo, I. (2010). Optimization of a solar powered absorption cycle under Abu Dhabi's weather conditions. *Solar Energy*, *84*(12), 2034-2040. Retrieved from http://www.sciencedirect.com/science/article/pii/S0038092X10003051

Aprile, M. (2006). *Simulation Study of an Innovative Solar Absorption Refrigeration System*. Högskolan Dalarna. Retrieved from http://dalea.du.se/theses/?itemId=2696

Aprile, M., & Motta, M. (2007). SIMULATIONS OF A NOVEL SOLAR ABSORPTION COOLING CONCEPT: A COMPARISON OF STATIC AND DYNAMIC SYSTEM MODELS. *2nd International Conference Solar Air-Conditioning*. Tarragona, Spain.

Assilzadeh, F., Kalogirou, S. A., Ali, Y., & Sopian, K. (2005). Simulation and optimization of a LiBr solar absorption cooling system with evacuated tube collectors. *Renewable Energy*, *30*(8), 1143-1159. Retrieved from http://www.sciencedirect.com/science/article/pii/S0960148104003817

Ayadi, O. (2007). *Measurements, moldelling and simulation of thermo chemical accumulator used for solar cooling.*Hogskolan Dalarna.

Ayadi, O., Motta, M., Aprile, M., Doll, J., & Nunez, T. (2008). Solar energy cools milk. *Eurosun 2008* (p. 355). Lisbon. Retrieved from http://www.iea-shc.org/publications/downloads/task38-Solar_energy_cools_milk..pdf

Bales, C. (2001). *Parameter identification manual for TRNSYS models at SERC*. *Högskolan Dalarna* (p. 37). Borlänge. Retrieved from http://dalea.du.se/research/default.aspx

Balghouthi, M., Chahbani, M. H., & Guizani, A. (2005). Solar Powered air conditioning as a solution to reduce environmental pollution in Tunisia. *Desalination*, *185*(1–3), 105-110. Retrieved from http://www.sciencedirect.com/science/article/pii/S0011916405006132

Beausoleil-Morrison, I., Mottillo, M., Brandon, R., Sears, P., & Ferguson, A. (2004). The simulation of a residential space-cooling system powered by the thermal output of a cogeneration device. *The biennial conference IBPSA-Canada's*. Vancouver, BC. Retrieved from http://www.esim.ca/2004/documents/proceedings/PA163FINAL.pdf

Bourdoukan, P. (2009). *Description of simulation tools used in solar cooling*. Retrieved from http://www.iea-shc.org/publications/downloads/Report_C2A_Simualtion-tools-in-solar-cooling.pdf

Dudley, V. (1995). *SANDIA Report test results for industrial solar technology parabolic trough solar collector, SAND94-1117*. Albuquerque, USA.

Duffie, John A., & Beckman, W. A. (2006). *Solar Engineering of Thermal Processes* (p. 928). Wiley. Retrieved from http://www.amazon.com/Solar-Engineering-Thermal-Processes-Duffie/dp/0471698679

Döll, J., & Núñez, T. (2007). Simulation of a Medium Scale Solar Cooling System for Industrial Processes. *2nd International Conference Solar Air-Conditioning*. Tarragona, Spain.

Eames, I. W., & Adref, K. T. (2002). Freezing and melting of water in spherical enclosures of the type used in thermal (ice) storage systems. *Applied Thermal Engineering*, *22*(7), 733-745. Retrieved from http://www.sciencedirect.com/science/article/pii/S1359431102000261

Edwards, C. (2011). *Performance Assessment of Solar Absorption Cooling for Ontario Housing.Optimization*. Carleton University.

Eicker, U., & Pietruschka, D. (2009). Design and performance of solar powered absorption cooling systems in office buildings. *Energy and Buildings*, *41*(1), 81-91. Retrieved from http://www.sciencedirect.com/science/article/pii/S0378778808001734

Florides, G. A., Kalogirou, S. A., Tassou, S. A., & Wrobel, L. C. (2002). Modelling and simulation of an absorption solar cooling system for Cyprus. *Solar Energy*, *72*(1), 43-51. Retrieved from http://www.sciencedirect.com/science/article/pii/S0038092X01000810

Ghaddar, N. K., Shihab, M., & Bdeir, F. (1997). Modeling and simulation of solar absorption system performance in Beirut. *Renewable Energy*, *10*(4), 539-558. Retrieved from http://www.sciencedirect.com/science/article/pii/S0960148196000390

Hellmann, H. M., & Ziegler, F. (1999). Simple absorption heat pump modules for system simulation programs. *ASHRAE Transactions*, *105*, 780-787.

Hellmann, H. M., Schweigler, C., & Ziegler, F. (1999). The characteristic equations of absorption chillers. *Proc. of the Int. Sorption Heat Pump Conf., ,* (pp. 169–172). Munich.

Häberle, A., Berger, M., Luginsland, F., Zahler, C., Baitshc, M., Henning, H.-M., & Rommel, M. (2007). Linear concentrating Fresnel collector for process heat applications. *Estec 3rd European solar thermal energy conference*.

Johnson, G. (2011). *Design and Commissioning of an Experiment to Characterize the Performance of a Lithium-Bromide Absorption Chiller By*. *Test*. Carleton University.

Joudi, K. A., & Abdul-Ghafour, Q. J. (2003). Development of design charts for solar cooling systems. Part I: computer simulation for a solar cooling system and development of solar cooling design charts. *Energy Conversion and Management*, *44*(2), 313-339. Retrieved from http://www.sciencedirect.com/science/article/pii/S0196890402000456

Joudi, K. A., & Lafta, A. H. (2001). Simulation of a simple absorption refrigeration system. *Energy Conversion and Management*, *42*(13), 1575-1605. Retrieved from http://www.sciencedirect.com/science/article/pii/S0196890400001552

Klein, S. A., Beckman, W. A., Mitchell, J. W., Duffie, J. A., Duffie, N. A., & Freeman, T. L. (2006). TRNSYS 16. Retrieved from http://www.trnsys.com/

Kruger, D., Heller, A., Hennecke, K., & Duer, K. (2000). Parabolic trough collectors for district heating systems at high latitudes: a case study. *Eurosun 2000*. Copenhagen, Denmark.

Kühn, A., & Ziegler, F. (2005). Operational results of a 10 kW absorption chiller and adaptation of the characteristic equation. *First Int. Conference Solar Air Conditioning,*. Bad-Staffelstein.

METEOTEST. (1999). Meteonorm 4.0. Bern, Switzerland.

Mertins, M., Lerchenmüller, H., & Häberle, A. (2004). Geometry Optimization of Fresnel-Collectors with economic assessment. *Eurosun2004*. Freiburg.

Puig-Arnavat, M., López-Villada, J., Bruno, J. C., & Coronas, A. (2010). Analysis and parameter identification for characteristic equations of single- and double-effect absorption chillers by means of multivariable regression. *International Journal of Refrigeration*, *33*(1), 70-78. Retrieved from http://www.sciencedirect.com/science/article/pii/S0140700709001947

Schumacher, J., Cotrado, M., Pietruschka, D., & Eicker, U. (2011). Simulation of solar cooling systems. *4th INTERNATIONAL CONFERENCE SOLAR AIR-CONDITIONING 2011*. Larnaca, Cyprus.

Thermal Energy System Specialists. (2004). *Tess Documentation Library, chapter 10.Solar Library Technical Reference*.

Wetter, M. (2009). Generic Optimization Program User Manual. *Energy*, (c), 1998-2009.

Witte, K. T., Albers, J., Krause, M., Safarik, M., Besana, F., & Sparber, W. (2008). Absorption chiller modelling with TRNSYS - requirements and adaptation to the machine EAW Wegracal SE 15. *Eurosun 2008, 1st International Congress on Heating, Cooling, and Buildings* (pp. 1-8). Lisbon.

Xavier, G. C. (2006). Solar absorption cooling in Spain: Perspectives and outcomes from the simulation of recent installations. *Renewable Energy*, *31*(9), 1371-1389. Retrieved from http://www.sciencedirect.com/science/article/pii/S0960148105001783

7. Chapter Seven: System optimization and potential definition

Results obtained from the monitoring activities of the system's performance were utilized for the simulation models validation. These validated models were used for further simulation campaigns aiming at defining the optimum operating points of the whole system and trace a path towards plant performance improvement. For a comprehensive assessment of the system's optimizations outcomes, not only energy but also economic and environmental factors have been taken into account. The work in this chapter was done in three steps:

1. Optimization of the installed system to identify the optimum operating parameters and best control strategy. Applying the results of this optimization step does not require hardware changes and can be implemented without causing long stand-by of the plant.

2. Investigate the optimization potential related to the components design and installation. e.*g.* the pressure drop of the heat transfer fluid in the chiller's generator and the optical losses of the solar collector. The optimization results of this step addresses possible improvements of the components both to be considered by the components producers as well as to be considered in the design for future plants.

3. A simulation campaign was carried out to study the behavior of different configurations of solar cooling system in different climatic zones and under varying loads and operation conditions aiming at identifying the optimal system design under certain circumstances.

7.1. Installed system optimization

In this optimization step, the optimal control strategies and operating parameters of the installed system were id and implemented to the real system, and the optimization outcomes were verified through experimental activ

One of the most representative performance figures for solar cooling systems assessment is the primary energy PE_{saved}. In this section the primary energy saving PE_{saved} is defined and the procedure to calculate it is presented. Si were carried out to optimize system's operating parameters to ensure the highest primary energy savings of the s annual bases. The main studied parameters are the solar loop pump control strategy and the chiller's hot dri temperature. Compared to the parameter identification process presented in the modelling chapter, for an optin process there is not a real system, and the filter is not required. The target function for y_{sim} in this case was set to

7.1.1. Primary energy saving PE_{saved}

To calculate the primary energy efficiency, the theoretical primary energy demand of a conventional reference syst has to be calculated assuming that all the cold produced by the solar cooling system is produced by a compressio powered by electricity. Assuming a seasonal performance factor SPF value of 2.5 for the reference chiller and the energy conversion factor for electricity production of ε_{elec} = 0.4 (kWh of electricity per kWh of primary energy), the energy consumption of a reference system PE_{ref} can be calculated as:

$$PE_{ref} = \frac{Qsolarcooling}{SPF.\varepsilon_{elec}} \ [kWh] \qquad \text{Equation 1}$$

The solar system will also have a demand for electrical energy (the tracking system of the solar collector mirrors, s pump, chiller's solution pump, heat rejection fan) which are highlighted in the system scheme in Figure 7-1. T consumption will be converted to PE as well, resulting in the figure of the primary energy consumed by the solar PE_{solar}.

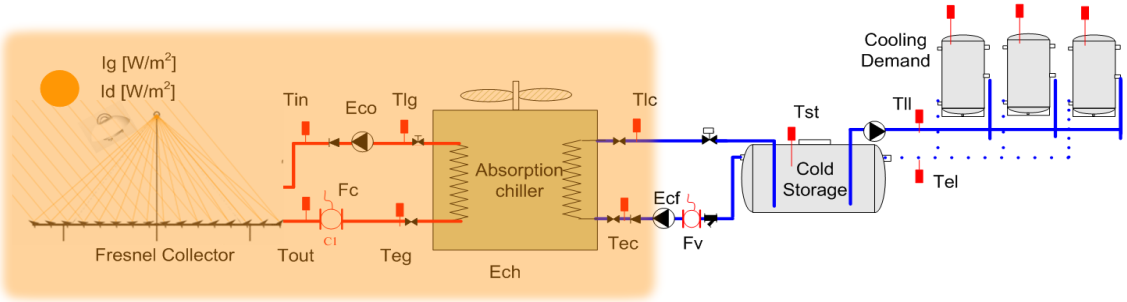

Figure 7-1 Solar cooling system scheme, highlighting the components considered for the primary energy consumption assessment.

The difference between both energy quantities is the saved primary energy PE_{saved} by the use of a solar system and of this optimization step is to maximise this value.

$$PE_{saved} = PE_{ref} - PE_{solar} \qquad [kWh] \qquad \text{Equation 2}$$

In the solar cooling system, electricity is mainly consumed by the solar loop pump and the absorption chiller with rejection unit. In order to reduce the electrical consumption of the system, it is necessary to optimize the control s regulating the performance of these two units. It has to be mentioned that, within the experimental setups used project, the pressure drop in the generator of the prototype chiller is higher than average. This explains the high consumption (800 W) of the solar loop pump which has to overcome this high pressure drop.

7.1.2. Solar loop pump

The control of the solar loop pump can be either based on a scheduled operating hours "Time" mode, or based availability of the solar radiation "IR" mode. A diagram showing the two logical paths is given in the flow chart in F In the "Time" control mode, the solar loop pump starts at tset1 in the morning, and shut down at tset2 in the even am – 6 pm).

In the "IR" mode, the solar radiation is measured and the value is compared to the starting set value "IRok", the s pump starts if the measured value is higher that the set value. Afterward, if the measured radiation value falls be "IRok" due to sunset or clouds for a certain period "delay" the pump shuts down. A typical value of the delay peri minutes to avoid frequent on/of operation in cloudy days.

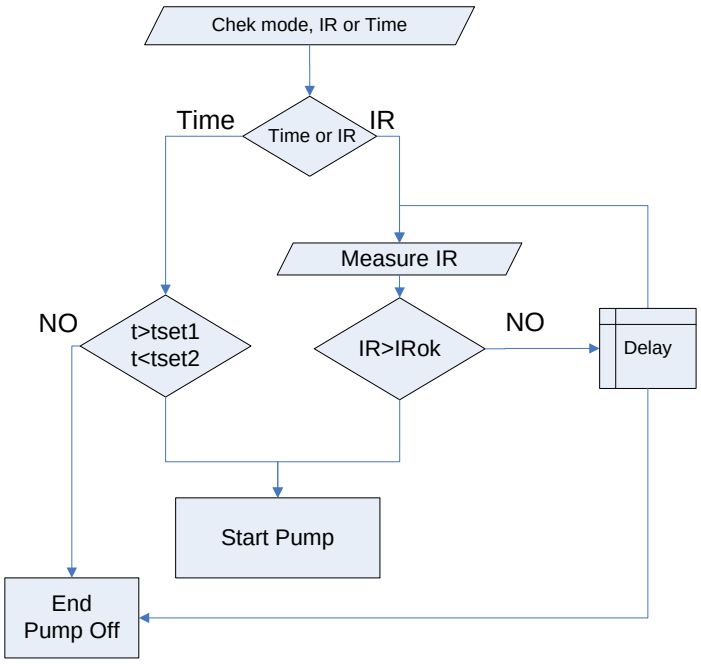

Figure 7-2 Control options of the solar loop pump

Two TRNSYS system simulation models were created, one to simulate the system with "IR" control mode wher radiation level at which the chiller starts "IRok" and the hysteresis were defined as variables. The latter could be v the optimization software GenOPT aiming at finding the highest energy savings. And the second was done to opti system with the "Time" control.

Simulation results showed that a very small energy savings can be achieved when applying the "Time" control mo the fact that in winter months the solar pump works and consumes electricity, but the solar radiation is genera enough to produce enough heat to run the chiller and the consumed electricity is wasted.

On the other hand, using the "IR" control mode ensures that the solar pump works only if there is enough solar r that could increase the temperature of the thermal fluid and drive the absorption chiller. Optimization process wa out to determine the optimal value of "IRok" that results in the highest primary energy savings.

The left vertical axis of Figure 7-3 presents the primary energy consumption of the solar and the reference systems right vertical axis presents the difference between them which is the saved primary energy PE_{saved}. Both, the prima consumption and the primary energy saved are plotted as a function of the selected level of radiation at which th loop pump should start "IR_{ok}".

Figure 7-3 shows that if the radiation level at which the system starts is low e.g. 200 W/m^2, the collector pump w early in the morning and the both the collector and the chiller will produce more energy than if it is started at hig radiation e.g. 400 W/m^2. However, the drawback is that the pump and the chiller will consume more electricity

On the other hand, if the system starts at high radiation level e.g. 400 W/m^2 then the electricity consumption by t and the chiller will be less. On the other hand, lower will be the collector and the chiller production too. And thu optimization process is required to find the optimal set radiation level at which the system will achieve the highest energy savings.

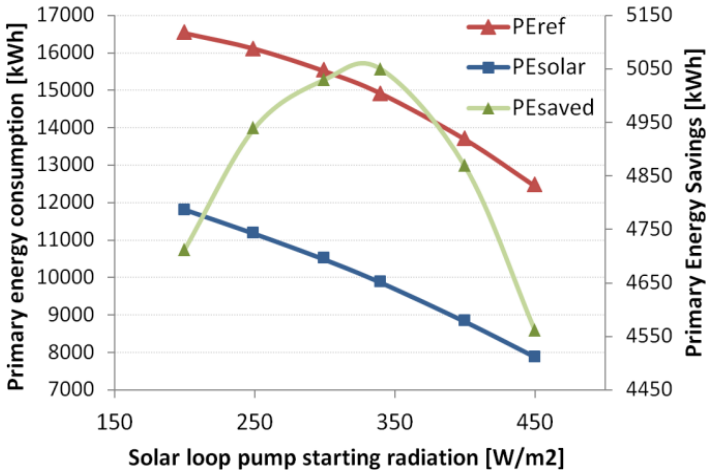

Figure 7-3 Primary energy consumption and savings at different solar loop pump starting radiation.

Applying the optimization algorithms, the optimum solar loop pump starting radiation "IR_{ok}" was found to be W/m^2.Figure 7-3 presents the simulation results for the operation of the system at different starting radiation l showing the optimum operation point. 7% and 20% increment in primary energy savings were achieved by runn system at the optimum operation point compared to starting at low radiation 200W/m^{2}or high radiation 450W/m^{2}respectively.

7.1.3. Absorption chiller

The chiller starts its operation when the input temperature from the hot circuit is higher than the set temperature the chiller "T_{set}". The hot inlet temperature to the chiller's generator has a great influence on the performance of t and the higher this temperature is the better the performance of the chiller. Compared to other parameters that i the performance of the chiller such as the ambient temperature, the hot inlet temperature is adjustable, and w optimization process we are aiming at finding the optimal set temperature T_{set}.

Considering one day, enabling the chiller to start at low starting temperature i.e. *100°C ensures that the chiller w working early and will work for many hours. However, its performance will be low until the hot temperature will around midday. On the other hand, if the chiller is set to start at higher temperatures* i.e. *160°C, the chiller will st but the chiller performance will be better for the shorter period of operation for that day.*

This temperature was varied between (100°C-160°C) and through the optimization process it was found that the starting temperature T_{set} is 145°C as can be seen in Figure 7-4.

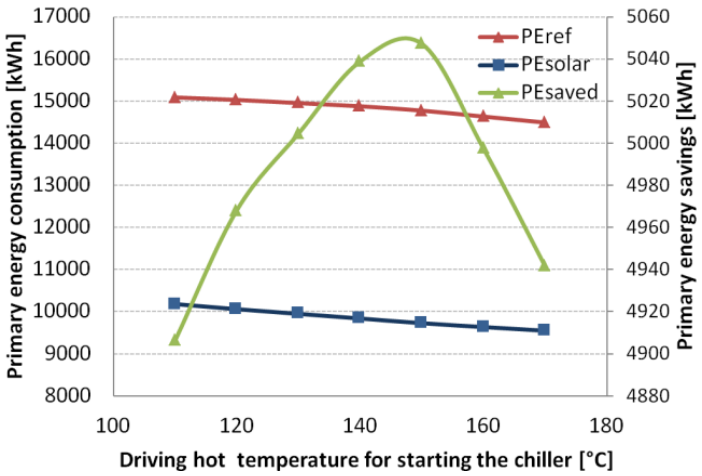

Figure 7-4 Primary energy consumption and savings at different driving hot temperatures for chiller starting.

7.1.4. Implementation and verification of optimization results

Based on the optimization process outcomes, the control strategy of the system was changed from "Time" mode mode with (IR_{ok} = 340 W/m^2) in April 2010. And the starting temperature of the chiller was set to output value optimization (T_{set} = 145 °C).

The average electrical COP of the solar cooling system was in the range of 3 during the months of (May to July) 2009, the value has been improved to the range of 4 during the same months of the next year. And the average of the primary energy ratio PER was improved from 112.5% during the months of (May-July) 2009 to reach a value of 162% during the same months of the year 2010 with an improvement of 44% (see Figure 7-5).

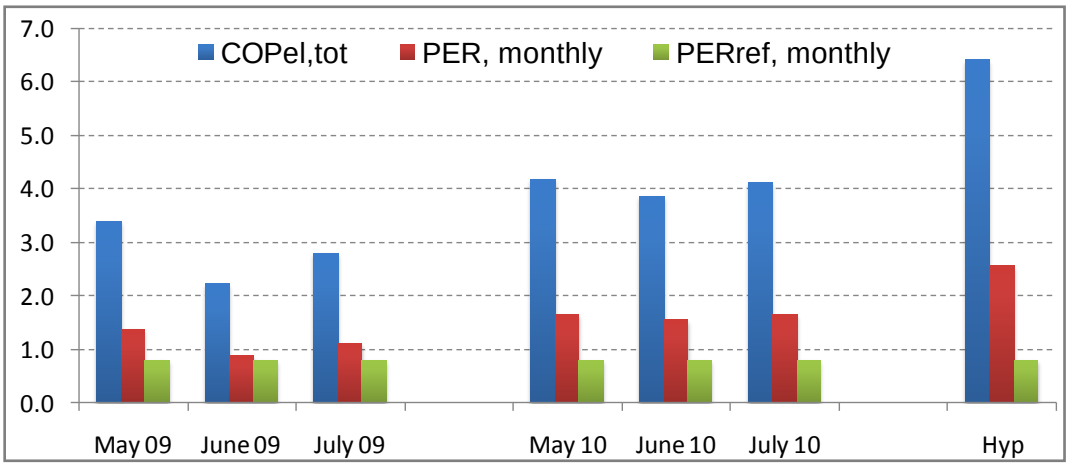

Figure 7-5 Electrical COP and primary energy ration for the solar and the reference systems for different months.

7.2. Optimization potential related to the system components

In this optimization step, the primary energy savings potential associated with the design of system components is investigated.

7.2.1. Pressure drop in the solar loop

The absorption chiller used in this project is a gas fired absorption chiller that was adapted to cope with the solar heat by replacing the gas burner placed at the bottom side of the generator with a heat exchanger. However, the hot water from the solar collector suffers a high pressure drop in this prototype heat exchanger of the generator, resulting in the necessity of using a large circulation pump with high electricity consumption.

This problem can be solved in future installations if the chiller's manufacturer can optimize the hydraulic performance of the heat exchanger. For the current installed system, the potential of primary energy savings related to the reduction of pressure drop in the system by varying the flow rate and the use of variable speed pump is investigated.

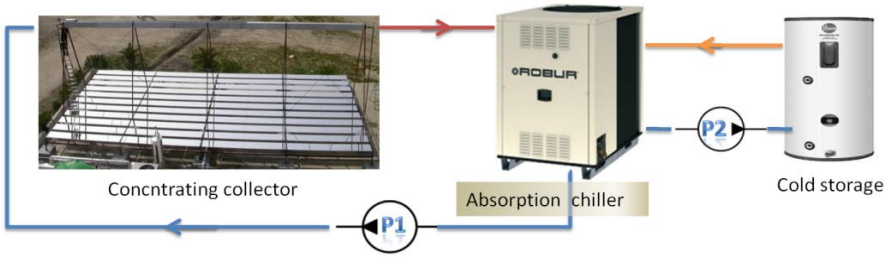

Figure 7-6 simplified scheme of the solar cooling system, presenting the solar loop pump, the solar collector and the chiller.

The solar loop pump (P1) was selected based on the nominal flow rate required by the absorption chiller and the pressure drop of the loop. The nominal flow rate required by the chiller is 3.5 m^3/h, this flow rate is adequate for the solar collector (40l/h/m^2). (See Figure 7-6)

Before the fluid temperature reaches 140°C the hot water circulates in the complete solar loop at the chiller set flow rate 3.5m^3/h for about 90 minutes (in average) for a normal sunny day "warm up period". However, in this period the chiller is not working and the fluid suffers from high pressure drop in the chillers generator. Energy savings can be achieved during the fluid "warm up period" by circulating the water at low flow to reduce the pressure drop in the chiller's generator, but at the same time this level of flow should guarantee a good heat transfer inside the solar collector absorber to ensure a god performance of the collector.

7.2.1.1. Similarity analysis of the pump

Based on similarity laws in pumps, a reduction of the flow rate (V) during the water warm up period from V1= 3.5 m^3/h to V2=1 m^3/h (71%) will reduce the break horse power of the pump's motor by (97%).

V2/V1 =ω2/ω1=0.29

bhp2=bhp1* (ω2/ ω1)^3 =0.023*bhp1.

7.2.1.2. Flow rate limits based on the heat transfer analysis

Based on the steady state one-dimensional model developed by NREL (Forristall, 2003) shown in Figure 7-7, analysis of the heat transfer between the receiver absorber and the heat transfer fluid at different flow rates and temperatures analysis were carried out to determine which is the minimum flow rate that ensure good heat transfer in the collector's absorber. The detailed model implemented in Matlab is given in Appendix [1].

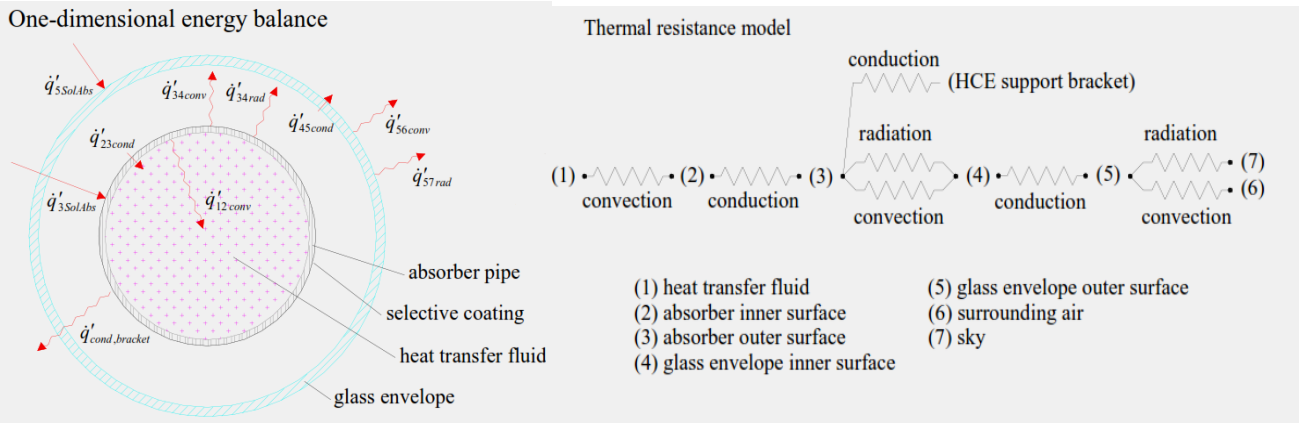

Figure 7-7 a) One-dimensional steady-state energy balance and b) thermal resistance model for a cross-section of an HCE.

The following assumptions have been taken.

1. Solar radiation of 500 W/m^2. (Reasonable value for operation early in the morning), considering that 5.5 m^2 of mirrors are focusing their radiation toward the 1 meter long of absorber, and that the optical efficiency of the absorber is η_0=0.5, then the total absorber radiation by the absorber tube is 1375 W/m-long of the absorber tube.
2. Ambient and sky temperature are equal at the same temperature of 25°C.
3. All receiver geometrical and material characteristic data are based on Schott PTR 70 tube catalogues.
4. The fluid temperature was set to 120°C and the heat losses were calculated at flow rates rising from 1 to 5 m^3/h.

Solving the set of equations describing the heat transfer mechanisms of the one-dimensional steady state model provided detailed information about the heat losses from the absorber at different flow rates at different fluid temperatures. Basically, a low flowrate value down to 1 m^3/h guarantees turbulent flow and good heat transfer characteristics in the absorber tube.

At a temperature of 120 °C of the heat transfer fluid in the absorber tube, the heat loss was calculated to be (17.7 W/m @ 1m^3/h, 14.3 W/m @ 5m^3/h) (see Figure 7-8). This slight increment of the heat losses from the absorber tube when circulating the water at low flow is insignificant compared to the electricity savings by the pump.

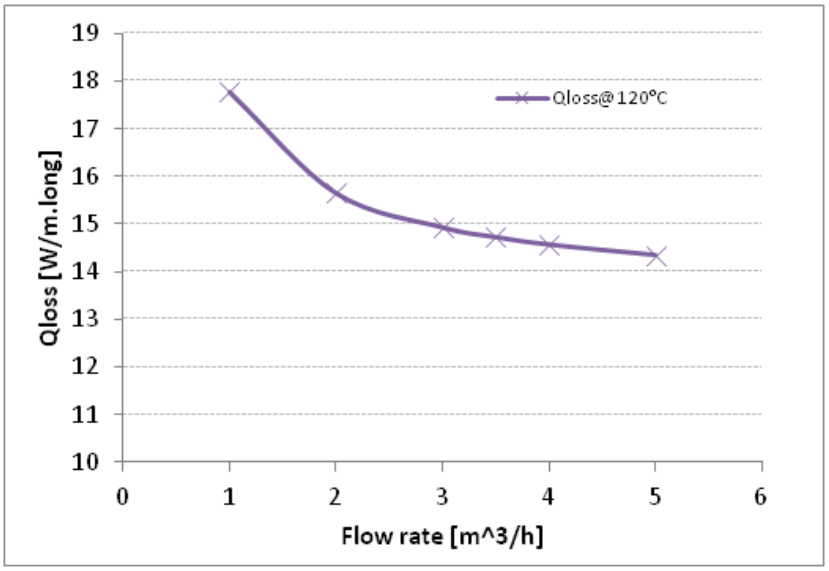

Figure 7-8 The heat loss per meter long of the absorber tube as a function of the flowrate at 120 °C fluid temperature.

A detailed analyses of the pressure drop in the solar loop at different flow rates have been carried out, considering all hydraulic components in the circuit; Receiver tube, steel tubes, hydraulic fittings: valves, bends, filter, tee pieces, flanges, expansion and contractions.

Pressure drop in the chiller's generator is the main contributor to the pressure drop in the solar loop circuit. The curve of the pressure drop of the thermal fluid in the generator provided by the manufacturer was given for diathermic oil at two operating temperatures 190°C and 240°C. The heat transfer fluid used in the installation was selected to be pressurized water rather than diathermic oil due to water's high heat capacitance and low cost compared to oil. In order to plot the pressure drop curve of water in the chiller's generator, and due to the unknown geometrical characteristics of the generator's heat exchanger, thee non-dimensional analysis based on Buckingham theorem were applied to correlate the pressure drop of water to that of thermal oil. The detailed analyses are pretend in Appendix [2].

The total pressure drop versus the flow rate is then calculated, and presented in Figure 7-9 for the solar loop with and without the chiller's generator. Two main results could be concluded from the pressure drop analysis:

1. Circulation the fluid in a closed loop is a situation where the friction losses are dominant and no static head affects the pressure drop in the circuit, and that the system head is proportional to the square of the fluid velocity.
2. It is clear from the pressure drop calculation that a high reduction in the pressure drop in the solar loop can be achieved when running the system at low flow rate.

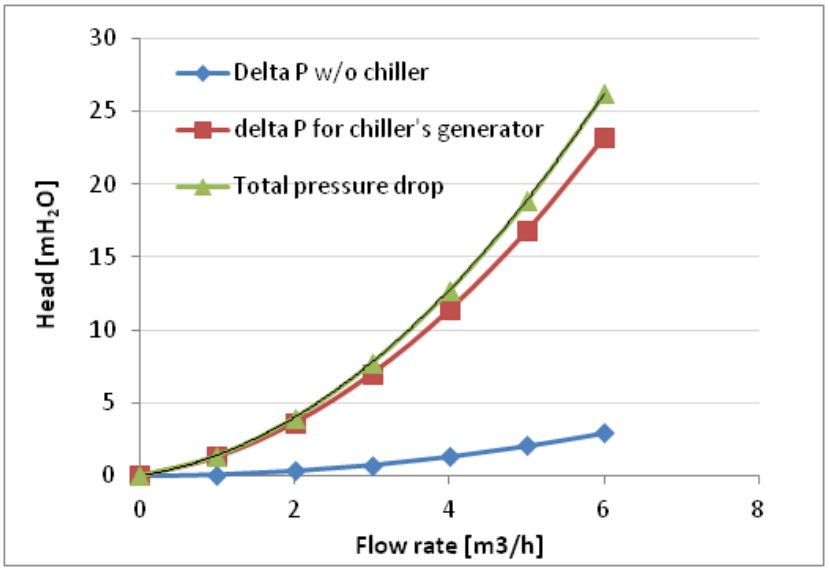

Figure 7-9 Pressure drop in solar loop as a function of the flow rate.

A study of the electricity savings of the pump was done by selecting a variable speed drive that runs the pump at low flowrate during the warm up period. The intersections between the system curve and the performance curves of the pump at different flow rates is presented in Figure 7-10.

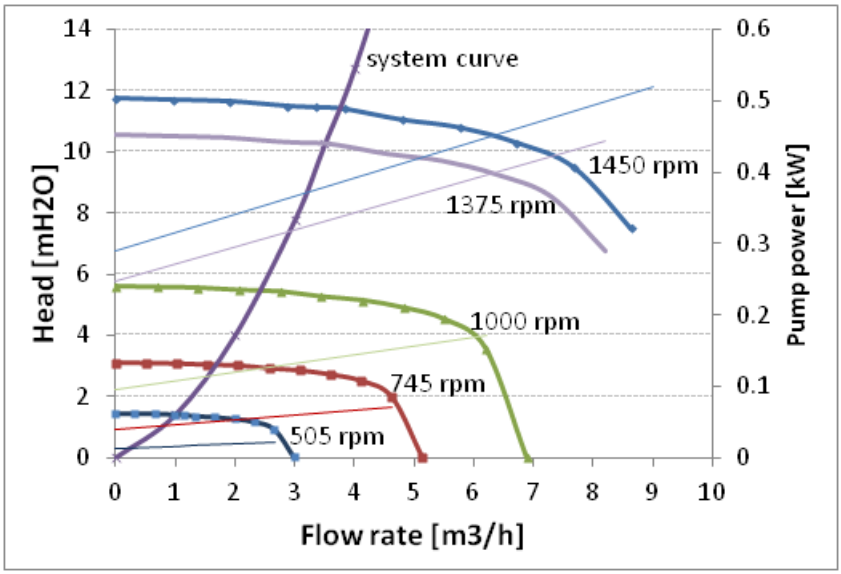

Figure 7-10 Pump performance curve at different rotational speeds.

An annual simulations of the solar cooling system utilizing a constant versus variable speed pump was done, and the results showed that the pump worked at the low speed for about 19% of its operation time which corresponds to 23% savings in the pump electrical consumption which corresponds to energy savings of 466 kWh annually and improvement of the primary energy savings of 30%. (See Table 7-1).

Table 7-1 Operating hours and energy consumption of systems utilizing constant and variable speed pumps.

	TIME [hours]	*E pump [kWh]*	*E chiller [kWh]*	*total pump operation [h]*	*High flow pump operation [h]*	*Low flow pump operation [h]*
Variable speed	8760	1563.7	1856.2	2537.7	2062.4	475.3
Const speed	8760	2030.1	1831.3	2537.7		

7.2.2. Solar collector scale up

For the LFR collector, it was mentioned in the modeling chapter that for collectors with different length but otherwise identical geometry, the transversal IAM remains the same, while the longitudinal IAMs differ due to end losses. The gross heat production (GHP) of collectors with the same width but various lengths was calculated by (Häberle et al., 2007) using the weather data of Seville (see Figure 7-11). As expected, end losses become significant for short collectors like the one installed in the first plant in Tunisia (16 m long) (see Figure 7-12) and the end losses accounted for about 17% of the gross heat production of the collector.

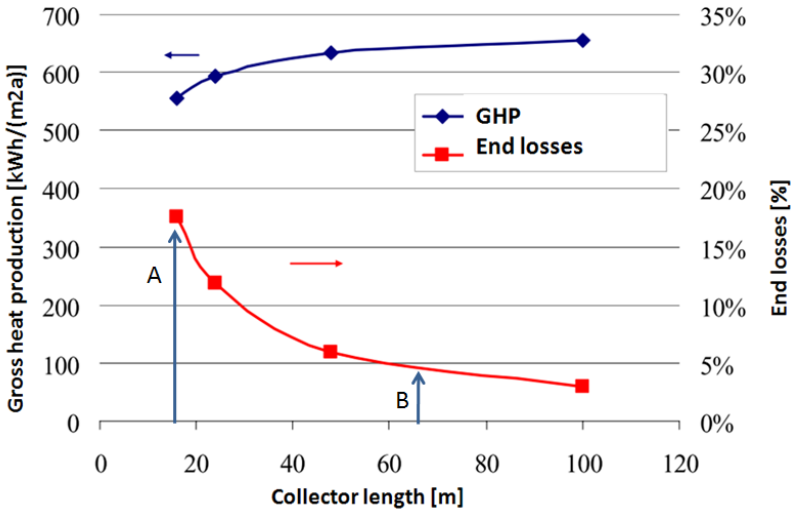

Figure 7-11Gross hear production and end losses for different collector sizes for a fluid temperature of 200°C using the weather data of Seville. (Häberle et al. 2007)

For a larger LFR collector area, for example for the collector installed for the solar cooling plant in Seville University with an aperture area of 352 m^2 and 64 m length (see Figure 7-13), the end losses accounted for only 4% which is 75% less than that of the short collector as can be seen in Figure 7-11.Assuming all the heat produced by the collector is used by the chiller, the scaling up of the collector will result in 15% improvement of the primary energy savings.

Figure 7-12 The LFR collector installed in Tunisia, Area: 88 m^2 Length 16 m

Figure 7-13 The LFR collector installed in Seville University, Area 352 m^2, Length 64 m.

7.2.3. Second optimization step outcomes

Based on the outcomes of the second step of optimization with respect to utilization of a variable speed pump in t loop and the scale up of the solar collector, the outcomes were used for a system simulation that showed a 4 improvement of primary energy savings of the system, which is presented in Figure 7-5 as a Hypothetical mo

7.3. Potential definition

In the previous sections, the optimization of the installed systems was done with a technical perspective only, thus performance indicators have been defined without considering costs. However, the main motivation for deploying solar air-conditioning systems is to save energy, this in turn means a lowering of the running costs for the operator. Therefore solar cooling systems will only have a chance in the industrial sector in the long term if the energy saving and cost reduction aspects can be reconciled with one other. The main objective of the here presented simulations is the definition of the system concept with the lowest cost of saved primary energy (CSPE).

7.3.1. Methodology

In this section, developing the basic system concept in order to achieve better system economics has been carried out. The aims of these developments are to maximize the utilization of the solar system and to augment the cold production of the system, thus, several configurations have been investigated:

1. A compression chiller system. To be used as a reference case.
2. Solar cooling system with direct connection between the solar collectors and the absorption chiller, without hot or cold storages.
3. A solar cooling system with a hot storage connected directly to the solar collectors.
4. A solar cooling system with a hot storage that can be connected through a heat exchanger to the solar collector or bypassed when no excess heat is produced by the collector.
5. Utilize a heating backup to derive the chiller when no solar heat is available.

6. Vary the size of the absorption chiller and the cold tank.

The developed configurations have been simulated through a parametric study, the best control strategy and the optimized operating parameters were identified, and different performance indicators have been calculated. Even thought the absolute energy outcomes of a configuration using the PTC or LFR will be different, the trend of the two systems will be the same when comparing one configuration to another. This lead to the use of one type of collectors in the simulations; as the aim of these simulations is to compare diverse configuration rather than focusing on the absolute outcomes of a specific configuration. The collector used in these parametric studies is the PTC collector.

7.3.1.1. Sites geographical location selection

For the simulation study, different climate scenarios have been selected. In order to limit the number of locations to a reasonable amount on the one hand and – on the other hand get representative results for the potential study – an expedient choice was made. Looking on the World map of Köppen-Geiger climate classification Figure 7-14**Error! Reference source not found.**, five different climatic zones can be found in the Mediterranean. These climatic zones are indicated by three letters. The first one indicates the main climate, the second the precipitation and the last one the temperature.

Three climates where chosen for the simulation study. Since the climatic zones BWh (equatorial, desert, hot arid) and CSa (warm temperate, summer dry, hot summer) not only represent most of the geographic area but also most of the Agro food industry companies are located in one of these two zones. Moreover, the climatic zone BWk (equatorial, desert, cold arid) was due to its favorable conditions of high direct radiation and low ambient temperatures. Weather profiles of these zones were generated using Meteonorm weather data. (METEOTEST, 1999)

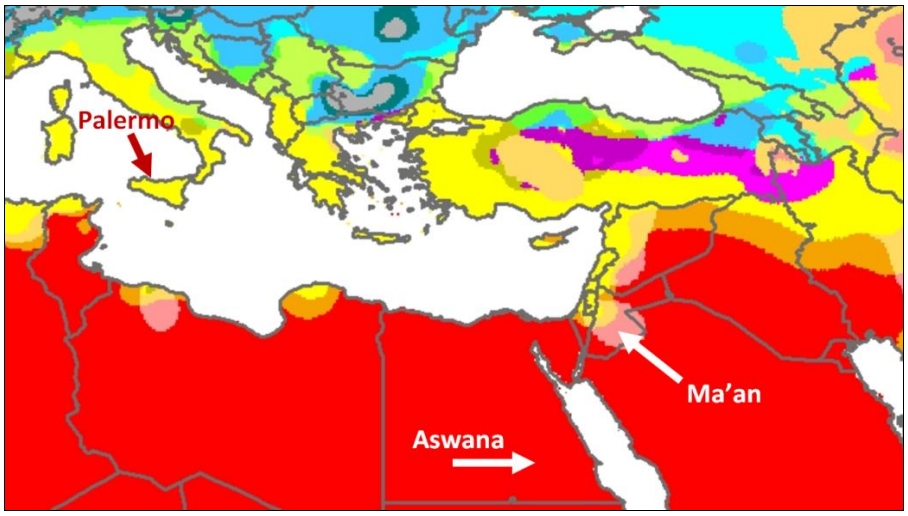

Figure 7-14 World map of Köppen-Geiger climate classification. (Peel, Finlayson, & McMahon, 2007)

The legend of the map colors can be seen in the table below.

	BWh – equatorial, desert, hot arid
	BWk – equatorial, desert, cold arid
	BSh – equatorial, summer dry, hot arid
	BSk – equatorial, summer dry, cold arid
	CSa – warm temperate, summer dry, hot summer

Within these three climatic zones, three cities were selected and their information is presented in the table below. (See Table 7-2)

Table 7-2 Selected sites data.

City	*country*	*Longitude*	*Latitude*	*Altitude [m]*	*Avg. mean Daily ambient Temperature [°c]*	*Annual DNI [kWh/m^2]*
Aswan	Egypt	24 N	32° 53’ E	85	25.9	3137
Ma’an	Jordan	30 11’ N	35° 44’ E	1108	17.3	2360
Palermo	Italy	38 6’ N	13° 22’ E	20	18.3	1681

The weather profiles of the selected three locations were not only used for the simulation of ambient temperature and radiation in the simulation study, but also for the generation of the cooling load profiles for the refrigerated warehouse in the three locations.

7.3.1.2. Cooling load profiles

One of the main requirements in the agro-food industry (AFI) is the ability to conserve the produced fruits and vegetables for certain periods to deal with the market needs. This should be done while keeping in mind the quality of the frozen products.

The analysis of the agro-food industry in the Mediterranean countries showed a high potential for the applications of refrigerated warehouses, and the high share of the AFI total revenue. For example, in Tunisia - the “warehouse” activity includes 770 companies and 22 800 employees (38% of the total employees of the AFI) and the turnover represents 17% of the AFI (ANME, 2008).

For the parametric study analysis, a real refrigerated warehouse project has been selected (See Figure 7-15), all the realistic data concerning the type and quantity of products and their required conserving temperatures, utilization factors for the zones, internal gains (lights, forklift, labor …) were used for the cooling load profile creation.

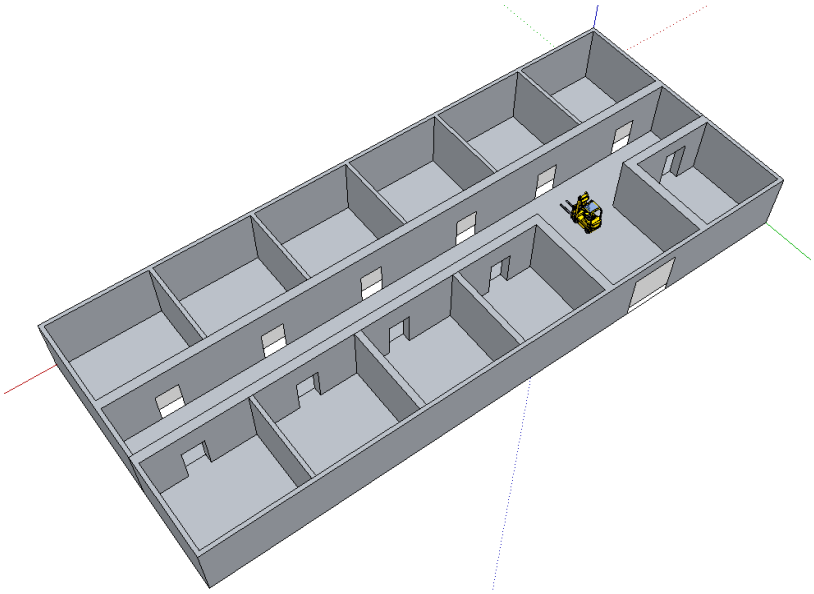

Figure 7-15 Plan of the refrigerated warehouse.

The warehouse consisted of eleven rooms “refrigerated cells” of two different volumes in addition to the connecting corridor. The small cells with a volume of 912 m^3 have room for up to 19500 kg of vegetables, with a maximum daily new products introducing of 3000 kg. The larger cells have room for up to 28700 kg of vegetables, with a maximum daily new products introducing of 5000 kg. In both cases the vegetables introduced with a temperature of 20°C and need to be cooled to 2°C within 20 hours. The maximum cooling load for each zone is presented in Table 7-3. It has to be mentioned that a utilization factor of 0.5 has been used after this analysis was done, which means that the maximum instantaneous cooling load is 245 kW, and the selection of the compression chiller for the reference case was based on this capacity.

Table 7-3 Characteristics of the refrigerated warehouse zones.

ID	zone	length	width	Heigh	Surafce area m2	Volume m3	Temp. operating °C	Temp. introd. °C	kg product day	Time processing hour	Q. -15/+35 kw
1	cell c°1	15	11.4	8	171.0	1,368.0	2	20	5,000	20	40
2	cell c°2	15	11.4	8	171.0	1,368.0	2	20	5,000	20	40
3	cell c°3	15	11.4	8	171.0	1,368.0	2	20	5,000	20	40
4	cell c°4	15	11.4	8	171.0	1,368.0	2	20	5,000	20	40
5	cell c°5	15	11.4	8	171.0	1,368.0	2	20	5,000	20	40
6	cell c°6	15	11.4	8	171.0	1,368.0	2	20	5,000	20	40
7	cell c°7	10	11.4	8	114.0	912.0	2	20	3,000	20	30
8	cell c°8	10	11.4	8	114.0	912.0	2	20	3,000	20	30
9	cell c°9	10	11.4	8	114.0	912.0	2	20	3,000	20	30
10	cell c°10	10	11.4	8	114.0	912.0	2	20	3,000	20	30
11	cell c°11	10	11.4	8	114.0	912.0	2	20	3,000	20	30
12	corridors	50	9	5	450.0	2,250.0	12	20			100
											490

The cooling load profile of the warehouse was created by simulating the building using type 56 in TRNSYS. This simulation considers the climatic conditions around the building taking into consideration the building walls and roof structure and layers as well as the internal gains. As result the major contribution to the cooling load resulted from the refrigeration of the vegetables, which accounts for more that of 50% of the cooling load. The annual cooling load for warehouse on the three selected sites is presented in Table 7-4.

Table 7-4 Annual cooling energy demands for storage on the three selected sites

	Aswan	*Palermo*	*Ma'an*
Annual cooling demand [MWh]	1715	1691	1688

The difference between the cooling load of the three location is not large as one could expect; this is due to the fact that all the vegetables to be refrigerated arrives at the same temperature (20 °C) for the three locations as they are usually pre-cooled. Moreover the warehouse is well insulated and the main contributor to the load which is the refrigeration of the vegetables contributes with the same amount to the three locations due to the same temperatures of the operation in the three sites.

Figure 7-16 presents the cooling load profile for the warehouse building (empty) in the three locations without considering the vegetables refrigeration. The cooling load in Aswan is the highest all over the year due to the high ambient temperatures and solar gains. The low ambient temperatures of the mountain city of Ma'an results in a lowest cooling load in the winter months, however in the summer with the high solar gains, the cooling load increase up to almost the same level of Palermo. The daily average cooling load for the warehouse in Aswan including the vegetables refrigeration load ranges from 185 to 205 kW.

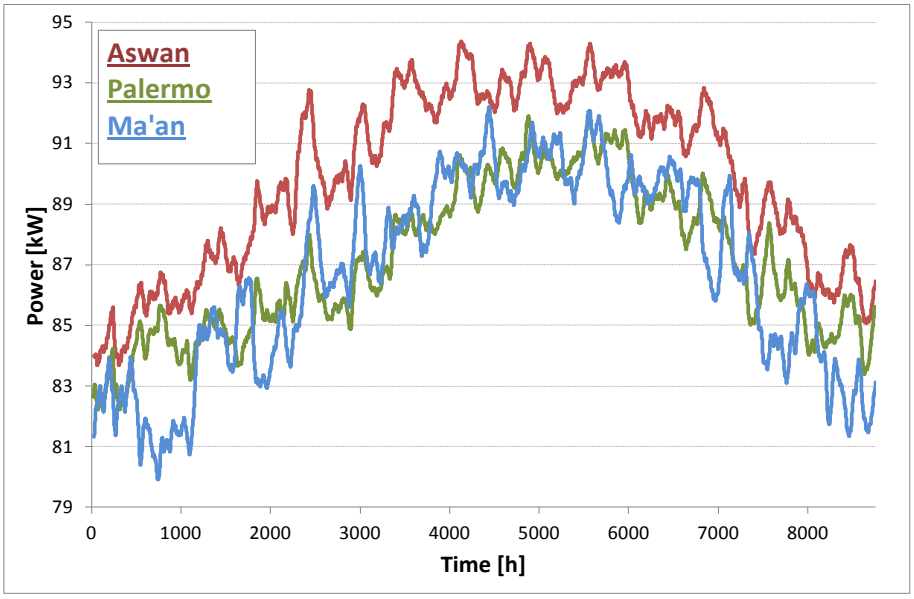

Figure 7-16 Cooling load profile for the warehouse without vegetables for the three selected sites.

7.3.1.3. Parametric studies

7.3.1.3.1. Reference case (Compression chiller)

An air cooled compression chiller that is capable of working at the required temperatures and load has been selected for the simulations of the reference case. The selection was done using Magellano selection software of the company Aermec, and the model NY1500Y was selected. The characteristic and performance data of the selected compression chiller are presented in Table 7-5 and Figure 7-17 .

Table 7-5 Characteristics of the selected compression chiller.

- Refrigerant R410A.
- Electronic thermostatic valve also for low
- water temperature (down to -6°C)
- High-efficiency scroll compressors
- Axial flow fans with reduced noise level
- Aluminum condensing coils.

Nominal operating conditions:

- Cooling capacity: 375 kW
- Total input power: 161 kWel
  @ 35°C ambient temperature
  7°C water outlet temperature
  ΔT = 5°C
  COP=2.33

Figure 7-17 A photo of the selected compression chiller for the reference case simulations

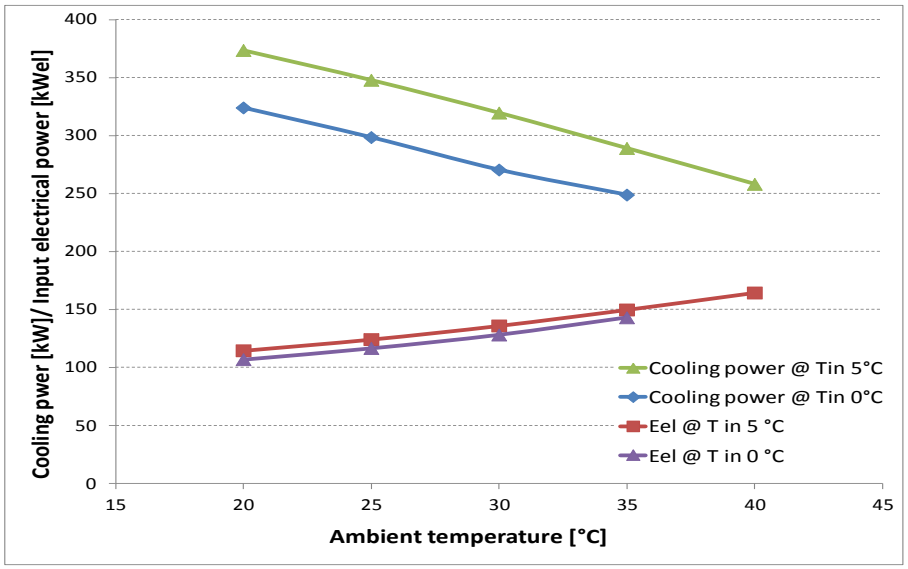

Figure 7-18 Performance data of the compression chiller at different operating conditions.

7.3.1.3.2. Basic case; direct connection between solar collector and absorption chiller.

This is the simplest configuration of a solar cooling system, coupling the solar collectors directly with the absorption chiller without any hot or cold storage (see Figure 7-19).The control tracking system's control and the circulation pump P1 could be based on a time schedule or the availability of the solar radiation. It has been shown in the first part of the optimization chapter that the control based on the solar radiation is more feasible from energy savings point of view. As soon as the temperature reaches the set temperature to run the absorption chiller, the chiller starts running.

A simple improvement for this system can be done by installing a three-way valve V1, as seen in Figure 7-19.This valve directs the thermal fluid through the dashed line back to the circulation pump when the temperature of this fluid is below the temperature required to run the absorption chiller "Tset". The aim of this valve is avoiding the high pressure drop in the chiller's generator when the chiller is not working.

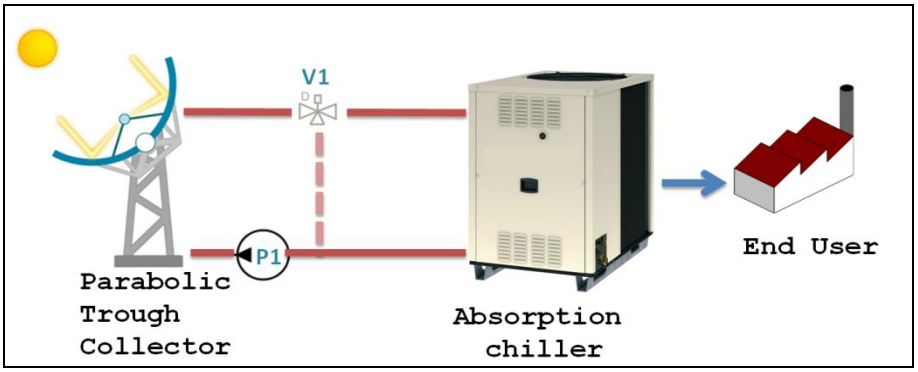

Figure 7-19 Basic case; direct connection between solar collector and absorption chiller.

The main advantage of this system is its simplicity and the elimination of additional cost of hot or cold storages. However, this configuration is suitable only when cooling loads are continuous during the solar radiation hours. In order to comment the simulation outputs, three definitions related to the collector output should be mentioned:

- Collector useful output: defined here as the real useful thermal energy delivered from the collector to the load, with considering the moments of collector defocus due to overheating.
- Collector potential output: defined in a similar way to the collector useful output, but calculated imagining that the collector have no temperature limits and never go into defocus mode.
- Dumped energy: is the difference between the collector potential output and the collector useful output, and represents the thermal energy lost due to the defocus of the collector during overheat moments.

The system was simulated with different numbers of collector modules (9 - 27 modules) which corresponds to (32 - 95 m^2) in terms of aperture area. (See Figure 7-20).

As expected, the collector potential output increases linearly with the increase of the collector field area. However, the collector useful output continues to rise linearly with the collector field area until it reaches a point where adding more collectors will just slightly improve the energy output mainly due to overheating and the defocusing of the collector. This is also presented by the increase of the dumped energy which is presented as the shaded region between the two curves of the collector output. The chiller output basically follows the curve of the collector useful output.

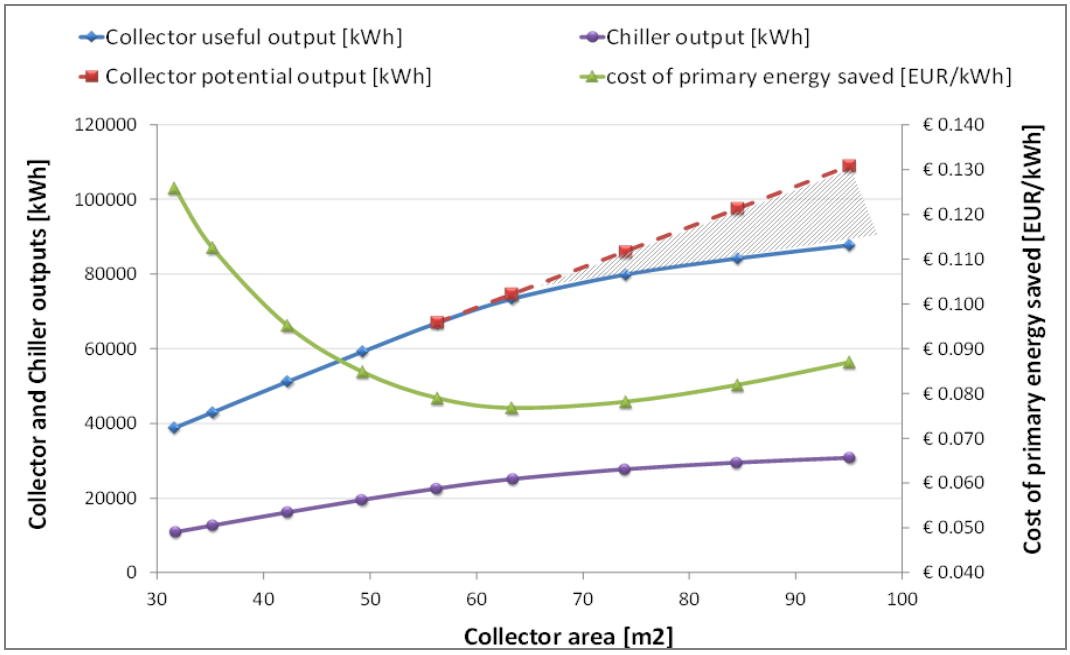

Figure 7-20 Collector and chiller outputs, and the cost of primary energy saved as a function of the collector area.

Increasing the collector field area results in increment of the thermal energy delivered to the chiller as well as the temperature of this supplied heat. And thus improves the performance of the absorption chiller, and as a result, the cost of primary energy saved is decreased.However, the curves show a typical saturation pattern which is due to an increasing number of hours in which collector is turned into defocus mode to prevent overheating, and thus the amount of dumped energy became high and does not justify additional collector area. As a consequence the cost of primary energy saved starts to increase again.

The lowest cost of saved primary energy is achieved by a collector area that produces enough heat with high temperature and with a minimum amount of dumped energy. Figure 7-21 presents the useful annual collector output and Figure 7-22 presents the cost of saved primary energy for different collector areas at the three selected sites. The annual useful collector outputs of the collectors installed in Aswan is the highest compared to the ones installed in Ma'an and Palermo, as a result of the high solar radiation there. And the increase of the useful output with the increase of the collector area tends to be less justifiable for collector areas larger than 63 m^2 (18 modules) due to the increasing amount of dumped energy.

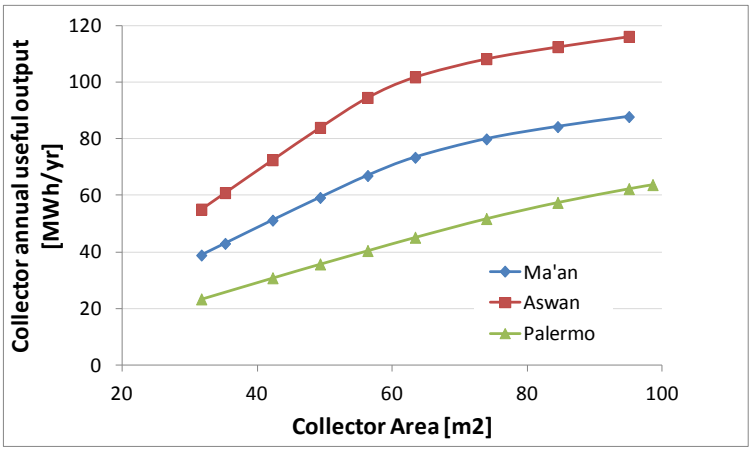

Figure 7-21 The Annual collector useful output [MWh/yr] for different collector areas at the three selected sites.

Based on a detailed economical analysis of the cost of the system components, design and installation, maintenance, the system life time as well as the local conventional energy costs, the cost of saved primary energy was calculated.

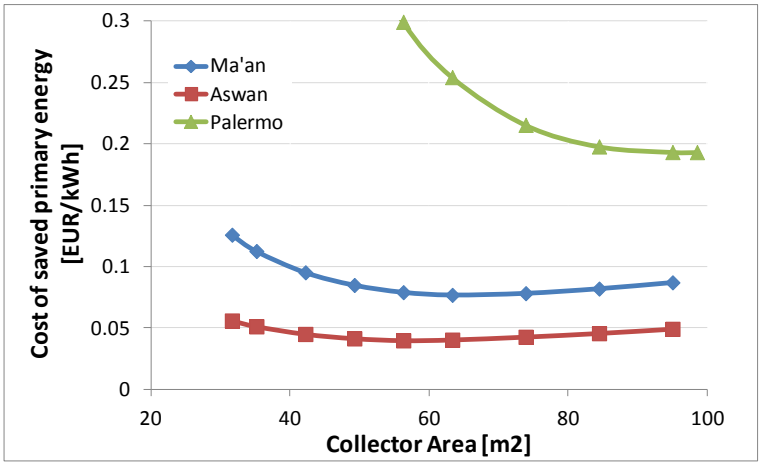

Figure 7-22 The cost of saved primary energy [EUR/kWh] for different collector areas at the three selected sites.

The minimum CSPE for the systems in Aswan, Ma'an and Palermo are 0.039 Eur/kWh, 0.076 Eur/kWh and 0.19 Eur/kWh for a collector field area of 56.3 m^2 (16 modules), 63.3 m^2 (18 modules) and 95 m^2 (27 modules) respectively.

7.3.1.3.3. System with a hot storage

The collector is designed to work at temperatures up to 200°C, above this temperature the collector tracking system will defocus the collector to prevent overheating. This defocusing will decrease the output temperature of the collector and protect the system components, but at the same time it reduces the energy output of the collector, and the lost energy during the defocus period is called the duped energy.

In order to reduce the amount of dumped energy lost during the defocus period, a hot storage could be used to conserve this excess heat to be use when no solar radiation is available.

Two configurations of the connection of hot storages with the solar collectors have been investigated; while the first configuration utilizes the hot storage as a buffer between the collector and the chiller, the second configuration allows a direct connection between the collector and the chiller, and connects the collector to the storage only when excess heat is available at the collector, and connects the storage to the chiller when the temperature of the storage is high enough to run the chiller and there is no availability of heat from the collector.

The two configurations and their outcomes are presented hereafter:

- *Configuration I (Figure 7-23)*

In solar thermal systems with non-tracking collectors, the solar loop pump in the solar thermal systems with hot storage starts when the solar panels temperature is higher than the temperature at the bottom of the hot storage with a ΔT.

However, for a tracking solar collector, the temperature of the thermal fluid will not increase until the collectors are put in tracking mode and the circulation pump circulates the fluid in the collectors' absorbers.

The control of the tracking system and the circulation pump P1 can be set as a function of time or the availability of the solar radiation.

At the beginning of the operation of the collector system, the output temperature of the collector is lower than that at the bottom of hot storage, so the three-way valve directs the flow to the circulation pump P1 to circulate and heat it in the collectors until the output temperature became higher than the temperature of the bottom of the hot storage with a certain ΔT, where at this point the three-way valve direct the flow toward the hot storage.

As soon as the temperature at the top of the hot storage reaches the set temperature to run the absorption chiller pump P2 starts to feed the chiller's generator with the hot fluid and the chiller starts running.

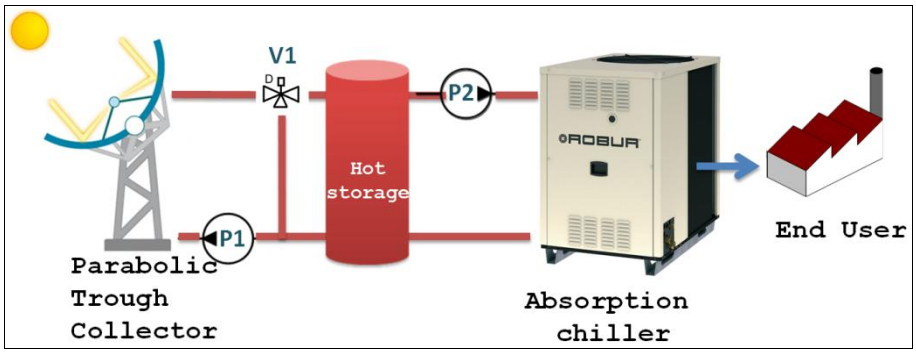

Figure 7-23 Solar cooling system scheme with a hot storage, Configuration I.

- *Configuration II (Figure 7-24)*

A hydraulic design which allows bypassing the hot storage can increase the overall efficiency, but makes the control more complex and requires more system components.

Basically, the system works similar to the direct coupling system during the preheating of the thermal fluid and the normal operation of the absorption chiller.

The additional functionality starts when the temperature out of the collector became higher than a certain value (about 180°C), at this point, the heat exchanger pump P-HX starts to extract heat from the flow returning from the chiller to the collector, thus reducing the temperature of the fluid entering the collector and as a consequence the output temperature of the collector.

When there is no more solar radiation available and the temperature of the hot storage is high enough to run the absorption chiller, the pump between the hot storage and the chiller P2 starts delivering heat to run the chiller while the three-way valve V2 direct the out flow from the chiller to the hot storage.

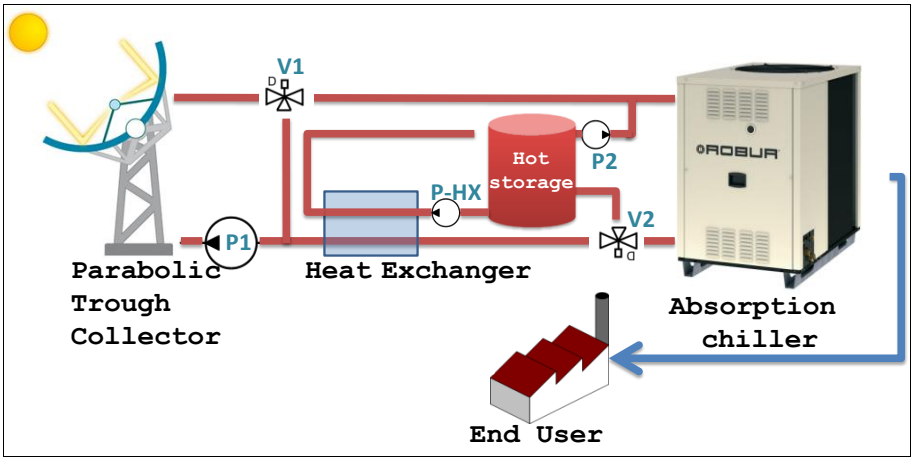

Figure 7-24 Figure 9 Solar cooling system scheme with a hot storage, Configuration II.

The system with its two configurations was simulated with different numbers of collector modules (9 - 32 modules) which corresponds to (32 - 112 m^2) in terms of aperture area and for different volumes of hot storage tanks (no storage tank, 1 m3 storage tank and 2 m3 storage tank).

Simulation results showed a very slight advantage of the second configuration. However, as the second configuration requires and additional pump and a heat exchanger which means additional costs, the improvement in the performance was not reflected in reduction of the CSPE.

Figure 7-25 presents the primary energy saved output and Figure 7-26 presents the cost of saved primary energy for different collector areas and hot storage volumes for the city of Aswan.

The primary energy saved for collector areas smaller than 63 m^2 is almost the same, due to the fact that no dumped energy happens for such a small collector areas. However, for larger collector areas, the hot storage can store the excess heat that would be dumped if no storage exists, and thus the saved primary for systems with a hot storage is higher.

The same amount of primary energy is saved by systems having a 1 m^3 and 2 m^3 coupled to collector field areas less than 84 m^2, this is due to the fact that 1m^3 hot storage can store all the excess heat for this collector field area, and the 2 m^3 hot storage is oversized and the additional cost of this large storage is unjustified for this collector area.

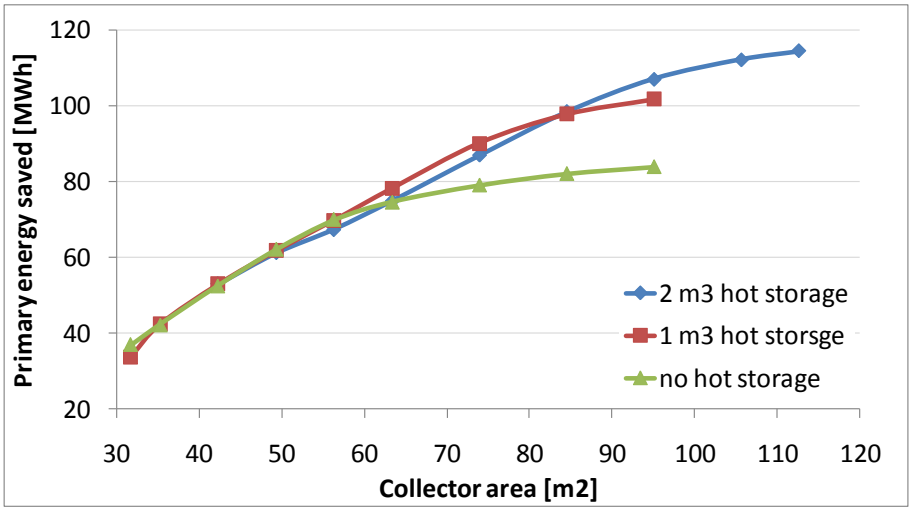

Figure 7-25The Annual collector useful output [MWh/yr] for different collector areas with different hot storage volumes.

Regarding the cost of saved primary energy (CSPE), the system with no hot storage has the lowest CSPE for small collector field area, and systems with a hot storage can only achieve this low CSPE if the amount of dumped energy they saved in the storage justifies the additional cost of the storage, and this happens for larger collector areas.

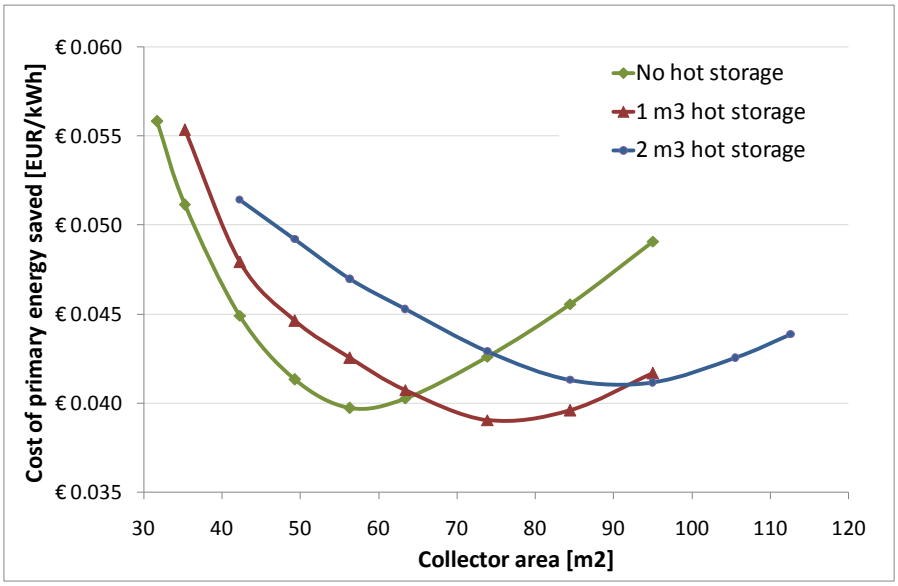

Figure 7-26 The cost of saved primary energy [EUR/kWh] for different collector and hot storage volumes in Aswan.

The economical analysis of the solar cooling system for this specific continuous cooling load showed that installing a hot storage would not reduce the CSPE of the system, but it would prolong the operating period of the system with an additional costs of a hot storage and larger collector field area.

It should be mentioned that for systems with different cooling load profiles that do not match with the solar radiation, a hot and or cold storage would be necessary to match the cold production with the cooling load. And for each specific case, a detailed analysis would be necessary to decide which kind of storages and collector volume are the most suitable and feasible.

7.3.1.3.4. Utilize a heating backup to derive the chiller when no solar heat is available.

The number of operating hours of the absorption chiller in a solar cooling system ranges between 2000-2500 hours per year, depends on the location and boundary conditions.

In order to maximize the utilization and increase the productivity of the system, the number of operating hours of the absorption chiller needs to be increased. This can be done by either integrating a hot storage with an over-sized solar field or by integrating a hot backup as can be seen in Figure 7-27. The previous simulations showed that large collector field areas requires hot storages to store the excess heat to avoid dumping it, which results in a higher system cost. In this section, the second option of integrating a back-up on the hot side is investigated.

When a back-up on the hot side is used, the annual useful solar heat for the cooling application, $Q_{g,sol}$, is given by equation 3.

$$Q_{g,sol} = Q_{g,tot} - Q_{g,back-up} \qquad \text{Equation 3}$$

Where $Q_{g,tot}$ is the total annual heat required for cooling, i.e., for operation of the thermally driven cooling system and $Q_{g,back\text{-}up}$ is the annual heat from a secondary heat source (back-up).

The solar fraction for cooling, SF_{cool}, is then given by equation 4.

$$SF_{cool} = 1 - \frac{Q_{g,back-up}}{Q_{g,tot}} \qquad \text{Equation 4}$$

Based on the low thermal COP of a single effect absorption chiller, the primary energy consumption of an absorption chiller driven by a gas backup alone is higher than that of a conventional compression chiller driven by electricity.

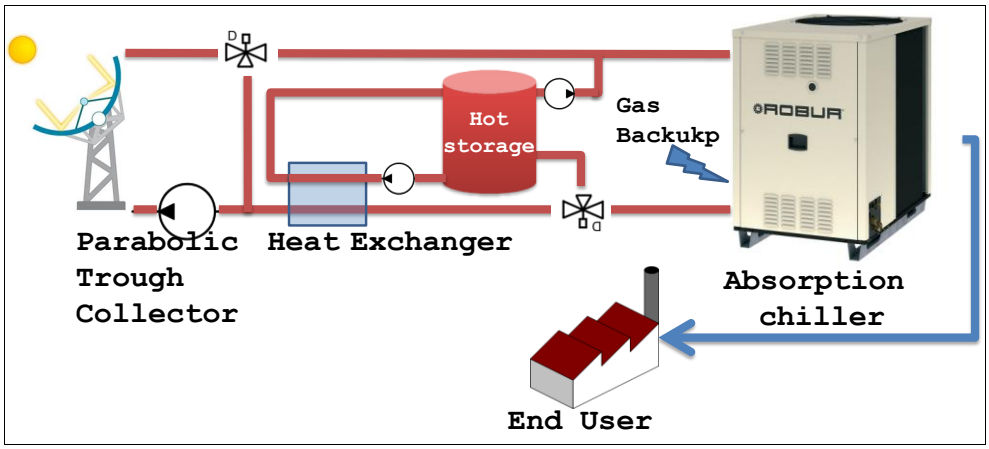

Figure 7-27A solar cooling system with a hot back connected to the absorption chiller.

Thus, the analysis shows that it is necessary to reach a certain value of the solar fraction in order that a solar-assisted cooling system achieves lower primary energy consumption than a conventional system using an electrically driven compression chiller. The system performance with regard to primary energy improves when the COP of the thermally driven chiller increases, the solar fraction increases and the specific electricity consumption of the cooling tower system decreases.(Henning, 2004)

Analyses were carried out to determine the minimum solar fraction the solar-assisted cooling system should achieve in order to save primary energy during its operation for the two locations of Aswan and Palermo.

The specific primary energy consumption of a conventional chiller, driven by electricity, $PE_{spec,conv}$, can be calculated as follows:

$$PE_{spec,conv} = \frac{1}{\varepsilon_{elec} \cdot COP_{conv}} \qquad \text{Equation 5}$$

Where COP_{conv} denotes the COP of the conventional chiller. $PE_{spec,conv}$ is expressed in kWh of primary energy per kWh of cold production.

For a solar-thermally driven chiller, which uses a fossil-fuelled back-up heater as a secondary heat source, the specific primary energy consumption, expressed in kWh of primary energy per kWh of cold production, is given by:

$$PE_{spec,sol} = \frac{1}{\varepsilon_{fossil} \cdot COP_{thermal}} \cdot (1 - SF_{cool}) + PE_{spec,elec} \qquad \text{Equation 6}$$

Where SF_{cool} is the solar fraction for cooling, $COP_{thermal}$ is the COP of the thermally driven chiller and $PE_{spec,elec}$ is the specific primary energy consumption of the electricity needs for the solar loop pump, the solution pump of the chiller and the heat rejection ventilator (kWh_{PE}/kWh_{cold}).

Figure 7-28 presents the primary energy consumption of a solar-assisted thermally driven cooling system with a fossil-fuelled heat back-up as a function of the solar fraction for cooling (i.e., the fraction of the heat needed for the thermally driven chiller that is produced by solar energy). A solar fraction with a value of zero means that all the heat is delivered from the fossil-fuelled backup heater. Analysis was done based on the energy conversation factors in Table 7-6.

Table 7-6 Energy conversion factors and COP in Aswan and Palermo

	Aswan	***Palermo***	
ε_{fossil}	0.9	0.9	
$\varepsilon_{elec.}$	0.3	0.4	
COP_{conv}	2.22	3.09	based on annual simulation
$COP_{thermal}$	0.58	0.53	based on annual simulation

Figure 7-28 also shows the primary energy consumption of a conventional, electrically driven compression chiller. The corresponding specific primary energy consumption, $PE_{spec,conv}$, is calculated using Equation 1. The upper line in the figures is valid for Aswan where the compression chiller showed an overall COP of 2.22, which is a quite low value due to the low evaporator temperatures and high ambient temperature as well as the low coefficient of conversion of electricity. The lower line is valid for Palermo where the compression chiller showed a COP of 3.09, and the electricity conversion factor is 0.4.

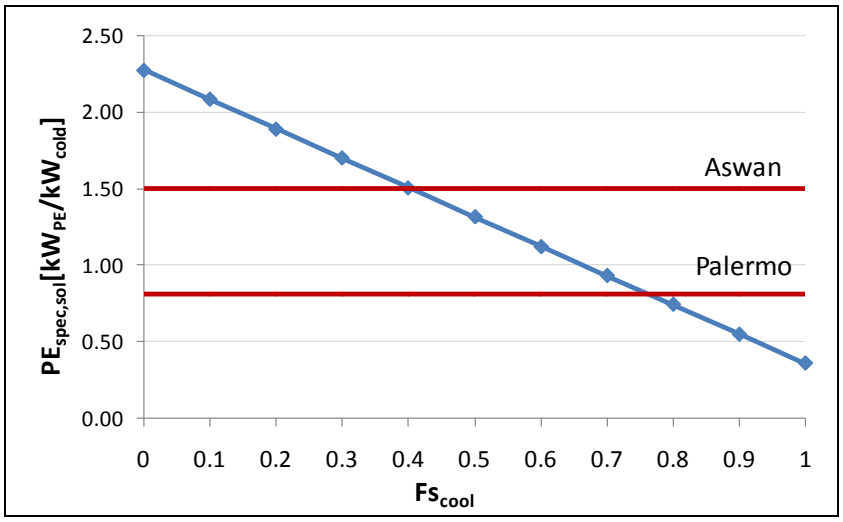

Figure 7-28 Primary energy consumption of a solar-assisted cooling system with fossil-fuelled thermal back-up as a function of the solar fraction.

Analysis presented in Figure 7-28 showed that for a solar-assisted cooling system in Aswan and Palermo should be designed to have a solar fraction higher than 40% and 77% respectively in order to achieve a primary energy savings.

Figure 7-29 presents a comparison between the costs of saved primary energy and cold production for systems without and with a hot backup for different collector areas. As expected, due to the high specific primary energy consumption of the absorption chiller fired by a gas backup, the utilization of the backup didn't result in an increase of the saved primary energy and thus didn't participate in a reduction of the cost of saved primary energy. On the other hand, the cold production of the chiller used in the system with a hot backup has been increased, and as a result the cost of cold produced has been decreased compared to the basic system without backup.

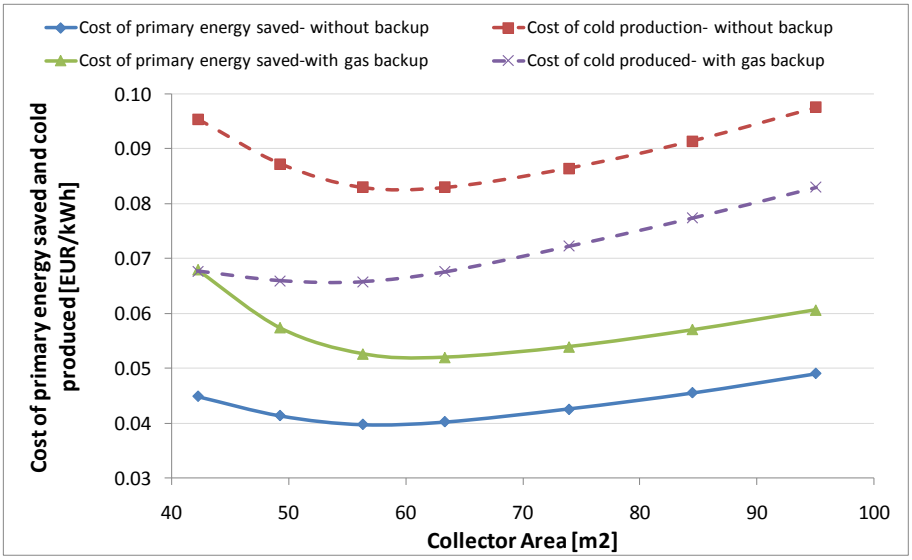

Figure 7-29 Comparison between the costs of saved primary energy and cold produced for systems without and with a hot backup for different collector sizes.

7.4.References

ANME. (2008). *Report on food and agro industries characterization in Tunisia, Morocco and Egypt*.

Forristall, R. (2003). *Heat Transfer Analysis and Modeling of a Parabolic Trough Solar Receiver Implemented in Engineering Equation Solver*.

Henning, H.-M. (2004). *Solar Assisted Air-Conditioning in Buildings A Handbook for Planners*. (H.-M. Henning, Ed.) (p. 150). SpringerWienNewYork.

Häberle, A., Berger, M., Luginsland, F., Zahler, C., Baitshc, M., Henning, H.-M., & Rommel, M. (2007). Linear concentrating Fresnel collector for process heat applications. *Estec 3rd European solar thermal energy conference*.

METEOTEST. (1999). Meteonorm 4.0. Bern, Switzerland.

Peel, M. C., Finlayson, B. L., & McMahon, T. A. (2007). Updated world map of the Köppen-Geiger climate classification. *Hydrology and Earth System Sciences*, *11*(5), 1633-1644. doi:10.5194/hess-11-1633-2007

8. Chapter Eight: Conclusion

The food industry relies heavily on the vapor compression refrigeration cycle for food preservation and processing as refrigeration has become an essential part of the food chain. Unfortunately, due to the scarcity of electricity sources that could run conventional cooling equipments large losses of post-harvest happens in developing countries. Consequently, the possibility to use solar cooling started to be considered an attractive solution.

The aim of this research is to develop, test and optimize solar thermally driven cooling concepts for the food and agro industry in the Mediterranean region, which under local conditions can result economically and socially sustainable. The objective is to asses which systems could better meet actual and future demands of the food and conservation industry sectors in the south edge of the Mediterranean basin and estimate in technical and economical terms the most appropriate approach for the implementation of solar thermal driven systems.

The developed system is intended for refrigeration at -5°C in hot climates, and consists of: medium temperature collector, single effect water ammonia absorption chiller and cold storage. The peculiarity of the configuration is the high temperature difference between the chilled refrigerant temperature, about –5 °C and the condenser temperature (ambient temperature, which could exceed 40 °C). Under these conditions, the absorption chiller must be driven by a medium temperature heat source (e.g. parabolic trough and Linear Fresnel reflector collectors). Moreover, the selected chiller is directly air cooled, and has the advantages of no water consumption, low maintenance work and no legionella problems.

Nowadays (2012), A total of about one thousand solar cooling systems driven by the solar thermal energy are reported worldwide, the vast majority of which are used for air-conditioning applications for residential and office buildings. System configurations including concentrating collectors are rare; less than thirty solar cooling system using concentrating collectors are reported in the detailed literature review conducted throughout this thesis work.

Beside the high capital cost of solar cooling systems, the small number of installed systems with concentrating solar collectors demonstrates the big gap between practical experience in the design and operation of this promising technology, which presents an important barrier against the growth of solar cooling systems.

Design and experimental activities carried out in this research project aim at improving the scientific and experimental knowledge of solar cooling systems utilizing concentrating collectors. To achieve this objective two agro-food industrial applications in the Mediterranean have been selected; a beverage factory in Tunisia, and a diary factory in Morocco.

In order to select the most suitable processes for cooling utilizing solar cooling systems, several site visits and energy audit were conducted to the plants and the best integration of the solar cooling system and the existing cooling systems was identified. The philosophy of the integration of the solar driven plant with the existent refrigeration system aimed at keeping the independence as high as possible, in term of regulation, control and moreover flexibility, feasibility and reproducibility.

In order to size the plant components and carry out the system's detailed design, different system solutions were set-up and simulated on a specific simulation platform (i.e., TRNSYS). For this reason, mathematical models of the main system components were developed, if necessary, implemented and validated. Moreover, several issues were investigated such as the implementation of energy storages hot and/or cold, different backup systems and various collector technologies with different axis orientations. The numerous annual simulation studies resulted in two system designs for the two end users.

A review of concentrating solar collectors and analysis of their thermo-economical performance as well as their availability was done to select the most suitable collectors for the two installations. The review was undertaken for collectors already available in the market and for prototypes in pre-market phase.

Detailed engineering analysis have been carried out in the detailed designs phase of the two plants considering the control system, pipes, valves and integration with existing systems.

The first experimental setup was installed for a beverage factory in Grombalia-Tunisia and consisted of a Linear Fresnel reflector (LFR) collector (North-South oriented /88 m^2 aperture area) connected to a water-ammonia absorption chiller (about 13 kW).The latter cools a cold water-glycol storage (3 m^3). The heat transfer fluid selected in the primary (i.e., solar) loop is pressurized water (up to 16 bar).

The second experimental setup was installed for a dairy factory in Marrakech-Morocco, the system consisted of a parabolic trough collector (32^o to the east from the North-South axis/58.5 m^2 aperture area) coupled with a water-ammonia absorption chiller (about 13 kW) that delivers cooling to the load directly or cools a phase change material PCM cold storage (2 m^3) when no cooling load exists. The heat transfer fluid selected for the primary loop is diathermic oil.

During my frequent participation in experts sessions related to data monitoring and analysis of solar cooling systems – Task 38: Solar Air-Conditioning and Refrigeration, within the International Energy Agency (IEA) Solar Heating and Cooling Programme – I contributed to the development of a comprehensive and unified monitoring procedure.The latter in order to allow a clear comparison between monitoring results of different installed systems, evaluating the primary energy ratio and other energy performance figures. The procedure describes the sensors required to evaluate a

specific performance factor and puts constrains on the acceptable uncertainty of the sensors and the monitoring system to ensure the quality of the analysis.

The developed performance figures established the basis on which the monitoring systems design and the analysis of the monitored data were carried out. The monitoring system consisted of global and diffused pyranometers, thermometers and electromagnetic and ultrasonic flow meters. All these sensors have been connected to a data acquisition system that is connected to a computer. A data acquisition application was developed using the platform LabView.

In order to ensure the reliability of the measured data, all sensors were selected and calibrated. An error propagation analysis was carried out to evaluate the uncertainty of the measured data and the calculated outputs.

During the first summer season of monitoring the system installed in Tunisia, both the solar collector and the chiller were able to operate at their maximum design temperatures (180°C for the collector and -8°C for the chiller). The electrical COP and the average primary energy ratio of the solar cooling system were in the range of 3 and 112.5% respectively during the months of (May-July) 2009.

After the first monitoring season, results obtained from the monitoring activities of the system's performance were utilized for the simulation models validation.

For the Linear Fresnel Reflector (LFR) collector model, this was done by identifying the model parameters by coupling the TRNSYS simulation software model to the generic optimization software GenOpt. The measured solar radiation, input temperature and flow rate to the LFR collector e(t) is applied as input signals to the TRNSYS models.The measured output (y_{meas}) is compared to the simulated output (y_{sim}), which is dependent on the parameters set *P*. The measured output (y_{meas}) is compared to the simulated output (y_{sim}) and the Generalized Pattern Search algorithm (Hooke-Jeeves) was used to derive the best parameter set *P* to minimize the difference between simulated and measured output temperatures.

For the absorption chiller model, data acquired from the quasi-steady state operation of the system during 2009 and 2010 were analyzed using a parametric-empirical approach to correlate cooling power and chiller's thermal COP to its operating conditions. Based on the validated correlations of the cooling power and COP of the absorption chiller, a performance map covering the entire range of possible operation conditions was created and used as input to the TRNSYS model.

Validated models were used for further simulation campaign to optimize the system performance. The first optimization step was carried out in order to identify the optimum operating parameters and best control strategy. Applying the results of this optimization step did not require hardware changes and was implemented without the necessity for long stand-by durations of the plant.

The saved primary energy was set as the objective function to be maximized by this optimization procedure aiming at defining the optimal control strategy for the solar loop pump and the absorption chiller. The control of the solar loop pump can be either based on a scheduled operating hours "Time" mode or on the availability of the solar radiation "IR" mode. The chiller starts its operation when input temperature from the hot circuit is higher than the set temperature to start the chiller "T_{set}". Based on the optimization process outcomes, the control strategy of the system was changed from "Time" mode to "IR" mode with (IR_{ok} = 340 W/m^2) in April 2010. The starting temperature of the chiller was set to the output value of the optimization process (T_{set} = 145 °C). As a result, electrical COP and average primary energy ratio of the solar cooling system were in the range of 4 and 162% respectively during the months (May-July) of 2010 with performance improvement of 30% compared to the same period of the previous year.

The second optimization step was undertaken to investigate primary energy savings potential related to components design and installation. This included a study of the pressure drop of the heat transfer fluid in the solar loop and the chiller's generator and the optical losses of the solar collector. This optimization step addressed possible improvements of components for consideration of components producers and design of future plants.

Thermal-hydraulic analysis of the solar loop was undertaken. This included a detail analysis of the heat transfer in the absorber of the LFR collector and a non-dimensional analysis for the pressure drop in the chiller's generator. The motive of the analysis was to study the feasibility of using a variable speed pump instead of the constant speed pump currently used. Annual simulations of the solar cooling system utilizing a variable speed pump was conducted and results showed 23% savings in electrical consumption of the pump which corresponds to energy savings of 466 kWh annually and improvement of the primary energy savings of 44 %..

In regards to the optical losses of the LFR collector, end losses became significant for short collectors such as the one installed in the first plant in Tunisia (16 m long) which accounted for about 17% of the annual gross heat production of the collector. For a larger LFR collector area such as the one installed for the solar cooling plant in Seville University with an aperture area of 352 m^2 and 64 m length, end losses accounted for only 4% which is 75% less than that of the short collector. Assuming all the heat produced by the collector is used by the chiller, the scaling up of the collector will result in 15% improvement of the primary energy savings.

Based on the outcomes of the second optimization step in respect to the utilization of a variable speed pump in the solar loop and the scale up of the solar collector, the outcomes were used for system simulation that showed 45 % improvement in electrical COP and primary energy savings of the system.

The third optimization step was carried out to study the behavior of different configurations of solar cooling systems in different climatic zones for the same type of application aiming to identifying the optimal system design under certain circumstances.

In this simulation step, parametric study analyses were done for an actual refrigerated warehouse project. The cooling load of the warehouse is based on the analysis of its actual operation data and climatic data of cities from three different climatic zones that accommodate the majority of Agro-food industrial activities in the Mediterranean; Aswan-Egypt, Ma'an-Jordan and Palermo-Italy.

Three solar cooling system configurations and a reference case using a compression chiller were simulated, the solar systems simulated are:

a) Basic case; direct connection between solar collector and absorption chiller.

The main advantage of this system is its simplicity. However, this configuration is only suitable when cooling loads are continuous during the solar radiation hours. Otherwise a hot and/or cold storage is required. The lowest cost of saved primary energy is achieved by a collector area that produces enough heat with high temperature and with a minimum amount of dumped energy. The annual useful collector outputs of the collectors installed in Aswan is the highest compared to the ones installed in Ma'an and Palermo due to its high solar radiation.

b) Solar cooling system with hot storage.

In order to reduce the amount of dumped energy lost during the defocus period, hot storage could be used to conserve this excess heat for utilization when no solar radiation is available. Two configurations of the connection of hot storages with the solar collectors were investigated.

The techno-economical analysis of the solar cooling system for this specific continuous cooling load showed that installing hot storage would reduce the CSPE of the system but would prolong operating periods with additional costs of the hot storage and require larger collector field area.

It should be mentioned that for systems with different cooling load profiles that do not match the solar radiation, a hot and or cold storage would be necessary to match the cold production and cooling load. For each specific case, detailed analysis is necessary to specify which kind of storages and collector volume are most suitable and feasible.

c) Solar-assisted cooling system with hot backup.

In order to maximize utilization and increase productivity of the system, the number of operating hours of the absorption chiller needs to be increased. This can be done by integrating a hot backup.

However, the analysis shows that it is necessary to reach a certain value of the solar fraction in order for the solar-assisted cooling system to achieve lower primary energy consumption than that of a conventional system using an electrically driven compression chiller.

The results of simulations showed that due to the high specific primary energy consumption of the absorption chiller fired by gas backup, the utilization of the backup did not result in increasing the saved primary energy and thus did not participate in a reduction of the cost of saved primary energy. On the other hand, the cold production of the chiller used in the system with hot backup has been increased and as a result the cost of cold production decreased compared to the basic system (without backup).

The study demonstrated that the presented solar refrigeration concept is technically viable and rentable from an energy point of view specially when considering the main advantage of the chiller being air cooled and can produce refrigeration effect even in hot areas with water scarcity if enough solar radiation is available.

Throughout this project, several optimization options have been studied, the results highlighted the higher impact of some optimization options. Monitoring results showed that 44% improvement of the primary energy savings of the system has been achieved by optimizing the control strategy. Further optimization options related to the components design showed that 45% improvement of the primary energy savings of the system could be achieved.

Appendix 1 One-dimensional steady state receiver model in Matlab

```
function f=reciver(x)
%Fluid
%T1=120; % T=MEAN BULK temperature of water. assume (150°C)
T2=150; %inside surface temperature of the absorber (160°C)
%T3=95.33; % outside surfece temperature of the absorber (162°C)
%T4= 25.979; % inner glas surface temperature [°C]
%T5=25.914; % outer glass surface tempearture [°C]

T=[130       260       30.284       29.932]
T1=T(1,1);
T3=T(1,2);
T4=T(1,3);
T5=T(1,4);


P=Xsteam('psat_T',T1)+2; %bar (saturation pressure is 4.76 bar) pressure of water.
assume 2 bar above saturation.
Miu=Xsteam('My_PT',P,T1); %dynamic viscosity [kg/m.s]
k=Xsteam('tc_PT',P,T1);%thermal conductivity of water
Cp=Xsteam('Cp_PT',P,T1);%specific heat at isentropic pressure [kJ/kg.K]
Rho=XSteam('rho_pt',P,T1); %Rho= density  [kg/m^3]
Pr= 1000*(Miu*Cp)/k; %Prandtl number (Miu*Cp/k)

%Glass cover
tg=3*10^-3; % glass cover thickness
D4=125*10^-3; % D=glass cover outer diameter [m]
D5=D4-2*tg; % D=glas cover internal diameter [m]

%pipe constans
tr=2.1*10^-3;% absorber tube thickness;
D3=70*10^-3; % D=reciever outer diameter [m]
D2=D3-2*tr; % D=reciever internal diameter [m]
L=16;%pipe length in meters [m]
A=D2^2/4*pi; %A= pipe cross section area [m^2]
R=0.15*10^-3; % roughness (Value based on NORSOK designers)
RR=R/D2; % relative roughness


% Flow
%Vdot = 3.5; %Vdot=flow rate [m^3/h]
Vdot=3.5;
V=(Vdot/3600)/A; % [m/s] %V=velocity [m/s]

format shortG
ln = @log; % necessary to be able to use ln() function.

%1. Convection heat transfer between the HTF and the receiver.
Re=(Rho*V*D2)/Miu; %Re=(Rho*V*D)/Miu
Lh_turbulent = 10*D2; % Entry length
f=colebrook(Re,RR);% friction factor based on Colebrook equation
%Nu=0.125*Re.*Pr.*f % Nusselt number
Nu1= ((f/8)*(Re-1000))/(1+12.7*(f/8)^0.5*(Pr^(2/3)-1))
h1=(k*Nu1)/D2 % convection heat transfer at T1 [W/m^2K]
```

```
%plot(Re,h,Re,f)
Q12conv= h1*D2*pi*(T2-T1)


%2. Conduction Heat Transfer through the Absorber Wall
k23=((0.013)*(T2+T3)/2)+15.2; % [W/mK] for stainless steel 304L
Q23cond=2*pi*k23*(T3-T2)/ln(D3/D2) %%maybe it should be T3-T2

%3. Heat Transfer from the absorber to the glass envelope
%3.a convection
epsilon= 3.53*10^-8;%? = molecular diameter of annulus gas (cm)
pa=1*10^-4; %annulus pressure in Torr.
lampda=2.331*10^-20*(((T3+T4)/2)+273.15)/(1*10^-4*(3.5.*10^-8)^2); %(lampda)= mean-
free-path between collisions of a molecule (cm
b=(9*lampda-5)/(lampda+1);
kst=0.2551; %thermal conductance of the annulus gas at standard temperature and
pressure (W/m-K)
h34=kst/((D3/(2*ln(D4/D3))+b*lampda*(D3/D4+1)));
Q34conv=pi* D3*h34*(T3-T4);

%3.b Radiation
% emisivity is assumed to be 10% for bothe the glass and the steel
Q34rad=(5.67*10^-8*pi*D3*((T3+273.15)^4-(T4+273.15)^4))/(10+0.9*D3/(0.1*D4))

%4. Conduction heat transfer in the glass envelope

k45=1.04; %thermal conductivity of glass 1.04 [W/m.°C]
Q45cond=2*pi*k45*(T4-T5)/ln(D4/D5) %

%5. Heat transfer from the glass envelop to the atmosphere.
%5.a convection
T6=25; % ambient temperature [°C]
Red5=1.184*4*125*10^-3/(1.849*10^-5);
Pr6=0.7296;
Pr5=0.7241;
k56=0.02514;
Nud5=0.26*Red5^0.6*Pr6^0.37*(Pr6/Pr5)^0.25 ;% Nussuelt number based on glass cover
outer diameter. avg. wind speed (4m/s)
h56=k56*Nud5/D5;
Q56conv=h56*pi*D5*(T5-T6)
%5.b radiation
T7=T6; % assume sky temperature equals ambient temperature during the day.
Q57rad=5.67*10^-8*D5*pi*0.1*((T5+273.15)^4-(T7+273.15)^4)




Qloss=Q34conv+Q34rad

%Doutput=[x1;x2;x3;x4;x5;x6;x7]
%csvwrite('output.txt', Doutput)
%dlmwrite('myfile.txt', Doutput, 'delimiter','\t', ...
%         'precision','newline', 6)
%type output.txt
```

```
%%Energy Balance equations%%

%solve('a*x^2 + b*x + c')
%1. Q12conv= Q23cond
%h1*D2*pi*(T2-T1)-2*pi*k23*(T2-T3)/ln(D3/D2)=0);

%2. Qsolabs= Q34cov+Q34rad+Q23cond
%2750=pi*                          D3*h34*(T3-T4)+(5.67*10^-8*pi*D3*((T3+273.15)^4-
(T4+273.15)^4))/(10+0.9*D3/(0.1*D4))+2*pi*k23*(T2-T3)/ln(D3/D2);
%3. Q45cond=Q34rad+Q34conv
%2*pi*k45*(T4-T5)/ln(D4/D5)=(5.67*10^-8*pi*D3*((T3+273.15)^4-
(T4+273.15)^4))/(10+0.9*D3/(0.1*D4))+pi* D3*h34*(T3-T4);
%4. Q45cond=Q56conv+Q57rad
%2*pi*k45*(T4-T5)/ln(D4/D5)=h56*pi*D5*(T5-T6)+5.67*10^-8*D5*pi*0.1*((T5+273.15)^4-
(T7+273.15)^4)

%Q23cond=2*pi*k23*(T2-T3)/ln(D3/D2); %%maybe it should be T3-T2
%Q34conv=pi* D3*h34*(T3-T4);
%Q34rad=(5.67*10^-8*pi*D3*((T3+273.15)^4-(T4+273.15)^4))/(10+0.9*D3/(0.1*D4));
%Q45cond=2*pi*k45*(T4-T5)/ln(D4/D5); %
%Q56conv=h56*pi*D5*(T5-T6);
%Q57rad=5.67*10^-8*D5*pi*0.1*((T5+273.15)^4-(T7+273.15)^4);

T1=x(1);
T3=x(2);
T4=x(3);
T5=x(4);
%1. Q12conv= Q23cond
f(1)=h1*D2*pi*(T2-T1)-(2*pi*k23*(T3-T2)/ln(D3/D2));

%2. Qsolabs= Q34cov+Q34rad+Q23cond
f(2)=-2750+pi*                     D3*h34*(T3-T4)+(5.67*10^-8*pi*D3*((T3+273.15)^4-
(T4+273.15)^4))/(10+0.9*D3/(0.1*D4))+2*pi*k23*(T3-T2)/ln(D3/D2);

%3. Q45cond=Q34rad+Q34conv
f(3)=2*pi*k45*(T4-T5)/ln(D4/D5)-(pi*                    D3*h34*(T3-T4))-((5.67*10^-
8*pi*D3*((T3+273.15)^4-(T4+273.15)^4))/(10+0.9*D3/(0.1*D4)));
%f(3)=2*pi*k45*(x(3)-x(4))/ln(D4/D5)-((5.67*10^-8*pi*D3*((x(2)+273.15)^4-
(x(3)+273.15)^4))/(10+0.9*D3/(0.1*D4))+pi* D3*h34*(x(2)-x(3)));
%4. Q45cond=Q56conv+Q57rad
f(4)=2*pi*k45*(T4-T5)/ln(D4/D5)-(h56*pi*D5*(T5-T6))-(5.67*10^-
8*D5*pi*0.1*((T5+273.15)^4-(T7+273.15)^4));
%f(4)=2*pi*k45*(x(3)-x(4))/ln(D4/D5)-(h56*pi*D5*(x(4)-T6)+5.67*10^-
8*D5*pi*0.1*((x(4)+273.15)^4-(T7+273.15)^4));


end
```

Appendix 2 Pressure drop analysis in the chiller's generator

The heat exchanger of the gas-fired absorption chiller was modified to be heated by the thermal hot fluid of the solar field as shown in figure 1. However, the data of pressure drop of the thermal fluid in the generator is given for diathermic oil at two operating temperatures 190°C and 240°C as shown in figure 2.

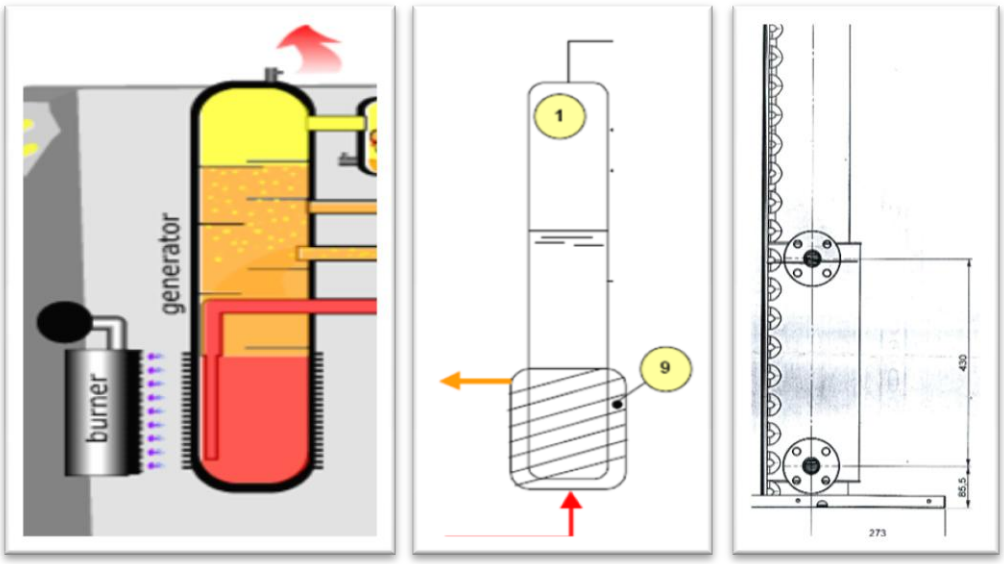

Figure 30 Absorption chiller generator, a. Gas-fired. b. Schematic of indirect fired. c. Scheme with dimensions.

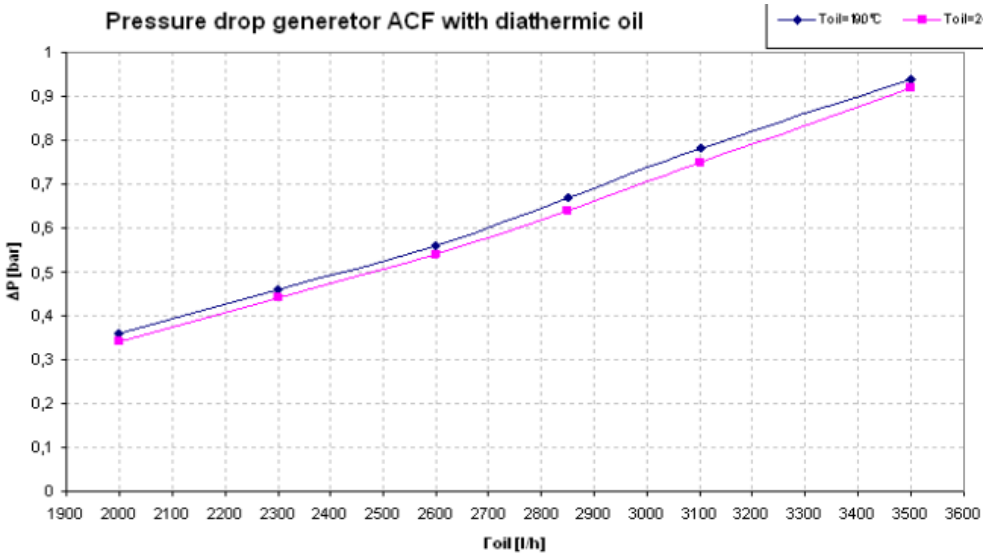

Figure 31 Pressure drop of diathermic oil at different flow rates and temperatures.

The heat transfer fluid in solar field of the installation was selected to be pressurized water rather than diathermic oil; due to water's high heat capacitance and low cost compared to oils. And the task here is to find the related chart of pressure drop of water in the generator at variable flow rates.

Heat exchanger geometry:

The internal geometry of the heat exchanger is unknown, however, a drawn to scale diagram presents the external dimensions of it. These dimensions were extracted. And a primary assumption of the heat exchanger as a jacket heat exchanger was done as shown in figure 3.

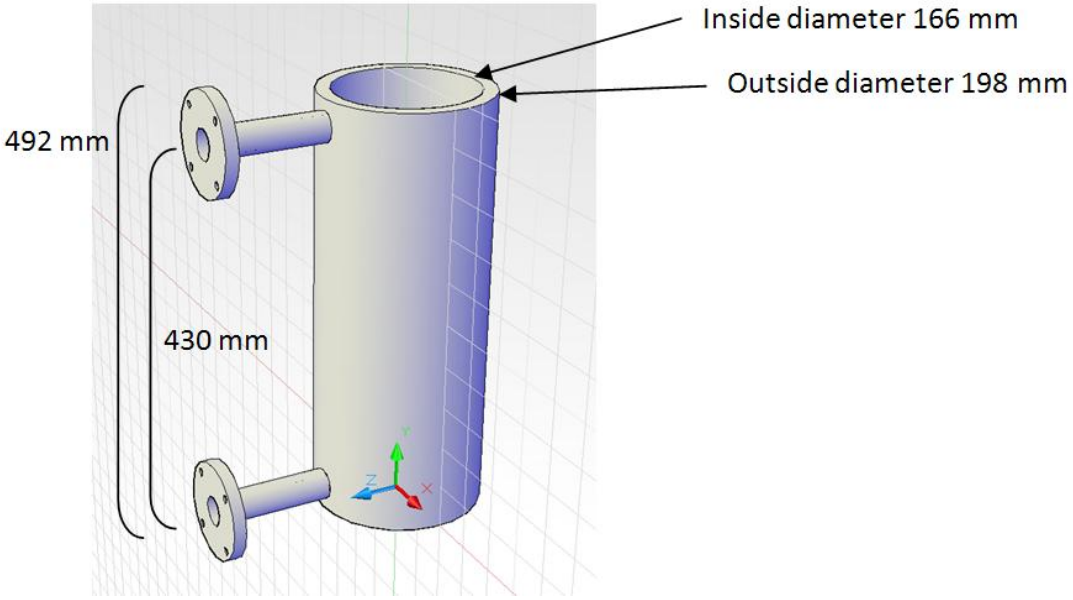

Figure 32 Assumed geometry of the heat exchanger.

Similarity analysis:

Regarding the fact that internal heat exchanger characteristics are unknown, and thus the normal pressure drop calculating approach can't be applied. Similarity analysis is planned to be used in order to find the relations that govern the pressure drop in order to use it to analyze the pressure drop of other fluids such as water in the heat exchanger.

Applying Buckingham theorem:

1) List the parameters in the problem and count their total number.

The pressure drop in the heat exchanger is written as a function of the variables affecting it, which are: the equivalent diameter Deq, the HX length, the internal surface roughness, the flow velocity V and the fluid density ρ and viscosity μ.

$$\Delta p = f(D_{eq}, L, V, \rho, \mu, \varepsilon) \quad (1)$$

The total number of the parameters n=7.

2) List the primary dimensions of each on the n parameters:

Parameter	Δp	D_{eq}	L	V	ρ	μ	ε
Primary dimension	$\{m^1t^{-2}L^1\}$	$\{L^1\}$	$\{L^1\}$	$\{L^1t^{-1}\}$	$\{m^1L^{-3}\}$	$\{m^1L^{-1}t^{-1}\}$	$\{L^1\}$

All the parameters could be calculated straight forward, while the equivalent diameter Deq was calculated based on equation 2. [Kern 1961]

$$D_{eq} = \frac{4 \times Flow\ Area}{Frictional\ wetted\ perimeter} = \frac{4 \times \frac{\pi}{4} \times \left({D_0}^2 - {D_i}^2\right)}{\pi(D_0 + D_i)} = D_0 - D_i \qquad (2)$$

3) Set the reduction j as the number of primary dimensions.

⇨ $j = 3$.

Calculate k, the expected number of II's,

K= n-j=7-3= 4.

4) Choose j repeating parameters.

D_{eq} , ρ, V

5) Construct the k II's, and manipulate as necessary.

Parameter	Δp	L	μ	ε
Non dimensional parameter	Π_1: $\Delta p/ \rho.V^2$	Π_2: L/D_{eq}	Π_3: $(\rho V D_{eq}/ \mu)$ Reynolds number	Π_4: ε/D_{eq} Roughness ratio

6) Write the final functional relationship.

$$\Pi_1 = f(\Pi_2, \Pi_3, \Pi_4)$$

$$\Delta p/ \rho.V^2 = f(R, L/D_{eq,} \varepsilon/D_{eq}) \qquad (3)$$

The dimensional analysis is completed at this point, and experimental data are required to define the relation between the parameters in the function (3).

It has to be mentioned that changing the fluid from oil to water has no influence neither on the independent parameters Π3 nor Π4 which remain constants, and only the Reynolds number changes. And thus the relation between Reynolds and the pressure drop is to be determined.

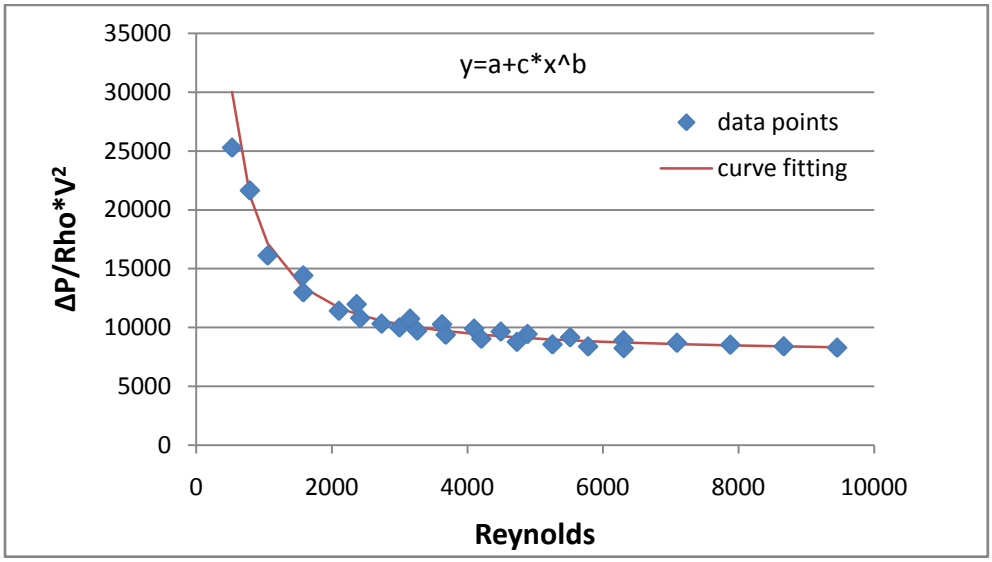

Figure 33 Relation between the non-dimensional numbers ($\Delta p/\rho v^2$) and Reynolds number.

Figure 4 shows the relation between the non-dimensional numbers (Δp/ρv2) and Reynolds number, which is fitted by the power function y=a+c*x^b, the parameters a,b and c were determined by the curve fitting.

$$\Delta p/\ \rho.V^2 = f\ (R,\ L/Deq,\ \varepsilon/Deq)$$

The best fitting achieved using the function Δp/ ρ.V2 = a+c*R^b where:
a= 7697.553, b= -1.24007, c= 52733813.

$$\Delta p = \rho.V2(\ 7697.553 + 52733813^*\ R\ ^{-1.24007}) \qquad (4)$$

It can be noticed that at large Reynolds numbers the Π1 (Δp/ρv2) curve tends to be horizontal, and thus in would be also independent of Reynolds number, and the flow would be fully rough turbulent flow. This can be presented more clearly in the extrapolated results for Reynolds number as shown in figure 5 with Π1 (Δp/ρv2) presented on a logarithmic scale.

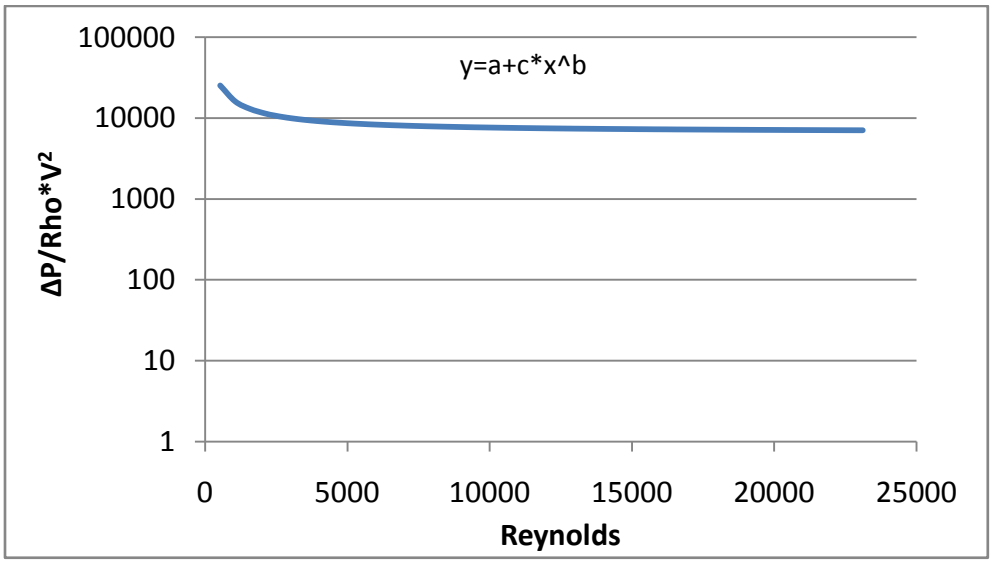

Figure 34 Relation between the non-dimensional numbers (Δp/ρv2) on logarithmic scale and Reynolds number.

Similarity between oil and water flows:

As the same heat exchanger is used in both cases with oil and water, the geometry related parameters (L/Deq "Π2", and ε/Deq "Π4") are constants.

$$\Pi_1 = f(\Pi_2, \Pi_3, \Pi_4)$$

$$L/D_{eq} = \text{const.} \Rightarrow \Pi_{2,oil} = \Pi_{3,water}$$

$$\varepsilon/Deq = \text{const.} \Rightarrow \Pi_{4,oil} = \Pi_{4,water}$$

And the only parameter affecting the dependent parameter ("Δp/ ρ.V2" Π1) is the Reynolds number (Π3). And thus based on the equation (4) which is a general equation extracted from the pressure drop of oil in the heat exchanger, the pressure drop of water in the heat exchanger was calculates as shown in figure 6.

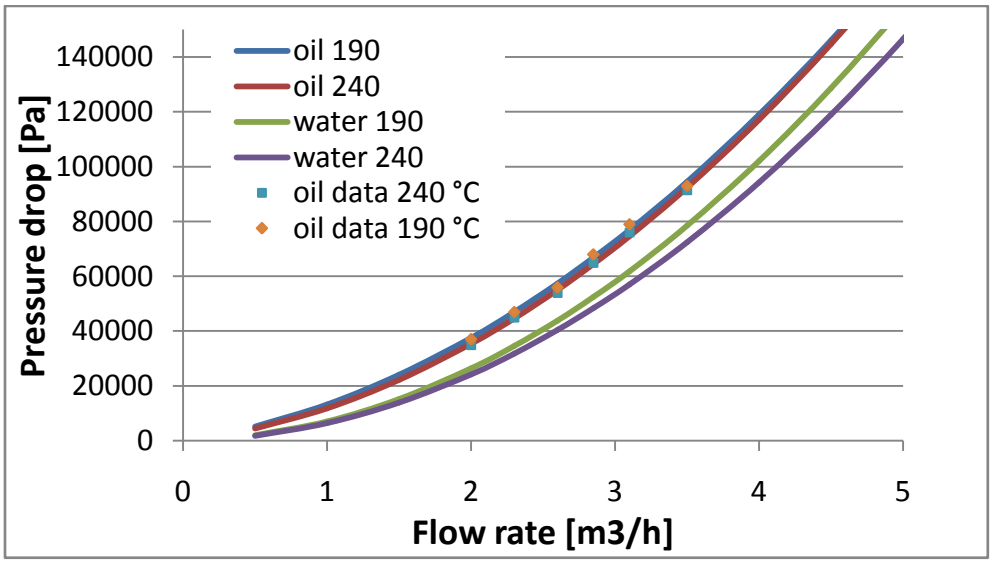

Figure 6 The pressure drop in the solar loop using both fluids, oil and water at different temperatures and flow rates.

The main difference between water and oil from flow dynamics point of view is their viscosity characteristics as shown in figure 7. And this results in much higher Reynolds number for water at the same flow rate of oil.

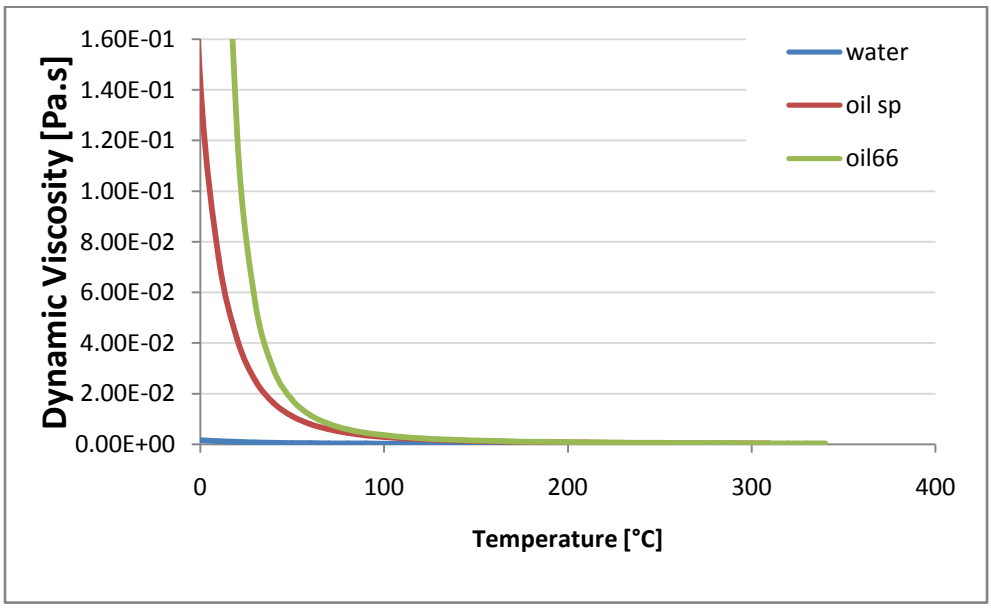

Figure 7 Dynamic viscosity of water and two types of thermal oils at different temperatures.